

ABSTRACT

Title of Document: INVESTIGATIONS IN INTERKINGDOM SIGNALING AND CONTROL OF QUORUM SENSING DEPENDENT PHENOTYPES

Amin Zargar, Doctor of Philosophy, 2015

Directed By: Professor William E. Bentley
Fischell Department of Bioengineering

Bacteria secrete and recognize communication molecules to coordinate gene expression in a process known as quorum sensing (QS). Through coordinated expression, bacteria are able to influence phenotypic changes on a larger population scale, such as biofilm formation. Recent studies into interkingdom communication have found cross-talk communication among bacteria and eukarya as well, which has been shown to influence actions pathogenicity and inflammation, among others. In this work, we developed *E. coli* ‘controller cells’ that guide and attenuate harmful bacterial QS phenotypes coordinated by the QS molecule autoinducer-2 (AI-2), as well as further the understanding of the interkingdom effects of these bacterial secretions (secretome) on human cells, particularly intestinal epithelial cells (IECs) that line the GI tract. Extending beyond natural networks, these ‘controller cells’ provide a useful tool in metabolic engineering, as synthetic biologists have incorporated QS networks to create sophisticated genetic circuits.

Through next generation RNA sequencing, we found that *E. coli* secretomes activate a number of defense-related signaling pathways in epithelial cells, including the cytokine-cytokine receptor pathway, the chemokine signaling pathway, and the NF- κ B signaling pathways. Further, we found the inflammatory cytokine interleukin-8 (IL-8) responded to AI-2 with a time-course pattern of initial upregulation followed by subsequent downregulation. We propose this pattern

fits the paradigm where bacterial metabolites cause changes in the host cell which are returned to homeostasis through negative feedback regulators.

To develop ‘controller cells’, we characterized the kinetics of the *lsr* operon in *E. coli* through the generation of a suite of bacterial strains that overexpress the components of AI-2 processing: uptake (LsrACDB), phosphorylation (LsrK) and degradation (LsrFG). These engineered ‘controller cells’ can regulate the extracellular AI-2 environment, silence bacterial communication, and modulate biofilm formation. Using the insight gained from our mathematical model of the AI-2 processing mechanisms, we developed a high-efficiency (HE) controller cell that could guide QS-dependent behaviors while being sequestered from the target population inside an alginate-chitosan capsule. This work has helped clarify the interkingdom interaction between IECs and commensal bacteria, and created a novel method to control bacterial communication.

INVESTIGATIONS IN INTERKINGDOM SIGNALING AND CONTROL OF QUORUM
SENSING DEPENDENT PHENOTYPES

By

Amin Zargar

Dissertation submitted to the Faculty of the Graduate School of the
University of Maryland, College Park, in partial fulfillment
of the requirements for the degree of
Doctor of Philosophy
2015

Advisory Committee:
Professor William E. Bentley, Chair
Assistant Professor Rohan Fernandes
Associate Professor Herman Sintim
Assistant Professor Kimberly Stroka
Associate Professor Ian White

© Copyright by
Amin Zargar
2015

Dedication

I dedicate this work to my parents, Sharif and Mahin, my older brothers, Arsalan and Ehsan, and my little sister Anita.

Acknowledgements

I would like to acknowledge the members of my committee for their time, advice and mentorship. In particular, I would like to thank my adviser, Dr. William Bentley. As a mentor, he has guided my research over the past four years, and as a role model, he has helped clarify the career path I wish to pursue for my future. I also wish to acknowledge my fellow lab members, past and present, for their contributions to this work. I especially would like to thank the senior members of the laboratory when I joined: Dr. David Quan, Dr. Chen Yu Tsao, Dr. Karen Carter and Dr. Hsuan-Chen Wu. They patiently trained and guided me at a time when I would have been completely lost without them, and I am indebted to their kindness and goodwill. I also thank all of my co-authors, collaborators, and undergraduate research assistants who helped shape this work. On a personal level, I would like to thank all of my friends who have supported me throughout my time at Maryland.

Contents

Dedication.....	ii
Acknowledgements.....	iii
List of Tables	vii
List of Figures.....	viii
Chapter 1: Introduction.....	1
1.1 Background	1
1.1.1 Quorum Sensing.....	1
1.1.2 Synthetic Biology.....	2
1.1.3 Interkingdom Communication	3
1.1.4 Quorum quenching	4
1.1.5 RNA Sequencing.....	5
1.2 Motivation	7
1.3 Dissertation Outline	8
Chapter 2: Bacterial secretions of nonpathogenic <i>E. coli</i> elicit inflammatory pathways: a closer investigation of interkingdom signaling	11
2.1 Abstract	11
2.2 Importance	12
2.3 Introduction	12
2.4 Materials and Methods	15
2.4.1 HCT-8 incubations with bacteria.....	15
2.4.2 HCT-8 incubations with AI-2.	15
2.4.3 AI-2 activity assay.....	16
2.4.4 RNA Downstream Analysis.....	16
2.4.5 Quantitative reverse transcription polymerase chain reaction (qPCR).	16
2.4.6 Enzyme-linked immunosorbent assay (ELISA)	17
2.5 Results	17
2.5.1 The secretome of BL21 and W3110 causes differential gene expression in HCT-8 cells.	17
2.5.2. BL21 and W3110 activate the cytokine-cytokine receptor pathway.....	20
2.5.3 BL21 and W3110 activate the NF κ B pathway and its negative feedback components.	23

2.5.4 Upregulation of gene expression by bacterial secretomes do not translate to increased cytokine protein expression.....	25
2.5.5 BL21 and W3110 cause differential expression in genes responsible for tissue structure.....	25
2.5.6 Strain-specific differentially expressed genes	26
2.5.7 AI-2 initiates upregulation of inflammatory cytokines before downregulation.....	29
2.6 Discussion	31
Chapter 3: Rational design of ‘controller cells’ to manipulate protein and phenotype expression	40
3.1 Abstract.....	40
3.2 Highlights.....	41
3.3 Introduction.....	41
3.4 Materials and Methods.....	44
3.4.1 Plasmid construction.....	44
3.4.2 AI-2 assay	44
3.4.3 AI-2 uptake profiles of ‘controller cells’	45
3.4.4 Modulation of AI-2 in co-cultures.....	45
3.4.5 Silencing of autoinduced protein expression.....	46
3.4.6 Biofilm studies and evaluation.....	46
3.4.7 Chemotaxis studies and assay	47
3.5 Results	48
3.5.1 Design of modular QS elements	48
3.5.2 Quenching of QS-dependent protein expression	51
3.5.3 Manipulation of ‘producer cell’ in co-cultures and extension of model	52
3.5.4 Chemotaxis and biofilm attenuation	56
3.6 Discussion	59
3.7 Supplemental material on mathematical model.....	61
3.7.1 Mathematical model of ‘controller cells’ with exogenously added AI-2	61
3.7.2 Extension of deterministic model to co-incubations with BL21	61
3.8 Supplemental figures	63
3.9 Supplemental Tables.....	68
3.10 Supplemental Material on Mathematical Model	73
Chapter 4: Generation of ‘quantized quorums’ through dose-dependent encapsulated bacteria...	75

The following work is prepared to be submitted into <i>ACS Synthetic Biology</i>	75
4.1 Abstract	75
4.2 Introduction	76
4.3 Materials and Methods	79
4.3.1 Plasmid construction.....	79
4.3.2 AI-2 Assay.....	79
4.3.3 Synthetic AI-2 uptake profiles.....	80
4.3.4 Modulation of autoinduced protein expression.....	80
4.3.5 Capsule preparation.....	81
4.3.6 AI-2 uptake profile in capsules.....	81
4.3.7 Modulation of protein expression through encapsulated bacteria.....	81
4.4 Results and Discussion	82
4.4.1 AI-2 uptake profiles of controller cells with and without glucose.....	82
4.4.2 Quenching of protein expression.....	84
4.4.3 Encapsulated bacteria remove extracellular AI-2.....	85
4.4.4 Encapsulated HE 'controller cell' can quench and tune quorum sensing.....	88
4.5 Supplemental Figures	92
Chapter 5: Autonomous cell-guided quorum quenching.....	94
5.2.1 Autonomous controller cell generates positive feedback loop.....	94
5.2.2 Autonomous controller uptake AI-2 in accelerated fashion and increases sensitivity .	96
5.2.3 Autonomous controller uptake provides signal of AI-2 uptake.....	97
5.3 Applications of autonomous controller cell	98
Chapter 6: Conclusions, contributions and future directions.....	99
6.1 Summary	99
6.2 Contributions to Science	100
6.3 Future directions	101
References.....	103

List of Tables

Table 2.1: Differentially expressed (DE) genes.	20
Table 2.2 SPIA significance.....	22
Table S2.1 Primers used for SYBR green qPCR.....	39
Table S3.1: All strains and plasmids used in Chapter 3.....	68
Table S3.2: Oligonucleotide primers used in Chapter 3.....	69
Table S3.3: Rate equations used in co-incubations of BL21 pTrcHisB with LW12 pTrcHisB.....	70
Table S3.4: Rate equations used in co-incubations of BL21 pTrcHisB and LW12 pLsrACDBFG ..	71
Table S3.5: Kinetic rate constants and parameters used in co-cultures	72

List of Figures

Scheme 1: Quorum sensing paradigms.	2
Figure 2.1: Interkingdom communication between microbiome and host in the GI tract.	14
Figure 2.2: Schematic of experimental setup.	18
Figure 2.3: Signaling pathway analysis.	23
Figure 2.4: Heatmap.	27
Figure 2.5: NGS sequenced reads mapped to annotated IL-8 gene as visualized in IGV.	28
Figure 2.6 qPCR of IL-8.	31
Figure S2.1: qPCR validation of RNA-Seq.	34
Figure S2.2: Signaling pathway analysis graphs.	35
Figure S2.3: Multi-analyte ELISA.	36
Figure S2.4: AI-2 standard curve.	37
Figure S2.5: qPCR of TNF and CSF2.	38
Scheme 3: <i>E. coli</i> <i>lsr</i> -system:	43
Figure 3.1 AI-2 uptake profiles of ‘controller cells’	49
Figure 3.2 Cell-cell modulation of protein expression.	52
Figure 3.3 LW12 pLsrACDBFG modulates AI-2 in the microenvironment.	55
Figure 3.4: Effects of AI-2 on biofilm production.	57
Figure 3.5: Effects of AI-2 on chemotaxis.	58
Figure S3.1: Optical density of individual strains.	63
Figure S3.2: Optical density of co-cultures.	64
Figure S3.3: Uninduced uptake rate.	65
Figure S3.4: QS reporter with control.	66
Figure S3.5: QS reporter with controller cell.	67
Scheme 4: Schematic of the <i>lsr</i> -system in <i>E. coli</i> and engineered plasmids.	77
Figure 4.1: AI-2 uptake profiles.	83
Figure 4.2. Modulation of protein expression.	85
Figure 4.3: Encapsulated bacteria uptake profiles.	87
Figure 4.4: Encapsulated bacteria silence cell-cell communication	89
Figure 4.5: Tuning protein expression with varying doses of encapsulated bacteria.	90
Figure S1: FACS histogram of EGFP expression with doses of encapsulated bacteria.	92
Figure S2: FACS histogram of EGFP expression with gating on side and forward scatter illustrated.	93
Figure 5.1: Schematic of ‘autonomous controller cell’	95
Figure 5.2: qPCR of autonomous controller cells.	96
Figure 5.3: AI-2 uptake of autonomous controller cells.	97
Figure 5.4: AI-2 uptake of autonomous controller cells.	98

1 **Chapter 1: Introduction**

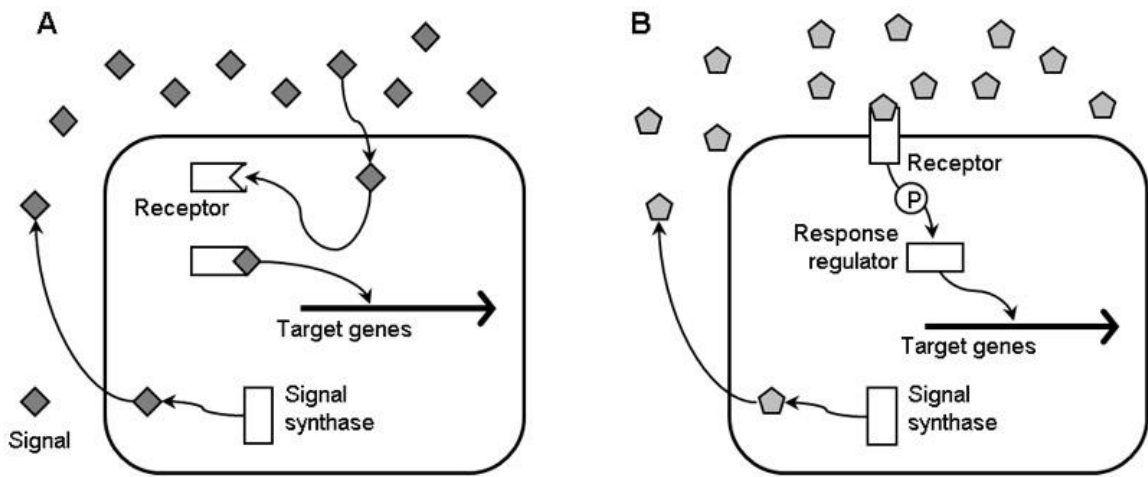
2 The goal of this work was to determine the interkingdom effects of bacterial secretions,
3 including autoinducer-2 (AI-2), on colonic epithelial cells of the GI tract, and then develop
4 engineered microbes that could regulate AI-2 and effect prokaryotic quorum sensing (QS)
5 dependent phenotypes. To better explore the concepts discussed, this chapter will first provide a
6 brief background into the fields of quorum sensing, synthetic biology, quorum quenching,
7 interkingdom signaling, and next-generation RNA sequencing. We will then explore the
8 motivation for this work and provide a brief summary of the work and the upcoming chapters.
9 Subsequent chapters are designed to be self-contained, and have been adapted from manuscripts
10 (accepted, submitted, or in preparation) to peer-reviewed journals.

11 **1.1 Background**

12 **1.1.1 Quorum Sensing**

13 QS bacteria produce and respond to their own signaling molecules for induction of gene
14 expression, hence classes of QS molecules are denoted as autoinducers. Quorum sensing is
15 involved in biofilm formation, bioluminescence, virulence factor secretion, sporulation and other
16 critical bacterial functions (reviewed by [1-4]). The first class of QS molecules described were
17 acyl homoserine lactones (AHLs), termed autoinducer-1 (AI-1) and is depicted in **Scheme1A**.
18 This QS system was first discovered with *Vibrio fischeri* [5], a bacterium that provided
19 bioluminescent light in a symbiotic process with its marine, eukaryotic host. Investigations
20 revealed that this process was performed through luxI synthesized the AHL, which once it reach a
21 concentration threshold, bound the luxR protein, and activated the luciferase promoter. This
22 luxI/luxR was later revealed to be a QS paradigm[6,7], with the generation and response to these
23 QS molecules considered species-specific.

24 A second class of autoinducers, AI-2, were found to consist as two classes (with or
 25 without boron), and in equilibrium in a mixture of isomers of 4,5-dihydroxy-2,3-pentadione
 26 (DPD) that rapidly interconvert (reviewed by [8]). Depicted in **Scheme 1B**, AI-2 is synthesized
 27 by LuxS from the precursor SAH, where it is secreted by TqsA into the extracellular space. AI-2
 28 is imported into the cell primarily through the LsrACDB complex, where it is subsequently
 29 phosphorylate din the intracellular space by the kinase LsrK. Phosphorylated AI-2 derepresses
 30 LsrR, the master regulator of the *lsr*-system, which allows genomic transcription of the *lsr*-
 31 operon. Phosphorylated AI-2 is degraded through a two-step process through enzymes LsrG and
 32 LsrF. Unlike AHLs, AI-2 is considered as a ‘universal’ QS molecule, as the *lsr*-system is
 33 widespread among prokaryotes[9].



34
 35 **Scheme 1: Quorum sensing paradigms.** A) AHL dependent quorum sensing is illustrated where a
 36 signal synthase produces the AHL signal that is exported out of the cell. The signal diffuses back
 37 into the cell and binds to a QS receptor that activates gene expression. B) AI-2 dependent quorum
 38 sensing is illustrated where the signal is imported into the cell by an ABC type transporter, and then
 39 binds to a response regulator that activates gene expression.

40 **1.1.2 Synthetic Biology**

41 The concept of biological parts that could process logical operations was first envisioned
 42 over 50 years ago[10], and the beginning of the 20th century coincided with the rapid emergence
 43 of the synthetic biology field as a simple toggle switch [11] was used to create the first of many

44 increasingly sophisticated gene circuits (reviewed by [12,13]). Most of our knowledge of
45 endogenous genetic circuits (interacting gene networks that guide cellular functions) has
46 consisted of top-down genetic perturbations that have proved to be challenging to develop
47 reliable outcomes. Synthetic biology provides a bottom-up approach to rationally design genetic
48 circuits and test them in living cells.

49 Synthetic genetic circuits allow the programming of complex, large scale cellular
50 behavior and phenotypes. A common method to connect synthetic circuits has been to leverage
51 the process of quorum sensing (QS), a natural cell-cell process that bacteria use to coordinate
52 action. For example, QS synthetic networks have been used to autonomously produce
53 proteins[14], detect arsenic[15], and produce a synthetic E. coli predator-prey system[16]. QS
54 synthetic networks have also been used to develop bacterial-directed therapies such as cancer-
55 fighting bacteria [17] and probiotic bacteria that can prevent cholera infections[18]. As more
56 complex circuits are being built, dynamic control over these signal molecules will be needed.
57 Through rational design and directed evolution [19], synthetic biology is developing tools that
58 influence the fields of metabolic engineering, biomedicine, and related biological processes.

59 **1.1.3 Interkingdom Communication**

60 The co-evolution of prokaryotes and eukaryotes over millions of years has resulted in
61 symbiotic, commensal, and parasitic interactions, and it is well-established that different bacterial
62 species modulate the host physiological system. Recently, a field has emerged from quorum
63 sensing involving interkingdom communication, specifically the communication between
64 prokaryotes and eukaryotes. The first observation of interkingdom signaling was made by
65 Telford et al., who discovered that an AI-1 molecule, OdDHL, N-(3-oxo-dodecanoyl)-l-
66 homoserine lactone, had immunomodulatory effects on murine and human leukocytes[20]. Since
67 then, OdDHL has been found to have many different effects on different tissues by entering and

68 functioning inside mammalian cells, but the mechanism of entry and OdDHL receptor remains
69 unknown[21,22].

70 Exploitation of interkingdom signaling networks could result in novel methods to combat
71 infections and develop therapeutics. As an example, while EHEC (enterohemorrhagic *E. coli*) can
72 hijack the hormones epinephrine and norepinephrine to activate pathogenicity [23], this activation
73 can be blocked through the use of α and β adrenergic antagonists[24]. Another example is the QS
74 signal produced from *Pseudomonas aeruginosa*, a common cause of infection in the lungs of
75 cystic fibrosis patients. *P. aeruginosa*-infected lungs secrete OdDHL, which in turn causes the
76 release of large quantities of IL-8, signaling high migration of neutrophils and resulting in
77 extensive tissue damage[25]. With this knowledge, therapeutics could be designed to not only to
78 attack *P. aeruginosa*, but to attenuate these pro-inflammatory signals. Almost all studies on
79 interkingdom communication have concerned AHLs and AI-2, while the interkingdom effects of
80 AI-2 has consisted of a single microarray study at 50 μ M of AI-2 with alveoli cells, which found
81 only 4 genes differentially expressed [22]. As a ‘universal’ signal, the understanding of AI-2 is
82 important not only in polymicrobial networks but also in regards to interkingdom communication.

83 **1.1.4 Quorum quenching**

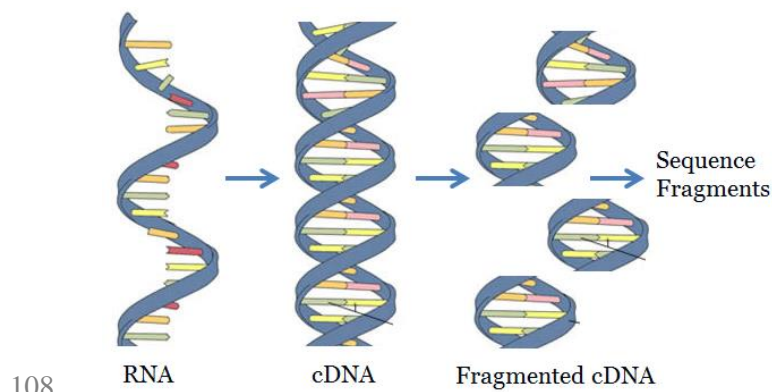
84 The emergence of multi-drug resistant antibiotic strains has ushered in an era where there
85 is no “magic bullet” to deal with patients with antibiotic-resistant infections [26]. The selective
86 pressure from these bacteriostatic or bacteriocidal agents exert help drive these microbes to
87 develop antibiotic resistance through genotypic or phenotypic agents [27]. While new research
88 suggests that quorum quenching should not be considered impervious to the development of
89 resistance [28], it is nonetheless a promising approach as quorum quenching studies have targeted
90 AHLs using lactonases, acylases and analogues, and AHL-consuming bacteria. Successful
91 applications include the use of AHL-consuming bacteria to reduce virulence of *V. cholera* in

92 mice[18,29] , the application of synthetic autoinducer peptides to reduce Staphylococcal lesion
93 formation in mice [30], among several others (reviewed [31]).

94 While most quorum quenching studies have targeted AHLs, there have also been studies
95 targeting AI-2. These AI-2 strategies have used compounds and enzymes to target the
96 extracellular signal, and the intracellular signal generator [27]. In our lab and with our
97 collaborators, we have developed both enzymes that target the extracellular AI-2 signal as well as
98 synthetic analogues to interfere with AI-2 mediated quorum sensing[32,33]. Additionally, an *E.*
99 *coli* double knockout mutant strain (*AhuxS ΔlsrR*) has been shown to interfere with
100 bioluminescence and alter the gut microbiome [34,35].

101 1.1.5 RNA Sequencing

102 RNA-seq has distinct advantages over microarrays. These include low background noise,
103 absolute transcript count, higher resolution, larger dynamic range, and increased accuracy [36].
104 The general outlines of upstream RNA-sequencing are shown in **Scheme 2**. The sequenced reads
105 from RNA-seq are mapped to the genome to quantify gene expression, and statistical software is
106 used to determine significantly differentially expressed genes and pathways. A brief overview of
107 the purification, analysis pipeline, and statistical software used is described below.



109 **Scheme 2: General outline of RNA- sequencing.** RNA is isolated from cells, synthesized to a
110 cDNA library, fragmented to smaller pieces and sequenced from either end.

111 Samples are sequenced with an Illumina HiSeq1000 at a sequencing facility. A TruSeq
112 RNA Sample Prep Kit (Illumina) is used to purify for polyadenylated mRNA, synthesize a
113 cDNA library from the RNA, and then shear the cDNA into an average library size of 200 base
114 pairs. The RNA is sequenced from both ends in 100 bp lengths with the HiSeq1000 (Illumina).
115 The raw reads obtained from the Illumina HiSeq1000 are first run on the FastQC software to
116 measure quality of the RNA reads based on Phred scores, which calculates a probability of the
117 accuracy of a base call based on peak resolution and peak shape [37]. All reads with an average
118 quality score over 20, which is the most commonly accepted cutoff for reliable RNA reads, will
119 be kept[38].

120 The sequencing results are analyzed with open-source software to determine biological
121 meaning. Each sample's reads will be aligned to the latest annotated human genome, hg19, using
122 the open-source software Tophat [39]. The output of Tophat are raw read abundances mapping
123 each transcript to its alignment on the human genome. Tophat uses a built-in program Bowtie[40]
124 to first align the cDNA reads to the genome, then uses Tophat to align reads that did not align
125 because of a splicing event and discards reads that cannot be aligned. Using the Integrative
126 Genome Viewer (IGV), the transcript abundances can be viewed at the genome level, the
127 chromosome level, the gene level, down to individual base pairs [41]. While lacking the
128 statistical power to analyze and group sample conditions, IGV provides useful graphical
129 illustrations of the data.

130 For determination of differential expression, raw read abundances from Tophat are
131 outputted into DESeq[42], an open-source program in R that analyzes the statistical significance
132 of differential expression. This software uses variance, transcript abundance, and fold-change to
133 determine differential expression, normalized by the size of each sample's cDNA library. High
134 abundance of transcripts and low variance in each gene transcript will result in a lower fold
135 change required for significant differential expression. DESeq outputs a significance value for

136 each gene and a multiple hypothesis tested adjusted p value for each gene. With the thousands of
137 simultaneous inferences being made, multiple hypothesis testing is needed to account for the
138 false discovery rate.

139 The significantly differentially expressed genes ($p_{adj}<0.1$) output of DESeq are outputted
140 into the open-source software Signaling Pathway Impact Analysis, SPIA[43]. These
141 differentially expressed genes are then fed into the software SPIA, signaling pathway impact
142 analysis, to determine the biologically relevant pathways that were activated or inhibited. SPIA
143 uses over-representation analysis (the prevalence of differential genes compared to all
144 background genes), functional class scoring (the similarity of functions in genes differentially
145 expressed) and pathway topology (a priori knowledge of signaling pathways).

146 **1.2 Motivation**

147 The symbioses of prokaryotes and eukaryotes in the GI tract leads to the question of what
148 is the role that bacterially produced secretions (secretome), including QS molecules, have on
149 eukaryotes. Interkingdom signaling is an emerging field of research that explores the ‘cross-talk’
150 between prokaryotes and eukaryotes. This relationship is of particular importance considering
151 there are over 400 indigenous species of bacteria that comprise the gut and oral cavity, and these
152 bacteria play an important role in proliferation and differentiation of epithelial cells, providing
153 nutrients, influencing and maintaining immune responses. While the mechanisms behind AI-2
154 quorum sensing networks have been well-studied, the interkingdom signaling relationship
155 between quorum signaling molecules and human cells is not yet understood. Therefore, before we
156 engineer a commensal microbe to remove AI-2, we sought to determine the impact bacterial
157 secretions have on epithelial cells, including in the presence or absence of AI-2.

158 The motivation behind engineering microbes to rapidly consume the QS molecule AI-2
159 extends to both natural and synthetic networks. As bacteria are developing resistance to
160 antibiotics at a faster rate than the development of new therapies [44], which is a worldwide

161 crisis, interfering with quorum sensing as a stand-alone or adjuvant therapy is looked as a
162 promising alternative. Quorum sensing inhibitors using synthetic, plant, or bacterial compounds
163 has shown promising results in attenuating QS-dependent phenotypes, but some of these
164 compounds have stability and toxicity issues, and all of these compounds have localized site of
165 delivery issues. Engineering commensal bacteria that can remove the QS molecule at the site of
166 infection could provide a promising alternative to antibiotics in human and health and disease.
167 Extending beyond natural networks, many synthetic biology applications have incorporated QS
168 networks, which lead to the need for developing tools to control these communication molecules.

169 **1.3 Dissertation Outline**

170 Chapter 2 describes the *in vitro* investigation into the interkingdom effects of the
171 bacterial “secretome”, particularly AI-2, on epithelial cells. Two different strains of *E. coli*, BL21
172 and W3110, and a negative control of growth media only are co-cultured with HCT-8 epithelial
173 cells. To ensure that interaction is only between soluble factors, a transwell was placed between
174 the epithelial cell culture and the bacterial cell culture (the negative control also uses a transwell).
175 After 6 hours, the effects of the secretomes on epithelial cells are determined by extracting the
176 colonic epithelial cell RNA and determining the transcriptome. We found that BL21 and W3110
177 *E. coli*, which exhibit phenotypic differences including production of flagella, acetate, and AI-2,
178 caused a similar reaction in epithelial cells, with the activation of cytokine-cytokine receptor
179 pathways and the upregulation of negative feedback components of these pathways.

180 Chapter 3 describes the development of a suite of QS consumers, ‘controller cells’, which
181 can be deployed to regulate the ‘universal’ QS molecule autoinducer-2 (AI-2) in a predictable
182 fashion using the well-characterized QS mechanisms of *E. coli*. In this design, we separately
183 overexpressed the three main components responsible for the uptake and degradation of AI-2
184 from the environment: AI-2 transport into the cell through the protein complex LsrACDB,
185 phosphorylation of AI-2 to AI-2P (a form of AI-2 that cannot cross the cell membrane) by the

186 kinase LsrK, and degradation of AI-2P by the two-step process of isomerase LsrG and cleavage
187 by LsrF. This study revealed that overexpression of the *lsr*-transporter, LsrACDB, causes the
188 greatest increase in AI-uptake rate, and that overexpression of the kinase, LsrK, results in
189 increased AI-2 uptake by limiting secretion of AI-2 back into the extracellular environment.
190 Further, we developed a simple mathematical model that recapitulates experimental data and
191 characterizes the dynamic balance among the various uptake mechanisms. We show that these
192 ‘controller cells’ modulate phenotypic outcomes such as biofilm formation and chemotaxis and
193 provide an orthogonal means of manipulation of natural and synthetic gene networks and
194 phenotypes (in press *Metabolic Engineering*). However, these controller cells needed large
195 numbers directly interacting with the QS-dependent bacteria to block communication, required
196 the addition of an exogenous inducing agent, functioned only in the absence of glucose—a
197 common nutrient in a variety of environments—and quenched, but did not tune QS-mediated
198 gene expression.

199 Chapter 4 describes an extension of this work to encapsulate a controller cell inside a
200 multifunctional polysaccharide capsule to tune protein expression of QS-dependent protein
201 expression systems, without direct interaction with the QS culture, the need for an inducing agent,
202 or the exclusion of glucose. Our previous work revealed that the separate overexpression of LsrK
203 and LsrACDB both resulted in increased uptake, and we hypothesized that the overexpression of
204 both mechanisms would result in greater uptake than each individual overexpression. Therefore,
205 we rationally designed a high-efficiency (HE) ‘controller cell’ through a two promoter
206 constitutive system on a single plasmid to overexpress all aspects of the *lsr*-system, save the *lsr*
207 repressor. Further, since the metabolic controls prevent AI-2 uptake and phosphorylation when
208 glucose is present, our previously engineered ‘controller cells’ could not be applied in glucose-
209 rich environments. The HE ‘controller cell’ constitutively expresses the *lsr*-system on the
210 plasmid independently of genomic transcription, which removes this constraint.

211 We show that the HE ‘controller cell’ provides the most rapid uptake of AI-2 compared
212 to all previously engineered cells, and that it is able to effectively remove all AI-2 from the
213 extracellular environment in the presence of glucose. Further, the HE cells can silence QS-
214 dependent protein expression at very low HE to target cell ratios, and also when encapsulated
215 inside a biocompatible capsule. We show that these encapsulated HE controller cells can quench
216 QS signaling, which can be envisioned to be used as a quorum quenching treatment to reduce the
217 expression of harmful phenotypes while sequestering the encapsulated bacteria. Our overarching
218 goal was to not only quench protein expression, but to guide a QS-dependent system that would
219 minimally interact with the controller cell populations. We show here that we can tune protein
220 expression by adjusting the quorum activated population through capsule dosage. We envision
221 that by enabling controlled manipulation of quorums, this tool could be used to assay threshold
222 responses, manipulate complex genetic circuits, and develop and interrogate spatially-patterned
223 cell populations.

224 Chapter 5 discusses the development of an autonomous system that only turns ‘on’ and
225 removes when AI-2 is present. This system not only uptakes and removes AI-2, but reports its
226 presence by fluorescing. The system is well characterized with growth rates, AI-2 uptake kinetics,
227 transcription and protein expression illustrated. We envision these cells could be used in in vivo
228 applications to report and function in a programmable fashion.

229 Chapter 6 provides a summary of the work, as well as discusses the contributions to
230 science and future work.

231 **Chapter 2: Bacterial secretions of nonpathogenic *E. coli* elicit**
232 **inflammatory pathways: a closer investigation of interkingdom**
233 **signaling**

234 This chapter was primarily reproduced directly or adapted from Zargar, Amin, et al.
235 "Bacterial Secretions of Nonpathogenic *Escherichia coli* Elicit Inflammatory Pathways: a Closer
236 Investigation of Interkingdom Signaling." *mBio* 6.2 (2015) with permission [45]

237 **2.1 Abstract**

238 There have been many studies on the relationship between nonpathogenic bacteria and
239 human epithelial cells; however, the bidirectional effects of the secretomes (secreted substances,
240 where there is no direct bacteria-cell contact) have yet to be fully investigated. In this study, we
241 use a transwell model to explore the transcriptomic effects of bacterial secretions from two
242 different non-pathogenic *Escherichia coli* strains on the human colonic cell line HCT-8 using
243 next-generation RNA-seq transcriptional profiling. BL21 and W3110 *E. coli*, while genetically
244 very similar (99.1% homology), exhibit key phenotypic differences including their production of
245 macromolecular structures (e.g., flagella, lipopolysaccharide), and secretion of metabolic
246 byproducts (e.g., acetate) and signaling molecules (e.g., quorum sensing autoinducer, AI-2). After
247 analysis of differential epithelial responses to the respective secretomes, this study shows for the
248 first time that a non-pathogenic bacterial secretome activates the $\text{NF}\kappa\beta$ -mediated cytokine-
249 cytokine receptor pathways while also upregulating negative feedback components including the
250 NOD-like signaling pathway. Because of its relevance as a bacteria-bacteria signaling molecule
251 and the differences in its secretion rate between these strains, we investigated the role of
252 autoinducer-2 (AI-2) on the HCT-8 cells. We found that the expression of inflammatory cytokine
253 IL-8 responded to AI-2 with a pattern of rapid upregulation before subsequent downregulation
254 after 24 hrs. Collectively, these data demonstrate that secreted products from non-pathogenic

255 bacteria stimulate transcription of immune related-biological pathways followed by the
256 upregulation of negative feedback elements that may serve to temper the inflammatory response.

257 **2.2 Importance**

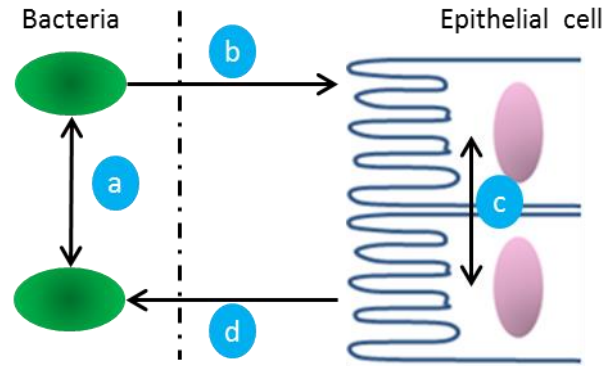
258 The symbiotic relationship between the microbiome and the host plays an important role
259 in the maintenance of human health. There is a growing need to further understand the nature of
260 these relationships to aid in the development of homeostatic probiotics and also in the design of
261 novel antimicrobial therapeutics. To our knowledge, this is the first global transcriptome study of
262 bacteria co-cultured with human epithelial cells in a model to determine transcriptional effects of
263 epithelial cells, while allowing epithelial and bacterial cells to “communicate” to each other only
264 through diffusible small molecules and proteins. By beginning to demarcate the direct and
265 indirect effects of bacteria on the GI tract, two-way interkingdom communication can potentially
266 be mediated between host and microbe.

267 **2.3 Introduction**

268 With approximately 10^{14} bacterial cells [46] populating the human GI tract, scientific
269 investigations have uncovered that interkingdom interactions play an important role in
270 maintaining homeostasis [47-49]. However, the normal microbiome can also elicit a dysregulated
271 immune response that can be a source of pathogenicity in inflammatory bowel diseases, most
272 commonly Crohn’s disease and ulcerative colitis. In the GI tract, intestinal epithelial cells (IECs),
273 which are an important part of the innate immune system, act as a bridge to the adaptive immune
274 system through their expression and secretion of inflammatory cytokines. IECs initiate this
275 mechanism through pathogen associated molecular pattern (PAMP) receptors, such as toll-like
276 receptors (TLRs) and nucleotide-binding oligomerization domain (NOD) receptors, which
277 recognize bacterial products such as lipopolysaccharides, flagella, and peptidoglycan. These
278 receptors activate signaling pathways, mainly through the transcription factor $\text{NF}\kappa\beta$, that
279 culminate in the production of cytokines [50-52]. As the first point of contact, IECs are

280 continuously exposed to huge numbers of Eubacteria (10^{10} - 10^{12} cells per gram) in the colon [53]
281 and therefore play an important role in bacterial-host communication [54-56].

282 An understanding of the mechanisms of response and communication between the
283 secretomes of epithelial cells and bacteria can aid in the understanding of the evolutionary
284 biology of signal development as well as interventional design strategies for maintaining
285 homeostasis (**Figure 2.1**) [56,57]. Moreover, signals that coordinate phenomena among bacteria
286 (e.g., quorum sensing) and signals that mediate bacterial – IEC interactions are of particular
287 interest as these communication networks are involved in pathogenesis and the progression of
288 disease [55,58,59]. Commensurate with the need to understand this interkingdom communication,
289 there have been many studies exploring the effects of non-pathogenic, commensal strains of
290 bacteria on human cells [60-64]. However, most of these involved direct bacterial – IEC
291 interaction, and those that investigated the secretome did not determine a global transcriptomic or
292 proteomic response, leaving the effects of bacterial secretions to be largely unexplored. We have
293 characterized the effects of the *E. coli* secretome, which is well-represented in the colon [65],
294 through the use of a transwell that separates bacteria from epithelial cells while allowing small
295 molecules and proteins to pass, and we have employed RNA-Seq because it provides several
296 advantages over DNA microarrays including lower background noise, an absolute transcript
297 count, and higher resolution [36]. By determining the global transcriptomic response of IECs to
298 bacterial incubations in a system that allows only indirect contact, we can then more closely
299 investigate the commonalities of interkingdom communication.



300

301 **Figure 2.1: Interkingdom communication between microbiome and host in the GI tract.** a) Quorum sensing (QS) molecules coordinate action among bacteria. b) Secretome of bacteria, including QS molecules, affect the host's cellular machinery c) Epithelial cells secrete signals to neighboring and distant cells through signaling molecules d) Soluble factors secreted by the host affect bacteria

306 In this work, we exposed nonpathogenic strains of two Gram-negative, Group A *E. coli*,
 307 BL21 and W3110, grown in the upper chamber of a transwell to the IEC line, HCT-8, cultured in
 308 a monolayer beneath the transwell. BL21, B strain derivative, and W3110, a K-12 strain
 309 derivative, have significantly different transcriptomes and proteomes leading to important
 310 phenotypic differences[66,67]. Our investigations show that the secretomes of either BL21 or
 311 W3110 activated the cytokine-cytokine receptor pathway (e.g. IL-8, TNF), while also
 312 upregulating the negative feedback regulators in $\text{NF}\kappa\beta$ and NOD-like signaling pathways, $\text{NF}\kappa\beta -$
 313 α and TNFAIP3, respectively. The upregulation of cytokines that activate the immune system as
 314 well as negative feedback regulators that reduce the transcription of these cytokines, could be part
 315 of the normal physiological response using a negative feedback loop [68] without which
 316 uncontrolled stimulation of inflammatory cytokines would lead to damaging inflammation to the
 317 host [47,68].

318 The role of AI-2 was investigated further by incubating the *in vitro* synthesized signal
 319 molecule at varied concentrations and time periods with IECs in follow on studies. The
 320 inflammatory cytokine, IL8, which plays an important role in attracting neutrophils, was found to
 321 be initially upregulated at all concentration levels of AI-2 tested (50, 150 and 400 μM) at 6 and

322 12 hours post-addition. It was subsequently significantly reduced at all concentrations relative to
323 the control after 24 hours. These data support a hypothesis that AI-2 is an IEC signaling molecule
324 and that bacterial secretions, including AI-2, may have an initial transcriptional inflammatory
325 response that is downregulated through alternative mechanisms, possibly including negative
326 regulators $\text{NF}\kappa\beta$ and TNFAIP3.

327 **2.4 Materials and Methods**

328 **2.4.1 HCT-8 incubations with bacteria.**

329 HCT-8 cells were plated in 6 well culture plates (Fisher Scientific) at a seeding density of
330 750,000 cells per well (375,000 cells/mL) in 10% Horse Serum (vol/vol) RPMI 1640 media
331 (ATCC). The culture was grown to confluence for 48 hours at 37°C in the presence of 5% CO₂
332 humidified air. A 0.4 µm transwell (Becton Dickinson) was placed in each culture plate and BL21
333 (2.6% overnight culture), W3110 (2.6% overnight culture) in 1.5 mL of RPMI media was added.
334 RPMI media alone was added as a negative control. The co-culture was then incubated for 6
335 hours at 37°C in the presence of 5% CO₂ humidified air. After incubation, the transwell and
336 enclosed media in the upper chamber were discarded, and the media of the lower chamber was
337 removed and harvested for the *Vibrio harveyi* BB170 AI-2 activity assay and ELISA assays. The
338 RPMI media is supplemented with phenol red, and there was no change in color in the lower
339 chamber, indicating that there were no significant pH changes during incubation. RNA was
340 extracted with the RNAqueous kit (Invitrogen) and eluted RNA was stored at -80°C until thawed
341 for sequencing and qPCR.

342 **2.4.2 HCT-8 incubations with AI-2.**

343 HCT-8 cells were plated and cultured in a similar manner as above. Synthetic AI-2 (10
344 mM) in water was generously provided by the Sintim research group. AI-2 at 50, 150 and 400
345 µM in 2 mL of fresh RPMI media and incubated with HCT-8 cells for 6, 12 and 24 hours.

346 **2.4.3 AI-2 activity assay.**

347 After incubation for 6 hours with the respective conditions, the media of the HCT-8 cells
348 were harvested and tested for the presence of AI-2 by inducing luminescence in *Vibrio harveyi*
349 reporter strain BB170, which was outlined Bassler and coworkers[69]. Briefly, BB170 was grown
350 for 16 hours with shaking at 30°C in AB medium and kanamycin, diluted 1:5,000 in fresh AB
351 medium and kanamycin, and aliquoted to sterile 12- by 75-mm tubes (Fisher Scientific). The
352 media of each condition was added to a final concentration of 10% (vol/vol) to these tubes.
353 Luminescence was measured by quantifying light production with a luminometer and obtained
354 values were in the linear range. Values represent fold change compared to negative control. All
355 conditions were taken in triplicate.

356 **2.4.4 RNA Downstream Analysis.**

357 Each sample's reads were aligned to the RefSeq annotated human genome, hg19, using
358 the software Tophat [39]. These read abundances were then outputted into DESeq [42], an open-
359 source program in R that analyzes the statistical significance of differential expression. The
360 abundance of sequenced reads, 'counts', of each gene were input into DESeq, a software that uses
361 variance, transcript abundance, and fold-change to determine differential expression, normalized
362 by the size of each sample's cDNA library. A modified Fisher's exact test with data fit to a
363 negative binomial distribution of the DESeq package was used to identify the differentially
364 expressed (DE) genes. Differentially expressed genes were outputted to SPIA [43] to evaluate
365 pathway activation.

366 **2.4.5 Quantitative reverse transcription polymerase chain reaction (qPCR).**

367 RNA was synthesized to cDNA using the BIO-73005 SensiFast SYBR Hi-Rox One Step
368 Kit. For the selected candidate genes, primers were taken from the literature or designed using
369 PrimerQuest. β -2-microglobulin, β 2M, was used as a housekeeping gene, and qPCR was

370 performed on the 7900HT real time PCR System (Applied Biosystems) and thermal conditions of
371 10 min at 45°, 2 min at 95°, and 40 cycles of 5 s at 95° and 20 s at 60°. The relative gene
372 expression level of each target gene was then normalized to the mean of β 2M in each group. The
373 control for each gene expression sample set data was selected to be 0 μ M AI-2 samples at each
374 time point. Fold change was calculated using the $\Delta\Delta$ CT relative comparative method. Data from
375 all the studies were analyzed using analysis of variance. Samples were completed in triplicate and
376 standard deviations are reported (n=3).

377 **2.4.6 Enzyme-linked immunosorbent assay (ELISA)**

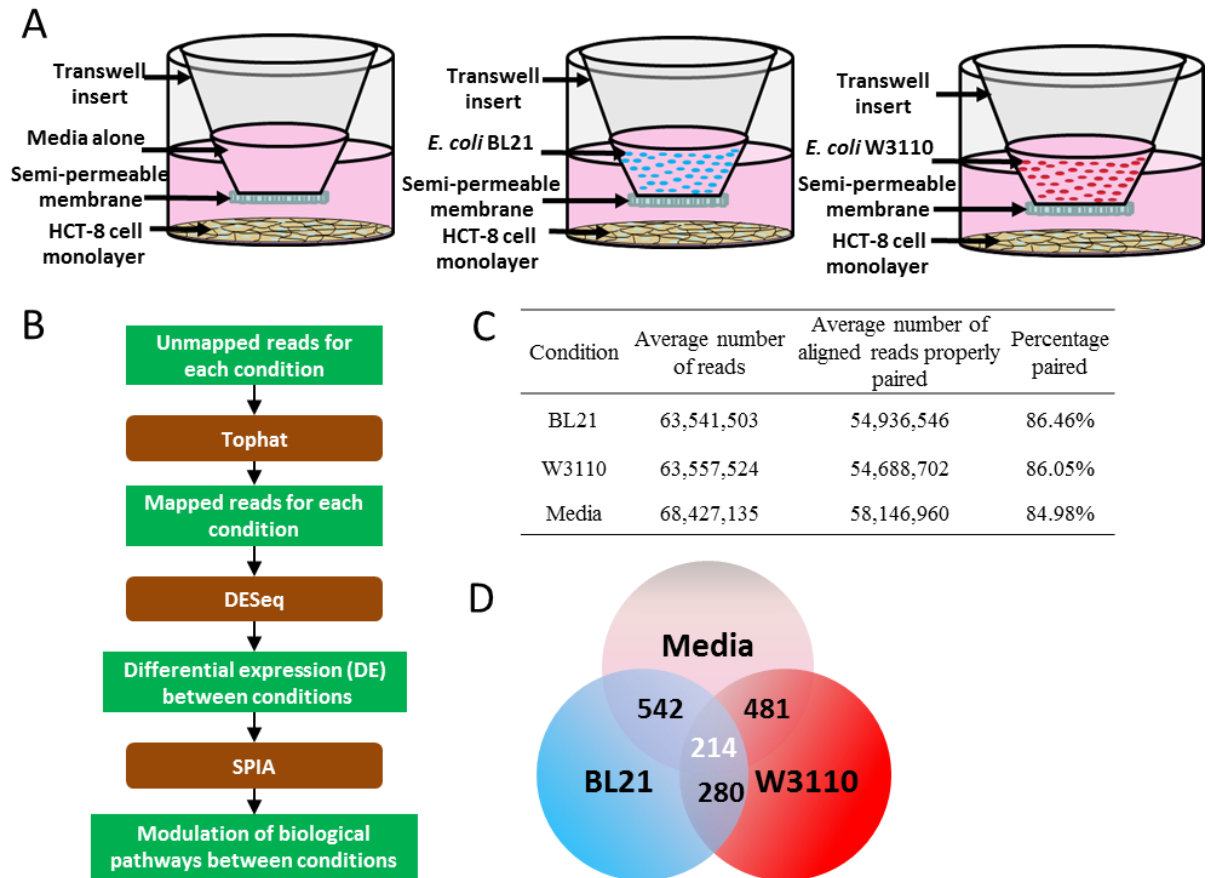
378 Cell culture supernatants of HCT-8 cells in transwell incubations with BL21, W3110, and
379 media alone were harvested and subsequently assayed with the Human Inflammatory Cytokines
380 Multi-Analyte ELISArray Kit MEH-004A (Qiagen)

381 **2.5 Results**

382 **2.5.1 The secretome of BL21 and W3110 causes differential gene expression in HCT-8 cells.**

383 In this study, we explored the transcriptomic changes of co-incubations of BL21 and
384 W3110 in a transwell model with the IEC cell line, HCT-8. We chose a coincubation model,
385 instead of using conditioned medium because bacteria themselves are affected by secretable
386 molecules from mammalian cells, and we chose to include any such crosstalk [70,71]. Toward
387 this end, overnight cultures of BL21 and W3110 were re-inoculated in fresh media in the upper
388 chamber of the transwell, and blank media alone was used as a negative control (**Figure 2.2A**).
389 The 0.4 μ M transwell does not allow measureable amounts of bacteria to pass through the upper
390 chamber (verified through optical density measurements of the lower chamber), but is large
391 enough to allow metabolites and signaling molecules to pass. After 6 hours of coincubation, both
392 bacterial strains reached similar cell densities ($OD_{600} \sim 1$, data not shown), and IECs appeared
393 visibly intact with a cell viability assay showing less than 5% cell death [data not shown]. The

394 RNA of the HCT-8 cells was extracted, and cDNA libraries were created from polyadenylated
 395 RNA.



396
 397

398 **Figure 2.2: Schematic of experimental setup.** **A)** HCT-8 epithelial cells were grown to
 399 confluency, and then incubated with BL21, W3110 or media alone in the upper chamber of a
 400 transwell. After 6 hours of incubation, the RNA of the epithelial cells were extracted and
 401 sequenced. **B)** Downstream RNA-Seq pipeline for analysis of sequencing data (red boxes indicate
 402 open-source program). **C)** Mapping results of HCT-8 NGS transcripts to Refseq annotated human
 403 genome, hg19, with 5 biological replicates using the software Tophat **D)** Differentially expressed
 404 genes using the software DESeq. 542 differentially expressed genes between HCT-8 cells
 405 incubated with BL21 or blank media, 481 genes between HCT-8 cells incubated with W3110 or
 406 blank media, 280 genes between HCT-8 cells incubated with BL21 or W3110. We found 214 DE
 407 genes in common in incubations of BL21 or W3110 compared to blank media.

408 The cDNA libraries of each condition were sequenced via NGS (see Methods) and then
 409 analyzed with downstream statistical software (**Figure 2.2B**). We performed five biological
 410 replicates, each constituting an average of over 60 million 100 bp paired-end reads mapping to

411 hg19, a RefSeq annotated human genome (**Figure 2.2C**). Mapping sequenced reads to the
412 genome was performed using Tophat [39] (which uses a built-in alignment tool) and Bowtie [40]
413 (which maps the cDNA reads to the reference genome). Tophat then aligns reads that did not
414 initially align because of a splicing event and discards reads that cannot be aligned. The aligned
415 reads were inputted into the open-source software DESeq [42], which was used to determine
416 significantly differentially expressed genes (Benjamini-Hochberg-adjusted p values below 0.05).

417 DESeq results indicated that BL21 and W3110 caused 542 and 481 differentially
418 expressed genes to be up or down-regulated when compared to blank media and 280 were
419 differentially expressed between BL21 and W3110 bacterial incubations. BL21 and W3110
420 affected 214 genes in common when compared to blank media (**Figure 2.2D**). A closer
421 examination of differentially expressed transcriptional levels between the three comparisons
422 illustrate that the majority of differentially expressed fold changes were small magnitude
423 differences that were less than two-fold (**Table 2.1**). With five biological replicates, we were able
424 to determine significant differential gene expression between conditions that displayed these
425 small differences. Additionally, we selected 8 genes for qPCR verification that spanned a wide
426 range of expression, and measured transcriptional levels with qPCR, which showed a high degree
427 of correlation, as expected (**Supplementary Figure 2.1**).

428

DE gene category	BL21	W3110	BL21
	/	/	/
	Media	Media	W3110
Upregulated genes			
1 < FC ^b < 1.5	154	154	66
1.5 < FC < 2	45	28	33
FC > 2	42	21	126
Total no. upregulated	241	203	225
Downregulated genes			
1 < FC < 1.5	262	166	39
1.5 < FC < 2	26	26	14
FC > 2	13	86	2
Total no. downregulated	301	278	55
Total number of DE genes ^a	542	481	280

DE is determined using open-source software DESeq. All genes listed have Benjamini-Hochberg-adjusted $p < 0.05$

^b FC is fold change

429

430 **Table 2.1: Differentially expressed (DE) genes.** DE genes in HCT-8 cells in incubations with BL21,
431 W3110, or media alone.

432

433 2.5.2. BL21 and W3110 activate the cytokine-cytokine receptor pathway.

434 The biological implications of these differentially expressed genes were determined using
435 Signaling Impact Pathway Analysis [43]. SPIA uses over-representation analysis (the prevalence
436 of differential genes compared to all background genes), functional class scoring (the similarity of
437 functions in genes differentially expressed) and pathway topology (*a priori* knowledge of
438 signaling pathways) to identify activated or inhibited pathways (**Supplementary Figure 2.2**).

439 Since epithelial cells are often damaged through extracellular stimuli, they often initiate
440 inflammation through the release of cytokines [72]. The cytokine-cytokine interaction pathway is
441 regulated through the chemokine and $\text{NF}\kappa\beta$ pathways, and as expected, these pathways were
442 activated in both bacterial incubations (**Table 2.2**). The toll-like receptor (TLR) pathway is not
443 listed in **Table 2.2** as the pathway was not activated. It has been shown that TLR receptors in

444 colonic IECs, unlike other types of epithelial cells, develop tolerance after exposure to PAMPs
445 such as LPS and lipoteichoic acid (LTA) [73,74], and only activate the TLR pathway after being
446 primed with interferon-gamma (IFN γ) [75].

447

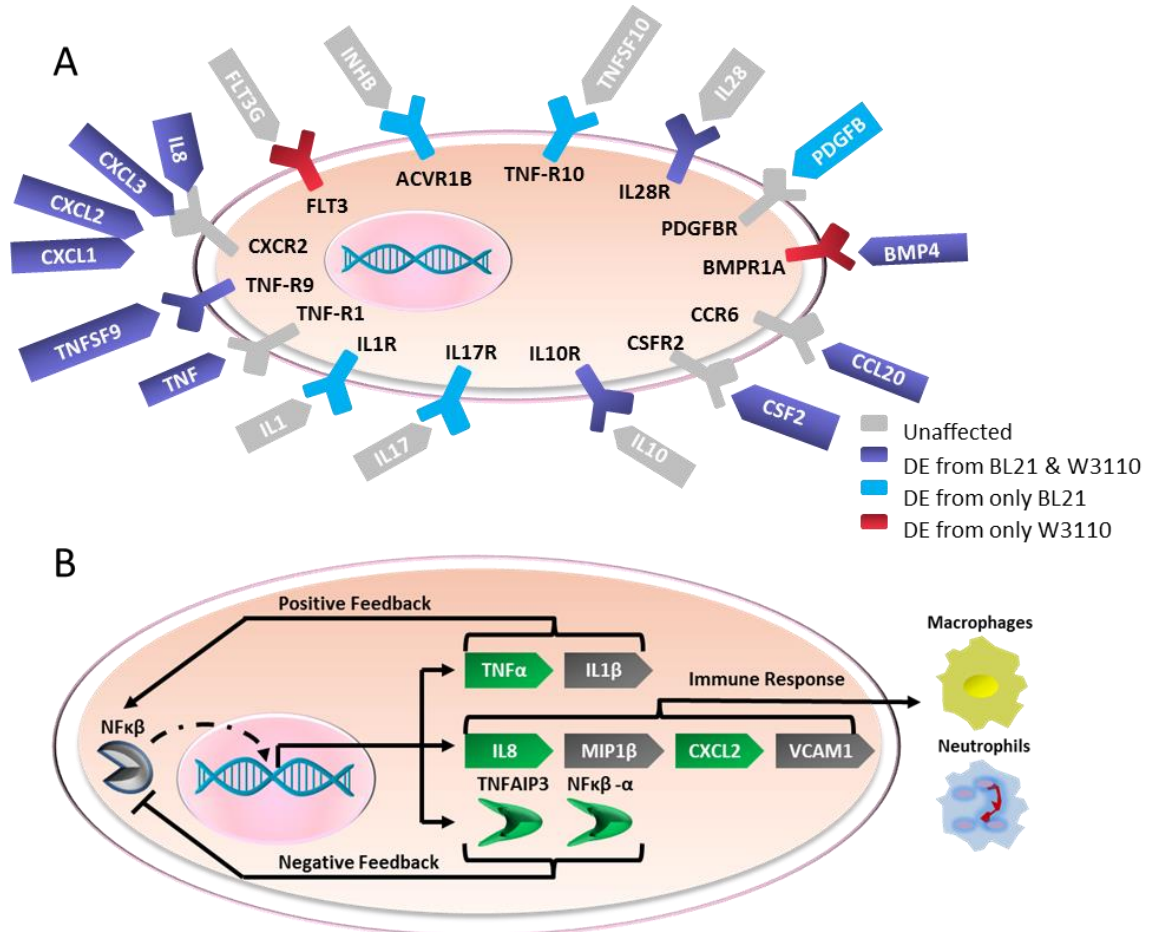
BL21 / Media			W3110 / Media		
KEGG Pathway	p-value ^a	Status	KEGG Pathway	p-value ^a	Status
Cytokine-cytokine receptor interaction	9.27E-06	Activated	Cytokine-cytokine receptor interaction	4.26E-05	Activated
Chemokine signaling pathway	4.06E-04	Activated	Chemokine signaling pathway	1.81E-04	Activated
Osteoclast differentiation	3.58E-03	Activated	NOD-like receptor signaling pathway	1.93E-04	Inhibited
NFκβ signaling pathway	1.10E-02	Activated	HTLV-I infection	2.67E-04	Activated
HTLV-I infection	1.18E-02	Activated	Epstein-Barr virus infection	4.10E-04	Activated
Chagas disease	4.10E-02	Activated	NFκβ signaling pathway	7.94E-04	Activated
NOD-like receptor signaling pathway	5.48E-02	Inhibited	Osteoclast differentiation	5.47E-02	Activated

^a pGFWER is Bonferroni adjusted global p-values

449 **Table 2.2 SPIA significance.** DE genes were inputted into SPIA (Signaling Pathway Impact
450 Analysis) software to determine activated or inactivated pathways. Incubations of BL21
451 compared to media alone resulted in the modulation of seven annotated KEGG pathways, and
452 incubations of W3110 compared to media alone also resulted in the modulation of seven
453 annotated KEGG pathways. Common to both sets were the activation of the cytokine-cytokine
454 receptor interaction, chemokine signaling pathway, osteoclast differentiation, NFκβ signaling
455 pathway, human T-lymphotropic virus-1 (HTLV-I) infection, and the inactivation of the NOD-like
456 receptor signaling pathway.

457 A closer investigation of the cytokine network found that 10 cytokines were significantly
458 differentially expressed in one sample or the other (**Figure 2.3A**). All of these cytokines were
459 upregulated, except BMP4, which is responsible for the regeneration of epithelial cells. The
460 upregulation of granulocyte macrophage colony-stimulating factor (CSF2) stimulates stem cells to
461 produce granulocytes (neutrophils, eosinophils, and basophils) and monocytes. The CXC
462 cytokines that were upregulated, (CXCL1, CXCL2, CXCL3, IL8) are chemotactic for
463 neutrophils, and all of the CXC chemokines upregulated act as agonists for the same receptor.
464 TNF, TNFSF9, and TNFRSF9 were upregulated and act as pro-apoptotic signals or receptors, as
465 well as promoting leukocyte chemotaxis through the induction of proinflammatory cytokines
466 [76]. CCL20, a CC motif cytokine, is weakly chemotactic for neutrophils, and strongly attractive
467 for lymphocytes. Taken together, the cytokines act collectively to induce activation and long-term

468 survival of neutrophils. This upregulation indicates that bacterial secretions have caused the IEC
 469 to signal the adaptive immune response due to the secretome of these nonpathogenic bacteria.



470
 471

472 **Figure 2.3: Signaling pathway analysis. A)** Activation of cytokine-cytokine receptor interaction
 473 pathway in incubations with BL21 or W3110. Schematic shows cytokines (ovals) and cytokine
 474 receptors (rectangles) upregulated only by incubation with BL21 (blue), only by incubation with
 475 W3110 (red). Incubations with either *E. coli* strain (purple), or with no change in regulation by
 476 either *E. coli* strain is also shown (grey). **B)** Schematic of genes involved in canonical NFκβ
 477 pathway, adapted from KEGG. Gene expression levels upregulated (green) and unaffected (grey)
 478 by incubations with both BL21 and W3110 compared to media alone are shown.

479 **2.5.3 BL21 and W3110 activate the NFκβ pathway and its negative feedback components.**

480 The NFκβ pathway is an integral part of the immune response, and functions as a protein
 481 complex that controls DNA transcription. To prevent uncontrolled inflammation, it is thought that

482 the negative feedback mechanisms associated with PAMP receptor activation are upregulated to
483 suppress the over-production of inflammatory cytokines [77]. Consistent with this hypothesis, the
484 canonical $\text{NF}\kappa\beta$ pathway was activated in both bacterial incubations, and the negative feedback
485 components (i.e. $\text{NF}\kappa\beta$ - α inhibitor) were upregulated as well (**Figure 2.3B**).

486 The function of the $\text{NF}\kappa\beta$ pathway is controlled by the $\text{NF}\kappa\beta$ kinase (IKK) complex,
487 which consists of NEMO, IKK- α and IKK- β . The IKK complex phosphorylates the $\text{NF}\kappa\beta$ - α
488 inhibitor, which causes its proteosomal degradation. The degradation of the $\text{NF}\kappa\beta$ - α inhibitor
489 leads to the free movement of $\text{NF}\kappa\beta$ into the nucleus and subsequent initiation of gene
490 transcription. In both BL21 and W3110 incubations, the end products of the canonical $\text{NF}\kappa\beta$
491 pathway were upregulated (inflammatory cytokines IL8, TNF α , and CXCL2) while the end
492 products of the atypical $\text{NF}\kappa\beta$ pathway (e.g. apoptosis regulator Bcl-XL) were unchanged. This
493 indicates that the bacterial secretomes stimulated the HCT-8 immune response through the
494 canonical $\text{NF}\kappa\beta$ pathway, and possible microenvironmental conditions such as hypoxia, which
495 activate the atypical $\text{NF}\kappa\beta$ pathway[78], did not elicit an immune response.

496 Critically, $\text{NF}\kappa\beta$ - α inhibitor, which is integral to the negative feedback in the $\text{NF}\kappa\beta$
497 pathway, was upregulated in both BL21 and W3110 incubations. Additionally, the NOD-like
498 receptor pathway was inhibited in both pathways, with its negative feedback response regulator,
499 TNFAIP3, also upregulated in both bacterial samples. NOD-like receptors (NLRs) act as
500 cytosolic sensors, and once activated, subsequently activate a receptor-interacting protein (RIP).
501 TNFAIP3 acts as the negative regulator of RIP, thereby quenching the signaling cascade despite
502 the continued presence of agonists of NLRs [79]. TNFAIP3 has also been shown to be a critical
503 negative feedback regulator to the $\text{NF}\kappa\beta$ pathway [80]. The activation of the $\text{NF}\kappa\beta$ pathway and
504 the negative feedback regulators $\text{NF}\kappa\beta$ - α inhibitor and TNFAIP3 suggest that components of the
505 bacterial secretions act as a stimulus to the immune system, and that the epithelial cells have

506 coincidentally upregulated the negative feedback components to prevent uncontrolled inflammation
507 from this nonpathogenic encounter.

508 **2.5.4 Upregulation of gene expression by bacterial secretomes do not translate to increased** 509 **cytokine protein expression.**

510 Using a 12 cytokine multi-analyte ELISA kit, we surveyed two of the upregulated
511 cytokines from incubations with BL21 and W3110 (TNF and IL8) as well as 10 other cytokines
512 involved in inflammation. We found that while inflammatory cytokine gene expression was
513 upregulated at the transcriptional level, there was no concomitant increase in secretion
514 **(Supplementary Figure 2.3)**. This finding is supported by Kamada et al. (2000), who similarly
515 used a transwell model and found that IL-8 secretion was unchanged in IEC HCT15 when
516 incubated with *E. coli* K-12 strain DH10 β for 4 hours [63]. These results indicate that the
517 transcriptomic upregulation is quenched either post-translationally or through the upregulation of
518 negative feedback mechanisms such as NF κ β and NOD-like signaling pathways.

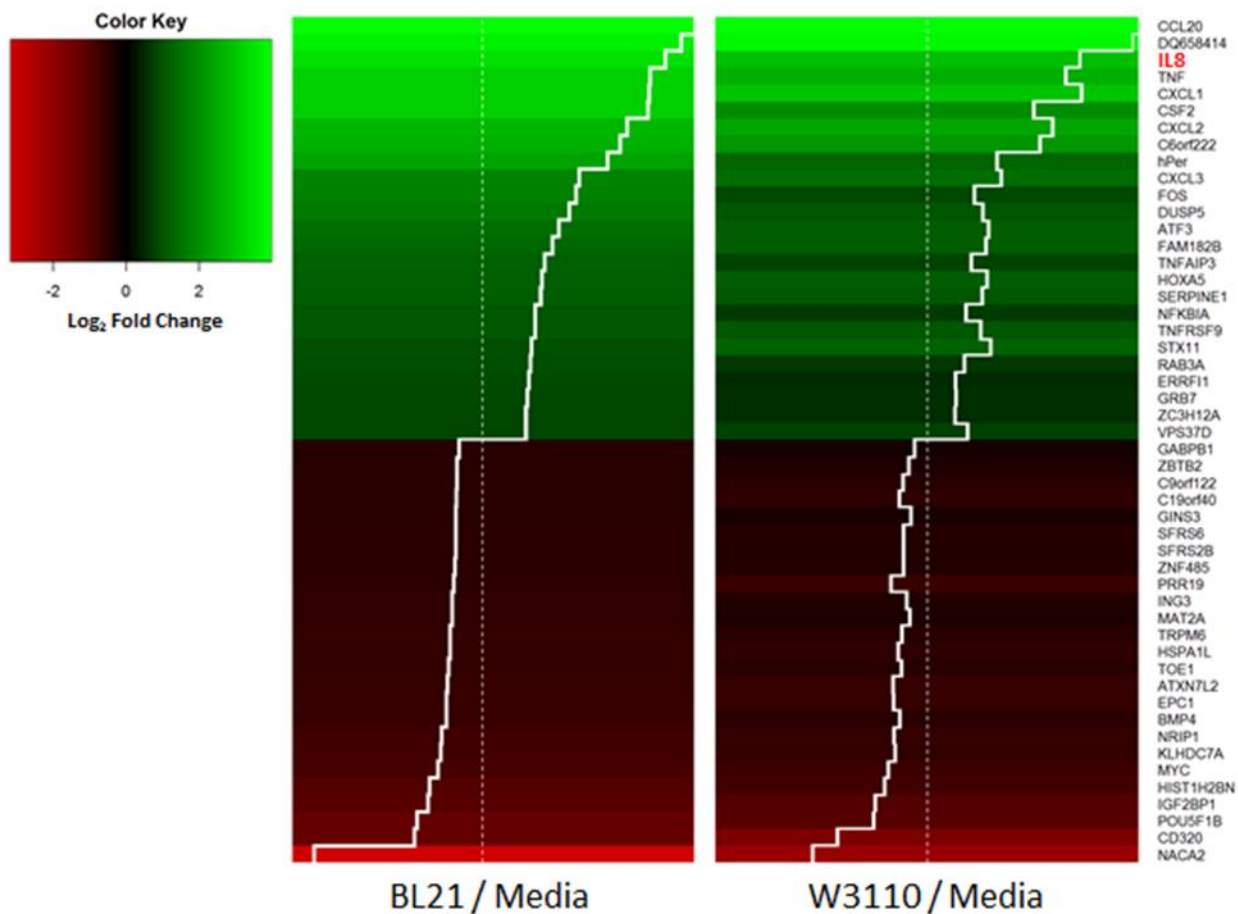
519 **2.5.5 BL21 and W3110 cause differential expression in genes responsible for tissue** 520 **structure.**

521 Since the bacterial secretome includes components such as LPS, an activator of
522 osteoclastogenesis to enhance bone resorption in both *in vitro* and *in vivo* studies [81,82],
523 differential expression of genes responsible for tissue structure was expected. Both BL21 and
524 W3110 resulted in the activation of the osteoclast differentiation signaling pathway. CTSK, an
525 end-product of this pathway, was upregulated in incubations with both BL21 and W3110 and
526 encodes for the protein cathepsin K, a protease that breaks down elastin, gelatin and collagen,
527 which are critical components of bone and cartilage. Furthermore, in the cytokine-cytokine
528 receptor pathway, the downregulation of BMP4 induces the increased epithelial stem cell
529 renewal. Collectively, these transcriptional differences indicate that the epithelial cells have been

530 insulted by the bacterial secretomes, causing the upregulation of genes responsible for cell
531 renewal.

532 **2.5.6 Strain-specific differentially expressed genes**

533 BL21 and W3110 are derivatives of the B and K-12 strains of *E. coli*, respectively, and
534 comprise the majority of all laboratory strains. Despite the similarity of their genomes, B strains
535 and K-12 strains show marked phenotypic differences. B strains grow faster in minimal media,
536 and have lower acetate production [66,67]. Furthermore, while B cells produce lower amounts of
537 intracellular proteases (e.g. Lon, ClpA, ClpP), they secrete higher total levels of extracellular
538 proteins, mainly through its Type II secretion pathway. K-12 strains have higher gene expression
539 levels of heat shock proteins, flagella that provide motility, and they more ably survive stress
540 insults (e.g. osmolarity, pH) than W3110 [66]. A closer investigation into the differential
541 regulation caused by each strain illustrates that both affect the directionality (i.e. upregulated or
542 downregulated) of differential expression in a similar manner. Of the 214 differentially expressed
543 genes that BL21 and W3110 share in comparison to blank media, 100% of them were regulated
544 in the same manner (i.e. upregulated or downregulated). **Figure 2.4** shows a heatmap of the two
545 strains organized by the 25 most up and downregulated genes in the BL21 coinubation. The
546 similarity in gene expression to incubations with W3110 was striking, with many cytokines as the
547 most upregulated genes.

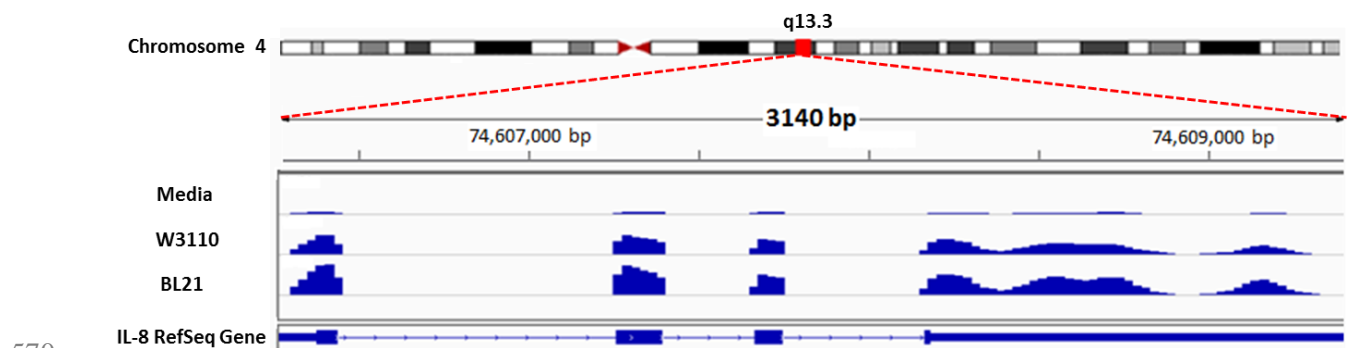


548

549 **Figure 2.4: Heatmap.** 25 most upregulated (green) and downregulated genes (red) in HCT-8 in
 550 incubations with BL21 compared to media alone and in incubations of W3110 compared to
 551 blank media. Trace line (white) indicates direction and extent of differential expression.
 552 Differential expression levels are similar between incubations of BL21 and W3110, and 100% of
 553 differential expression is regulated in the same manner (i.e. up or downregulated). DESeq was
 554 used to identify differential expression, and all genes listed have Benjamini-Hochberg-adjusted p
 555 < 0.05 . Cytokines, including IL8 (red text), were among the genes most upregulated.

556 While both strains showed similarity in fold change expression levels and directionality
 557 of regulation, we found the amplitude of the up and/or downregulation was higher in BL21
 558 incubations. This trend was also subtly revealed by more carefully considering the results from
 559 **Figure 2.1C**. Of the 214 genes that were commonly differentially expressed in both strains
 560 compared to blank media (**Figure 2.1C**), 96 were upregulated, and 76 of these (79.1%) were
 561 more upregulated in the BL21 sample. Of the 118 genes downregulated in common, 75 of these
 562 (63.5%) were more downregulated in the BL21 sample. Then, there were 280 genes differentially

563 expressed when comparing BL21 directly to W3110 (**Figure 2.1C**), and of these genes, 225
 564 (80.3%) were differentially expressed at a greater amplitude in incubations with BL21. Of
 565 particular importance is IL-8, a proinflammatory cytokine, as it shows greater abundance in
 566 incubations with BL21 as opposed to W3110 (**Figure 2.5**). These expression level differences
 567 indicate that secretions from BL21 induce a greater epithelial cell response than W3110.
 568 Importantly, cell densities of inocula were identical as were the final optical densities (data not
 569 shown).



570
 571 **Figure 2.5: NGS sequenced reads mapped to annotated IL-8 gene as visualized in IGV.** The IL-8
 572 gene is shown at the bottom with four exons separated by three introns. Each read is
 573 represented by a blue square, and the abundance of reads at each condition (BL21, W3110 or
 574 media alone) is shown. HCT-8 incubations with W3110 show greater abundance of IL-8
 575 transcription compared to media alone, while incubations with BL21 illustrate higher levels than
 576 W3110. One representative replicate sample of each condition is shown.

577 We then sought to investigate the cause of the greater perturbation caused by BL21
 578 compared to W3110. Because of the use of the transwell, the phenotypic differences that would
 579 require direct interaction can be ignored, and we can focus on secretable substances. One possible
 580 candidate, LPS, is more highly expressed in BL21 than W3110 [66], and it is well known that
 581 LPS induces inflammatory effects on cytokines [83,84] and through it, the activation of the $\text{NF}\kappa\beta$
 582 in colonic IECs [85]. However, in colonic epithelial cells, the addition of cytokine $\text{IFN}\gamma$ to the
 583 IEC is needed to express myeloid differentiation protein-2 (MD-2), which is required for LPS
 584 responsiveness [75,83]. Furthermore, priming of $\text{IFN}\gamma$ with subsequent LPS exposure shows a
 585 transient upregulation of IL-8 that returns to baseline levels after 6 hours, which is the time period

586 used in this study. On the other hand, BL21 produced much more extracellular AI-2 than W3110
587 (~ 35 μ M compared to 8 μ M, **Supplementary Figure 2.4**), and BL21 cells do not express the
588 ABC transporter for uptake of quorum sensing signal molecule, autoinducer-2 (AI-2) or the
589 intracellular kinase that sequesters AI-2 inside the cell [86]. BL21 showed much higher The
590 effect of autoinducer-2 on colonic cells is of particular interest not only because the highest
591 numbers of bacterial concentrations in the gut are found therein, but Eubacteria are almost
592 entirely concentrated in this area of the GI tract [53]. Furthermore, the LuxS/AI-2 production
593 system is highly conserved among the Eubacteria [9,87,88]; therefore we chose to investigate the
594 effect of autoinducer-2 on IECs. While we have shown that the robust transcriptional response of
595 epithelial cells to BL21 and W3110 is similar, the slightly greater amplitude shift in BL21 may be
596 caused by the much higher levels of AI-2 in BL21. We then sought to tease out this smaller effect
597 from the overall systematic response elicited from the secretome.

598 **2.5.7 AI-2 initiates upregulation of inflammatory cytokines before downregulation.**

599 Bacteria secrete and detect small molecules or autoinducers to coordinate gene
600 expression in a cell density-dependent manner (known as quorum sensing, QS). These QS
601 molecules are produced throughout the Eubacterial hierarchy and influence characteristics such as
602 swarming motility, biofilm formation, virulence, among others (reviewed by [1-4]). The terminal
603 synthase for one prevalent autoinducer, AI-2, has been found in over 80 species [9,87].

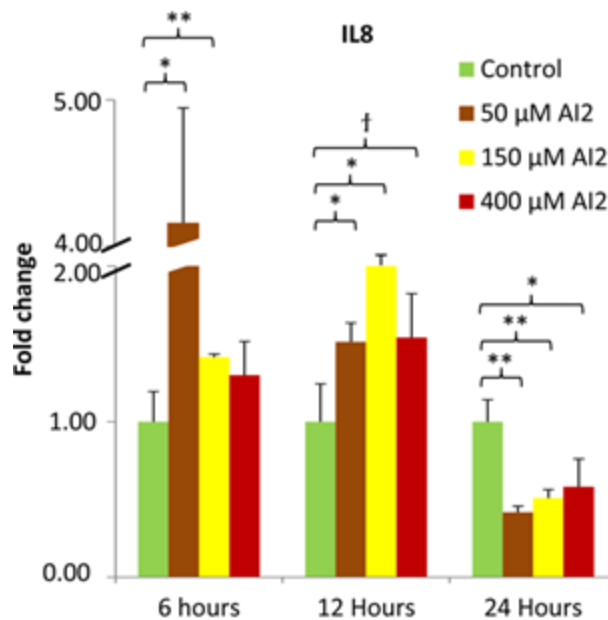
604 Studies have shown both beneficial and deleterious effects of QS molecules on human
605 epithelial cells. N-3-(oxododecanoyl)-L-homoserine lactone (OdDHL) produced by *Pseudomonas*
606 *aeruginosa* induces apoptosis in many mammalian cell types[89-91], while indole has been
607 found to decrease inflammation in IECs by attenuating IL-8 production, reducing TNF α mediated
608 NF κ B activation, and tightening cell junctions [49]. Investigations into interkingdom effects of
609 AI-2 on human cells have been limited to one study where Bryan et al. (2010) performed

610 microarray studies of alveolar cells exposed to AI-2 at 50 μ M, and found only 4 genes with over
611 2 fold changes in expression [22].

612 We chose to investigate the effect of AI-2 directly on IECs, and have performed a time
613 course analysis using a range of AI-2 concentrations: 50, 150 and 400 μ M. It must be noted that
614 the levels of AI-2, or any other quorum sensing metabolite, is unknown in the GI tract. However,
615 indole has been found in human feces at concentrations ranging from ~ 50-1100 μ M [92,93], and
616 interkingdom studies have used a range of concentrations from 0.4 to 250 μ M for the AI-1
617 molecule OdDHL[22,90,91]. In our study, 50 μ M of AI-2 was chosen as it is the concentration of
618 the only previous interkingdom study [22], and is a level approximating our coincubation studies
619 with BL21, which exposed the HCT-8 cells to much higher levels of AI-2 than W3110
620 **(Supplementary Figure 2.4)**. 150 μ M represents the upper limit reached by standard LB cultures
621 of *E. coli* BL21 [94]. Finally, since it has been shown higher concentrations of Eubacteria can
622 populate the colon than can be reached *in vitro* [53] and that QS molecules can reach much higher
623 in biofilms (~600 μ M) [95], we also selected 400 μ M of AI-2 as a possible representation of high
624 local QS molecule concentrations.

625 Thus, we exposed HCT-8 cells to 50, 150 and 400 μ M AI-2 for 6, 12 and 24 hours. We
626 performed AI-2 assays on samples after 24 hours and found that significant quantities of AI-2
627 were still present [data not shown]. After harvesting the RNA, we found that, IL-8, a
628 proinflammatory cytokine that is chemotactic to neutrophils, was moderately upregulated with the
629 average fold change for all three concentrations totaling 2.29 and 1.69 at 6 and 12 hour time
630 points, respectively, before being downregulated (-1.98) compared to blank media for all three
631 concentrations ranges at 24 hours **(Figure 2.6)**. This trend was consistent with the secretomes and
632 was found at all 3 concentrations. Interestingly, the same trend but at lower amplitude was found
633 for TNF and CSF2 at some concentrations **(Supplementary Figure 2.5)**. It is hypothesized that
634 the interplay between host and the microbiota is tightly regulated, and that microbial metabolites

635 induce changes in the host signaling pathways, which are restored through negative feedback
 636 loops[68]. The initial upregulation of IL-8 expression levels with exposure of BL21 and W3110
 637 to the HCT-8 cells, followed by abatement to lower levels is consistent with this hypothesis.



638

639 **Figure 2.6 qPCR of IL-8.** HCT-8 cells are incubated with AI-2 at 50, 150 and 400μM for 6, 12, and
 640 24 hours, normalized to media alone. At early times (6 and 12 hours), incubations with AI-2
 641 result in upregulation of IL-8 gene expression levels compared to media alone, while at 24
 642 hours, IL-8 expression levels are downregulated compared to media alone. qPCR fold level
 643 changes are shown.

644 † p < 0.10, * p < 0.05, ** p < 0.01

645 2.6 Discussion

646 Investigations into interkingdom communication in the GI tract can aid in treatment for
 647 diseases such as inflammatory bowel disease, which arises from the immune system causing
 648 inflammation from commensal bacteria, and colorectal cancer, which is believed to be promoted
 649 through chronic inflammation. In this study, we have shown for the first time that bacterial
 650 secretions from non-pathogenic *E. coli* upregulated a number of proinflammatory pathways in
 651 IECs leading to the transcription of cytokines involved in recruiting leukocytes, particularly
 652 neutrophils. The activation of biological defense-related pathways from secretions of two

653 different strains of *E. coli*, BL21 and W3110, illustrate that direct contact from flagella,
654 membrane bound proteins or secretion systems are not necessary to induce an immunological
655 response from IECs. That is, we have shown that *E. coli* secretions cause the upregulation of pro-
656 inflammatory cytokines through the activation of the mediation pathway, $\text{NF}\kappa\beta$, indicating that
657 the immune response was elicited through bacterial secretions.

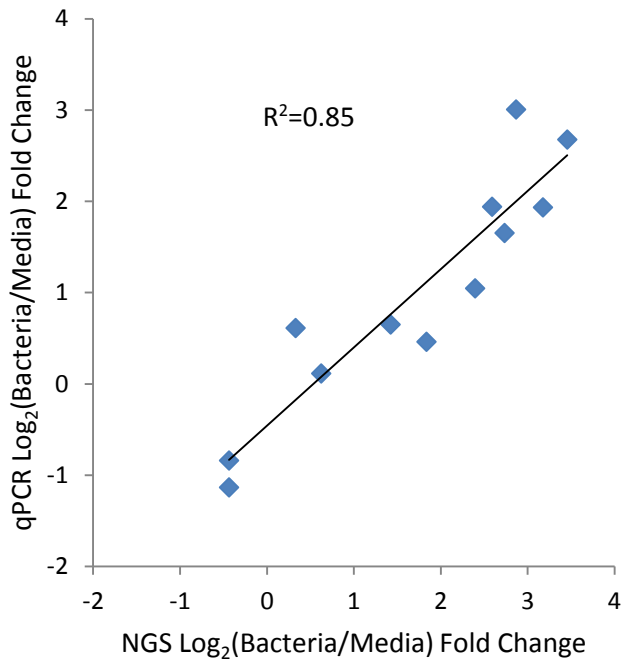
658 Our results also show that the negative feedback components of the $\text{NF}\kappa\beta$ pathways
659 ($\text{NF}\kappa\beta$ - α inhibitor) and NOD-like receptor pathways (TNFAIP3) were upregulated in the HCT-8
660 cells, indicating a negative feedback loop to control the upregulation of cytokine gene expression
661 from nonpathogenic *E. coli*. $\text{NF}\kappa\beta$ - α inhibitor acts to block the canonical and atypical $\text{NF}\kappa\beta$
662 pathways, and its upregulation directly inhibits the transcription of cytokines. TNFAIP3 is a
663 negative regulator of the NOD-like receptor pathway, the intracellular sensing mechanism
664 corollary to the extracellular TLR sensing mechanism. The inhibition of the NOD-like pathway
665 suggests a response to block the signaling cascade of bacterial products that were transported into
666 the mammalian environment. The upregulation of these negative feedback components may
667 suggest the IEC is preventing the physiological response from developing into a pathological
668 response.

669 While both bacteria elicited similar responses, BL21 appeared to cause greater
670 perturbations in HCT-8 cells. As noted above, phenotypic differences between BL21 and W3110
671 include flagella, LPS, heat-shock proteins, metabolic byproduct secretions, and AI-2 production.
672 Our investigations into the interkingdom effects of AI-2 revealed a moderate, but significant
673 upregulation in IL-8 at both 6 and 12 hours, followed by a significant downregulation found at 24
674 hours. Like the results from the full secretome, this may indicate that AI-2 as a single signal
675 molecule has an inflammatory effect, but after some period of modulation, the IEC inflammation
676 is controlled through negative feedback to prevent a pathological response to a non-pathogenic
677 stimulus.

678 In conclusion, while it may be expected that bacterial secretomes would affect IECs and
679 immune function in the gut, our study has demonstrated that a bacterial-bacterial signaling
680 molecule also influence the same. That is, IEC evidently “listen in” on the communication
681 between bacteria that reside in the lumen and alter their behavior based on these signaling
682 phenomena. Further exploration of the effects of bacterial soluble factors on IECs will aid in the
683 understanding of microbial disease, and modulation of existing interkingdom signaling networks
684 could result in novel methods to combat infections.
685

686

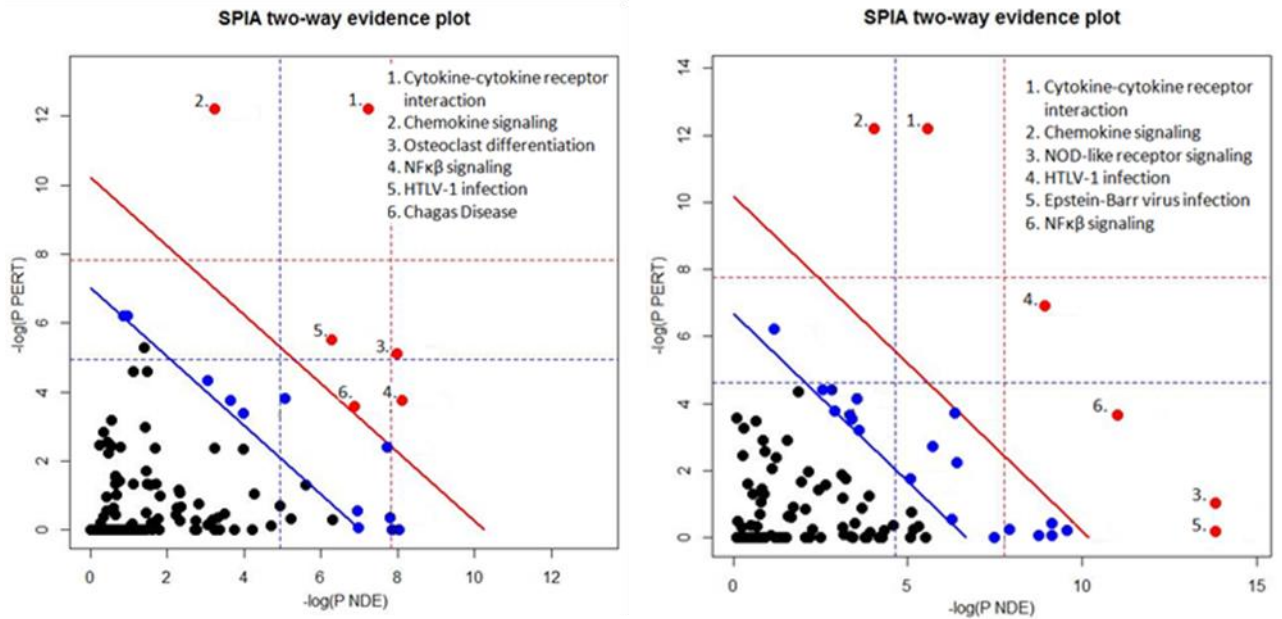
2.7 Supplemental Materials



687

688 **Figure S2.1: qPCR validation of RNA-Seq.** Results shows high correlation for range of expression
689 levels.

690



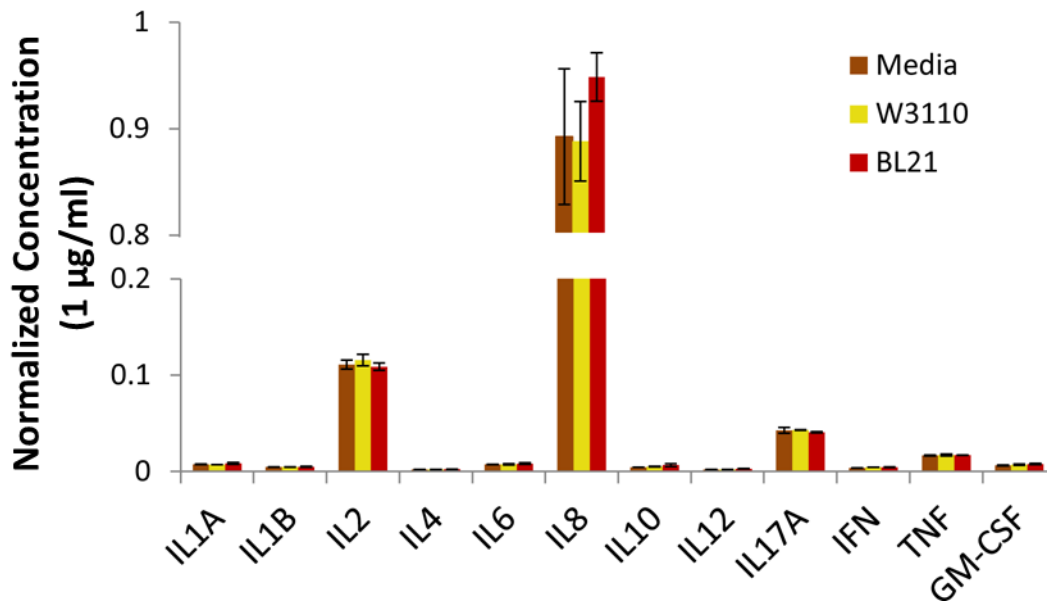
692

693 **Figure S2.2: Signaling pathway analysis graphs.** Significantly differentially expressed genes and
 694 expression levels from DESeq are inputted into SPIA (Signaling Pathway Impact Analysis) to
 695 determine activation and inhibition of entire biological pathways. All values to the right of the
 696 blue oblique line are significant after a False Discovery Rate adjustment of the global p-values.
 697 All values to the right of the red oblique line are significant after Bonferroni correction of the
 698 global p-values. a) HCT-8 cells incubated with BL21 compared to media significantly altered six
 699 biological pathways b) HCT-8 cells incubated with W3110 compared to media alone significantly
 700 altered six biological pathways. Common among both comparisons were the activation of the
 701 cytokine-cytokine receptor interaction, chemokine signaling pathway, osteoclast differentiation,
 702 NFκβ signaling pathway, human T-lymphotropic virus-1 (HTLV-I) infection, and the inactivation
 703 of the NOD-like receptor signaling pathway.

704 * pPERT probability of finding a greater total accumulation perturbation than compared to the
 705 preturbation accumulation in the pathway by chance

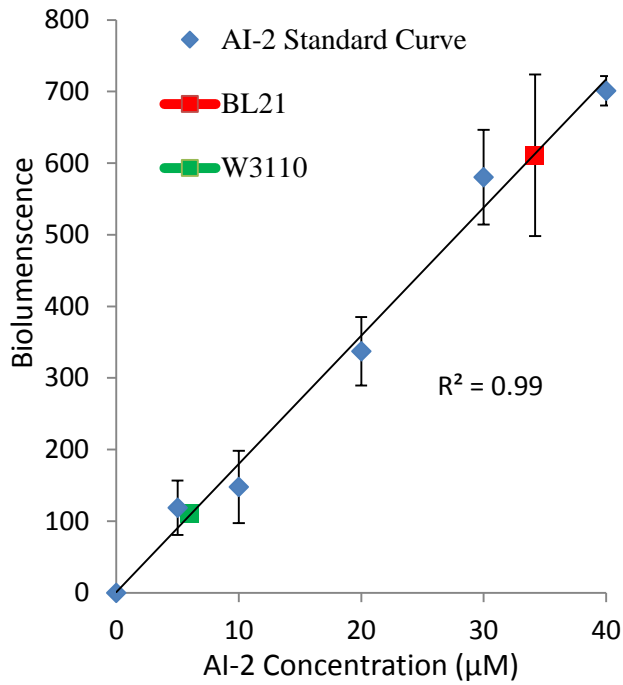
706 ** pNDE probability of finding at least x number of DE genes on the pathway using a
 707 hypergeometric model

708



709

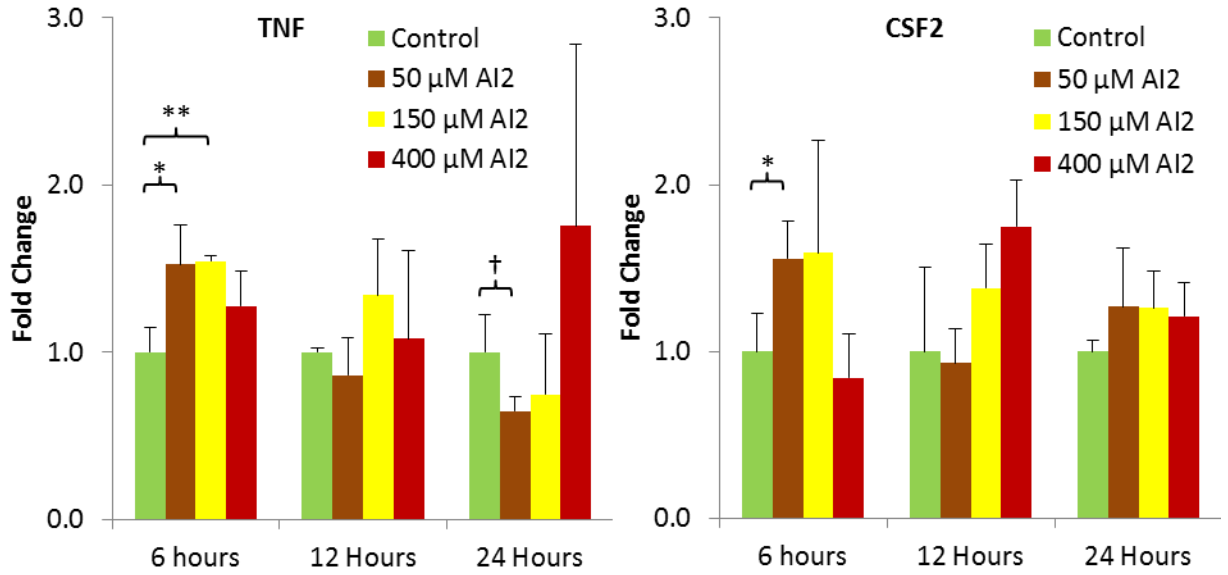
710 **Figure S2.3: Multi-analyte ELISA.** ELISAs were performed on cell culture supernatants of HCT-8
 711 cells in transwell cocultures with BL21, W3110, and media alone. Values are normalized to
 712 positive control (1µg/mL). ELISA data show no translational modulation in inflammatory
 713 cytokines with incubations of either W3110 or BL21 compared to media alone.



714

715 **Figure S2.4: AI-2 standard curve.** AI-2 concentration levels in HCT-8 supernatant from
 716 incubations with BL21 and W3110, respectively. An AI-2 standard curve was created from AI-2
 717 activity assays (see methods) with known AI-2 concentrations, and a best fit linear regression is
 718 shown ($R^2 = 0.99$). AI-2 concentration levels in the supernatant of the lower transwell (HCT-8
 719 supernatant) are shown in incubations with BL21 (red) and W3110 (green).

720



721

722 **Figure S2.5: qPCR of TNF and CSF2.** HCT-8 cells are incubated with AI-2 at 50, 150 and 400μM
 723 for 6, 12, and 24 hours. qPCR fold level changes are shown for colony stimulating factor-2 (CSF2)
 724 and tumor necrosis factor (TNF) and normalized to blank media (0 μM AI-2).
 725 † p < 0.10, * p < 0.05, ** p < 0.01

726

727

Gene	Primers
CXCL2	Upstream primer: TCCAAAGTGTGAAGGTGAAGTCCC Downstream primer: GGTTGAGACAAGCTTTCTGCCCAT
CXCL3	Upstream primer: CTGCAGGGAATTCACCTCAAGAAC Downstream primer: AGTGTGGCTATGACTTCGGTTTGC
PDGFB	Upstream primer: GGTGGGTTAGAGATGGAGTTTG Downstream primer: GAACCAGAGGAAGAGGTGAATC
IL8	Upstream primer: TCCTGATTTCTGCAGCTCTGTGTG Downstream primer: AATTTCTGTGTTGGCGCAGTGTGG
TNF	Upstream primer: AGCCCATGTTGTAGCAAACC Downstream primer: TGAGGTACAGGCCCTCTGAT
NFKB1	Upstream primer: GTGACAGGAGACGTGAAGATG Downstream primer: TGAAGGTGGATGATTGCTAAGT
B2M	Upstream primer: TGTGTCTGGGTTTCATCCATCCGA Downstream primer: TCACACGGCAGGCATACTCATCTT
CSF2	Upstream primer: AAATGTTTGACCTCCAGGAGCCGA Downstream primer: GGTGATAATGTGGGTTGCACAGGA

729 **Table S2.1 Primers used for SYBR green qPCR**

730

731

732 **Chapter 3: Rational design of ‘controller cells’ to manipulate protein**
733 **and phenotype expression**

734 This chapter was primarily reproduced directly or adapted from Zargar, Amin et al. " Rational
735 design of ‘controller cells’ to manipulate protein and phenotype expression " *Metabolic*
736 *Engineering* [96]

737 **3.1 Abstract**

738 Coordination between cell populations via prevailing metabolic cues has been noted as a
739 promising approach to connect synthetic devices and drive phenotypic or product outcomes.
740 However, there has been little progress in developing ‘controller cells’ to modulate metabolic
741 cues and guide these systems. In this work, we developed ‘controller cells’ that manipulate the
742 molecular connection between cells by modulating the bacterial signal molecule, autoinducer-2,
743 that is secreted as a quorum sensing (QS) signal by many bacterial species. Specifically, we have
744 engineered *E. coli* to overexpress components responsible for autoinducer uptake (*lsrACDB*),
745 phosphorylation (*lsrK*), and degradation (*lsrFG*), thereby attenuating cell-cell communication
746 among populations. Further, we developed a simple mathematical model that recapitulates
747 experimental data and characterizes the dynamic balance among the various uptake mechanisms.
748 This study revealed two controller “knobs” that serve to increase AI-2 uptake: overexpression of
749 the AI-2 transporter, LsrACDB, which controls removal of extracellular AI-2, and overexpression
750 of the AI-2 kinase, LsrK, which increases the net uptake rate by limiting secretion of AI-2 back
751 into the extracellular environment. We find that the overexpression of *lsrACDBFG* results in an
752 extraordinarily high AI-2 uptake rate that is capable of completely silencing QS-mediated gene
753 expression among wild-type cells. We demonstrate utility by modulating naturally occurring
754 processes of chemotaxis and biofilm formation. We envision that ‘controller cells’ that modulate
755 bacterial behavior by manipulating molecular communication, will find use in a variety of
756 applications, particularly those employing natural or synthetic bacterial consortia.

757 **3.2 Highlights**

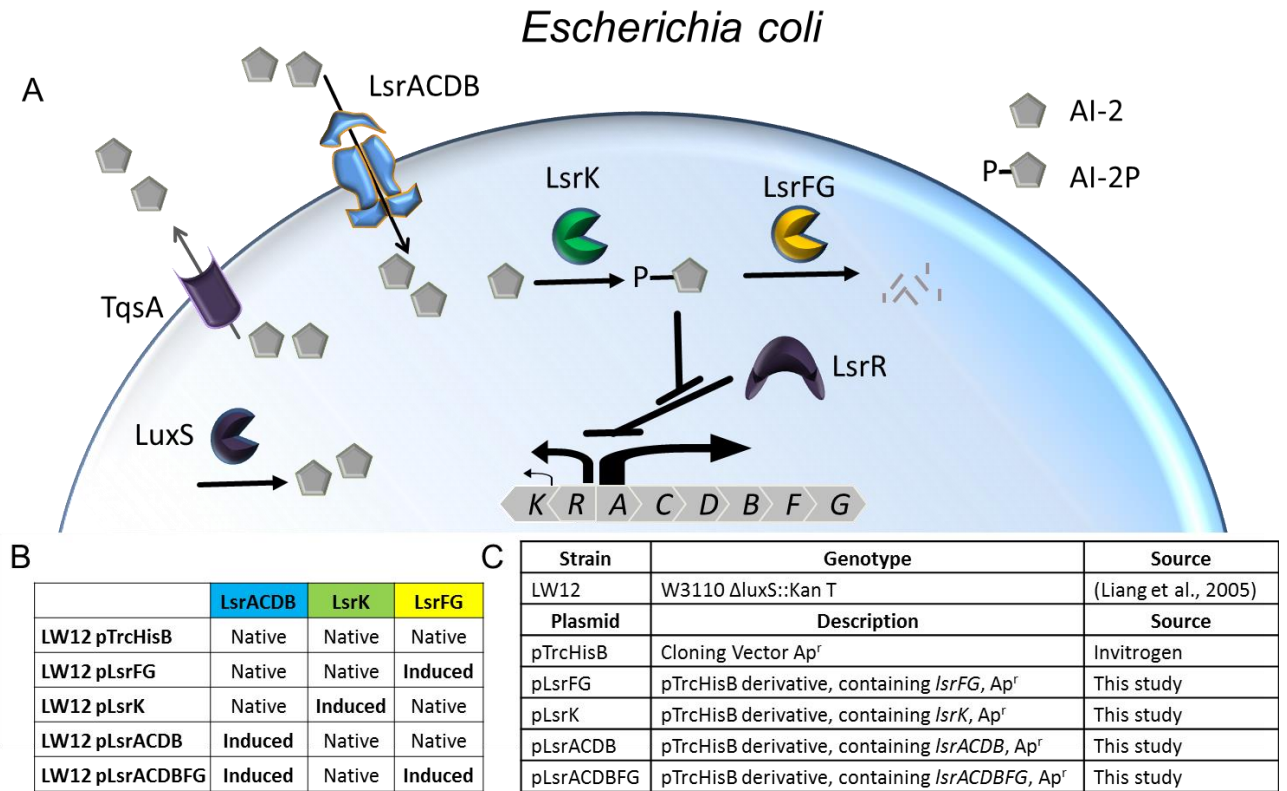
- 758 • ‘Modular’ quorum sensing systems manipulate the extracellular AI-2 environment
- 759 • Mathematical model characterizes mechanics of AI-2 signal transduction
- 760 • ‘Controller cells’ can modulate protein expression in synthetic QS-dependent systems
- 761 • Natural bacterial processes (chemotaxis and biofilm production) can be altered

762 **3.3 Introduction**

763 Metabolic engineering exploits the genetic modification of cellular pathways to improve
764 production of metabolites and proteins [97,98]. Many noteworthy examples have been
765 demonstrated wherein these cells serve as ‘factories’ for the environmentally sustainable
766 production of energy, materials, and chemicals [99]. Towards this aim, metabolic engineering has
767 incorporated finely tuned synthetic controllers and cells in the creation of artificial networks
768 [100-104]. The general structure of these synthetic networks is based on control devices that
769 respond to specific stimuli in a predictable fashion [105,106]. However, the task of coordinating
770 among and between cell populations remains a critical challenge that can limit the production of
771 desired end-products [13,107]. A further challenge is controlling the partitioning of resources that
772 (i) maintain native metabolism and (ii) adequately support product synthesis [108,109]. One
773 creative approach to address both of these challenges is through the leveraging of cell-cell
774 communication networks, and these have been the target of a variety of dynamic control systems
775 [110-112]. Using the native bacterial signaling network known as quorum sensing [113,114], we
776 have previously shown the ability to reduce the metabolic burden [115,116] and “program” cell
777 populations through the metabolic cue, autoinducer-2 [14,117]. However, while there has been
778 much development in multicellular systems that respond to metabolic cues [118-121], control of
779 the intensity of these metabolic cues to fulfill the potential of spatiotemporal control has not been
780 realized.

781 In this work, we have developed bacterial AI-2 consumers, ‘controller cells’, which can be
782 deployed to control AI-2 in a predictable fashion using the now well-characterized quorum
783 sensing mechanisms of *E. coli* (**Scheme 1A**). AI-2 is synthesized and recognized by a wide
784 variety of bacteria [9,87]; correspondingly its use as a potential target for modulating QS
785 activities among different cell types is of interest. The use of genetically engineered bacteria to
786 ‘quench’ extracellular AI-2 was first described by Xavier et al. [35], where genetic deletions of its
787 synthase (*luxS*) and its repressor (*lsrR*) were used to interfere with bacterial communication.
788 However, the interrelated complexity of QS networks renders the elucidation of its mechanisms
789 difficult, and the production of simple, “modular” networks would enrich the understanding of
790 these actions [122]. We have addressed this through the model-based design, construction, and
791 characterization of these ‘controller cells’ to modulate the external AI-2 environment. These cells
792 are designed via the compartmentalization of different aspects of AI-2 processing: uptake
793 (*lsrACDB*), phosphorylation (*lsrK*), and degradation (*lsrFG*) (**Scheme 1B-1C**).

794



795

796 **Scheme 3: *E. coli lsr*-system:** Panel (A) depicts the AI-2 quorum sensing network. LuxS
 797 generates AI-2 from metabolic precursors, which is then exported out of the cell by TqsA. AI-2 is
 798 primarily taken up through the ABC-type transporter Lsr, and then phosphorylated by LsrK to AI-
 799 2P. AI-2P depresses the response regulator LsrR, thereby activating transcription of the *lsr*
 800 operon. AI-2P is degraded by LsrF and LsrG. Panel (B) depicts the ‘controller cells’ that are
 801 engineered through the overexpression of distinct components of the *lsr* system. “Native”
 802 indicates native production, while ‘Induced’ indicates over-expression. Panel (C) illustrates the
 803 strains, plasmids, descriptions and sources used for these ‘controller cells’.

804 These ‘controller cells’ provide the ability to regulate extracellular AI-2 and modulate
 805 synthetic circuits. Further, we show that the ability to quench extracellular AI-2 through
 806 ‘controller cells’ can attenuate the native cell-cell behaviors of chemotaxis and biofilm formation.
 807 By teasing apart the regulatory network for AI-2, we have enhanced our understanding of the
 808 collective population-scale response to AI-2. In this way, systems can be designed wherein we
 809 decouple the consumption of AI-2 from bacterial population density and its emergent behavior.
 810 With the addition of ‘controller cells’, we provide an orthogonal means to modulate QS activity,

811 demonstrate their use as mediators of heterologous protein and phenotype expression, and
812 provide a modeling foundation to guide QS-communication.

813 **3.4 Materials and Methods**

814 **3.4.1 Plasmid construction**

815 The bacterial strains and plasmids used in this study are listed in **Table S3.1**, and were
816 constructed according to standard procedures [123]. Briefly, plasmid pTrcHisB (Invitrogen) was
817 used as the backbone to construct plasmids pLsrFG, pLsrK, pLsrACDB, and pLsrACDBFG. The
818 sequences for *lsrFG*, *lsrK*, *lsrACDB*, and *lsrACDBFG* were amplified by PCR using Q5
819 polymerase (New England Biolabs) from *E. coli* K-12 strain W3110. These PCR inserts were
820 ligated into XhoI-digested pTrcHisB using Gibson assembly [124] and then transformed into
821 LW12 (W3110 $\Delta luxS$) [125]. Oligonucleotide primers were obtained from Integrated DNA
822 Technologies (Coralville, IA) and are listed in **Table S3.2**. Cloning was verified with sequencing
823 and Western Blot.

824 **3.4.2 AI-2 assay**

825 Cultured media was tested for the presence of AI-2 by inducing luminescence in *Vibrio harveyi*
826 reporter strain BB170 [69]. Briefly, BB170 was grown for 16 hours with shaking at 30°C in AB
827 (AI-2 Bioassay) media. AB media is made by adjusting 400 mL of distilled (DI) water to pH 7.5,
828 and adding 7 grams of NaCl, 2.4 grams of MgSO₄, 0.8 grams casamino acid, and 8 mL of
829 glycerol. AB media is supplemented with 400 μ L of potassium phosphate buffer (K₂HPO₄ 10.71g
830 and 5.24g KH₂PO₄ in 100 mL of DI water), 400 μ L of 0.1M L-arginine (0.1742g in 10 mL of DI
831 water), 40 μ L of riboflavin (10 μ g/mL), 40 μ L of thiamine (1 mg/mL) and 40 μ L kanamycin (50
832 mg/mL).

833 Overnight cultures were diluted 1:5,000 in fresh AB media with kanamycin, and
834 aliquoted into sterile 12 x 75-mm tubes (Fisher Scientific). Test samples were added to BB170
835 cultures at a final concentration of 10% (vol/vol). Luminescence was measured by quantifying
836 light production with a luminometer (EG&G Berthold LB 9509 Jr) and assays were adjusted, if
837 needed, so that values were in the linear range. Data are presented as “fold change” compared to
838 negative controls. All conditions were tested in triplicate. In experiments with supplemented
839 chemically-synthesized AI-2, we report AI-2 activity normalized to the initial concentration, as
840 our previous study showed a linear correlation between AI-2 concentration and resultant
841 bioluminescent AI-2 activity [126].

842 **3.4.3 AI-2 uptake profiles of ‘controller cells’**

843 Chemically synthesized AI-2 [127] was generously provided by the Sintim research
844 group. Each strain was reinoculated by diluting an overnight culture to 3% volume in 10 mL of
845 LB; these cells were grown in a 50 mL culture flask to an optical density (OD) ~ 0.4-0.6 at 30°C
846 with 250 RPM shaking. Isopropyl β -D-1-thiogalactopyranoside (IPTG) and AI-2 were added to a
847 final concentration of 1 mM and 50 μ M, respectively. Every half hour, optical density was
848 measured (**Supplementary Figure 3.1**) and samples were harvested for analysis. The average
849 bioluminescence for samples at $t = 0$ was denoted 50 μ M, and subsequent AI-2 activity values
850 were normalized to this concentration.

851 **3.4.4 Modulation of AI-2 in co-cultures**

852 BL21 pTrcHisB, LW12 pTrcHisB, and LW12 pLsrACDBFG were reinoculated at 3% of
853 overnight culture in 25 mL of LB in 125 mL culture flasks and grown to an OD ~ 0.4-0.6 at 37°C
854 with ampicillin. Co-cultures of BL21 pTrcHisB incubated with either LW12 pTrcHisB or LW12
855 pLsrACDBFG were aliquoted in culture test tubes at ratios of 9:1, 3:1, 1:1, 1:3, and 1:9. IPTG (1

856 mM) was added and every 30 minutes optical density (**Supplementary Figure 3.2**) was
857 measured and samples were harvested, on which AI-2 activity assays were performed.

858 **3.4.5 Silencing of autoinduced protein expression**

859 LW12 pTrcHisB and LW12 pLsrACDBFG were reinoculated at 3% overnight culture
860 into 25 mL of LB in 125 mL flasks and grown to an OD ~ 0.4-0.6. The samples were induced
861 with IPTG (1 mM) for three hours, before being resuspended (2000 RPM for 10 minutes) to an
862 OD ~ 1. W3110 pCT6 pET-GFP_{uv} [14], a strain of *E.coli* that responds to the level of the AI-2
863 concentration by expressing GFP, was grown to an OD ~ 0.2, and then incubated with LW12
864 pTrcHisB or LW12 pLsrACDBFG. Flow cytometric analysis was performed using a FACSCanto
865 II™ Flow Cytometer (Becton Dickinson) and all raw data was analyzed with BD FACSDiva™
866 6.0 software (Becton Dickinson).

867 **3.4.6 Biofilm studies and evaluation**

868 W3110 pTrcHisB, LW12 pTrcHisB, and LW12 pLsrACDBFG were diluted to OD ~
869 0.05 and reinoculated at a total volume of 200 µL at a 1:1 (v/v) ratio. IPTG (1 mM) was added at
870 OD ~ 0.4, and biofilms were cultured for ~ 24 hours (+/- 30 minutes) at 30°C in static conditions.
871 After incubation, optical density was read on a plate reader (Molecular Devices SpectraMax M2)
872 at 600 nm. The supernatant was gently decanted, and each well was washed 3 times with 300 µL
873 of sterile PBS to detach loosely adhered cells. The plate was then incubated at 60°C with the lid
874 off for 60 minutes, and afterwards, 250 µL of 0.1% crystal violet was added to each well and
875 incubated for 15 minutes at room temperature. Crystal violet stain was aspirated with a pipette
876 and excess stain was washed off by gently submerging and mixing in a tray filled with distilled
877 water until washings were free of the stain. After the microplate was air-dried, the dye was
878 resolubilized by adding 250 µL of 95% ethanol, and incubated at room temperature with shaking

879 for 30 minutes. The optical density of each well stained with crystal violet was measured at 540
880 nm.

881 **3.4.7 Chemotaxis studies and assay**

882 Preparation of conditioned media: LW12 pTrcHisB and LW12 pLsrACDBFG were
883 inoculated from frozen cell stock in 20 mL of LB with ampicillin in a 125 mL culture flask and
884 grown overnight to OD ~ 0.4 at 23 °C with 150 RPM shaking. The cultures were induced with
885 IPTG (1 mM) for two hours (23 °C, 150 RPM shaking) before being washed and resuspended
886 with DPBS (with calcium and magnesium) to OD ~ 0.4. LW12 pTrcHisB and LW12
887 pLsrACDBFG cultures were incubated at 37 °C with 250 RPM shaking with 0 μM and 20 μM
888 AI-2. The cell cultures were spun down, and the supernatant (“conditioned media”) was syringe-
889 filtered and stored at -20 °C.

890 Transwell chemotaxis assay: CT104 pCT6 pET-dsRed cultures [128] were inoculated from
891 frozen stock into 30 mL of LB in 250 mL culture flasks and grown overnight to an OD ~ 0.4-0.6
892 at 23 °C with 150 RPM shaking. The cells were spun down at 1500 RPM with a fixed rotor for 15
893 minutes and washed twice with DPBS (supplemented with calcium and magnesium) to an optical
894 density ~ 0.4-0.6. A 3.0 μm transwell was placed in four wells of a 6-well plate (Corning). CT104
895 pCT6 pET-dsRed cells were first pipetted into the bottom of the wells with a volume of 2.5 mL
896 per well, followed by 1.5 mL of each of the “conditioned media” fluids added to the top of the
897 transwell. The plate was incubated at 30 °C for three hours; cells accumulating in the upper
898 transwell had swum vertically [129]. This method yields fewer motile cells than the reverse
899 scenario (swimming down), but precludes settling in negative controls. The optical density of
900 each sample from the top chamber of the transwell was measured at 600 nm. The experiment was
901 repeated in triplicate.

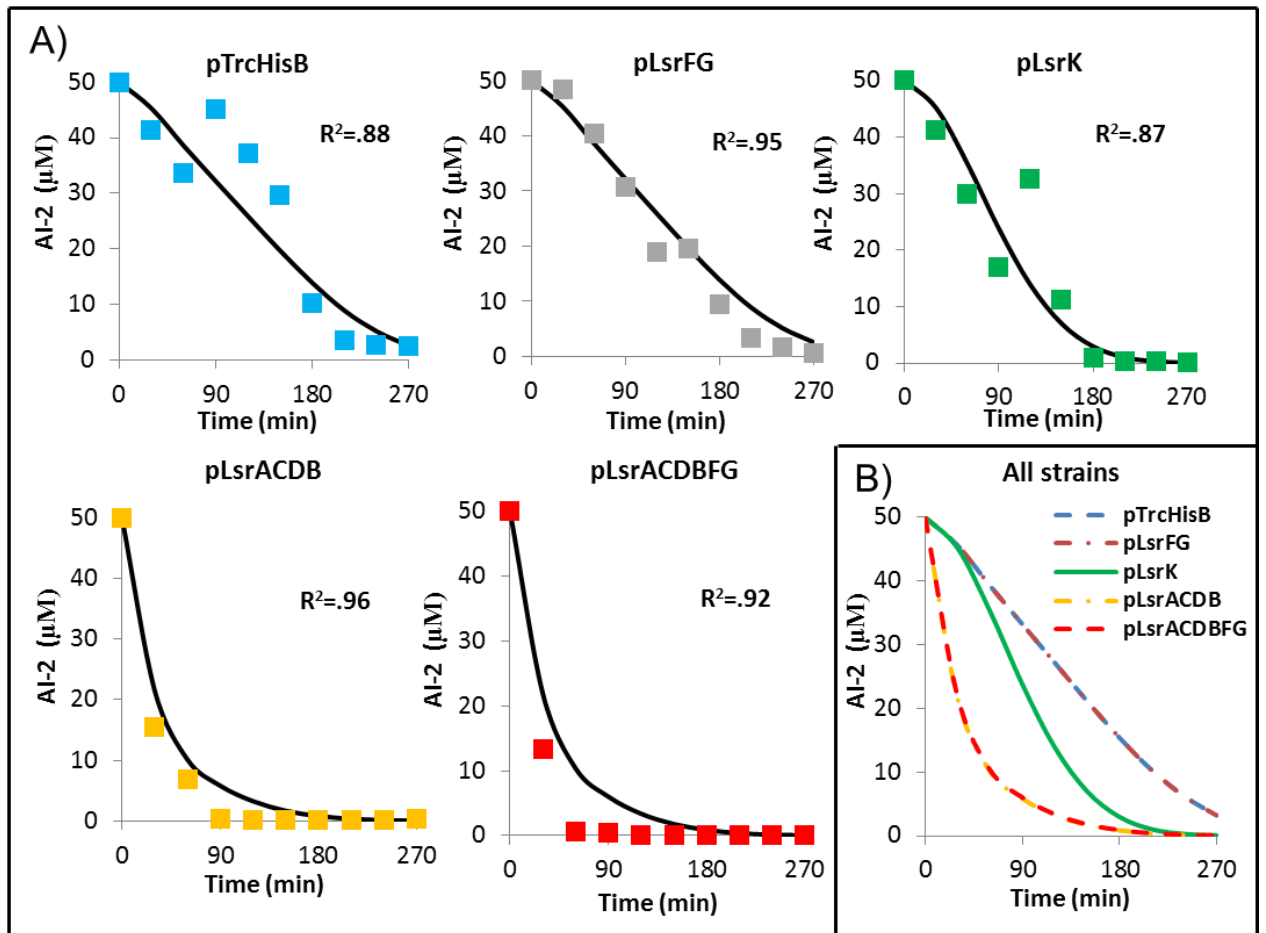
902 **3.5 Results**

903 **3.5.1 Design of modular QS elements**

904 As illustrated in **Scheme 1A**, the three steps involved in the processing of AI-2 from the
905 extracellular environment are (i) uptake, primarily through the LsrACDB transporter
906 [125,130,131], (ii) LsrK-mediated phosphorylation of AI-2 (to AI-2P), which blocks export back
907 to the extracellular milieu so that accumulated AI-2P binds the regulatory protein LsrR [132,133],
908 derepressing the Lsr transporter as well as enzymes, LsrF and LsrG, and (iii) degradation of AI-
909 2P through the two step process from isomerase LsrG followed with cleaving and thiolation by
910 LsrF [133,134]. In this study, we cloned *lsrFG*, *lsrK*, *lsrACDB*, and *lsrACDBFG* into the plasmid
911 pTrcHisB to enable overexpression of all proteins associated with these AI-2 processing
912 mechanisms (**Scheme 1B-1C**). We subsequently transformed each plasmid into LW12, a *luxS*
913 null mutant that cannot synthesize AI-2.

914 We first characterized the uptake rate of AI-2 by adding a fixed amount of exogenous AI-
915 2 and monitoring the extracellular concentration. Each strain was grown to mid-logarithmic phase
916 (OD ~ 0.4) with the subsequent addition of 50 μ M AI-2 and 1 mM IPTG (see Methods) and
917 optical density was recorded throughout (**Supplementary Figure 3.1**). **Figure 3.1A** shows the
918 uptake profile of each strain (colored dots), as well as the results of a topologically simple
919 mathematical model (black trendlines) comprised of several ordinary differential equations
920 (**Table 3.1**) for state variables AI-2, the molecular species that contribute to AI-2 uptake, and
921 optical density for each cell type. Note, we have included an empty vector control LW12
922 pTrcHisB that will consume AI-2 ($\Delta luxS$), but not in an accelerated fashion. We found that
923 overexpression of *lsrACDB* and *lsrACDBFG* genes showed the highest rate of uptake, indicating
924 that AI-2 transport into the cell is the slowest step involved in the processing of extracellular AI-2
925 into phosphorylated intracellular AI-2. Further, overexpression of *lsrK* resulted in an extracellular

926 AI-2 removal rate slower than overexpression of the transporter, but still faster than the host
 927 strain, LW12, with an empty vector or pLsrFG.



928

929 **Figure 3.1 AI-2 uptake profiles of 'controller cells'** A) Each plasmid was transformed into LW12
 930 (W3110 $\Delta luxS$) and grown to OD ~ 0.4 before the addition of IPTG (1 mM) and AI-2 (50 μM). AI-2
 931 levels were measured with AI-2 activity assays (see Methods) every 30 minutes (data points) and
 932 a mathematical model was created (black trendlines) to fit the data. B) Collation of
 933 mathematical models of each strain. Each experiment is performed in triplicate.

934

Reaction	Differential Equation
AI-2 outside the cell	$\frac{dAI2_{out}}{dt} = -k_{in} * (LsrACDB) * (AI2_{out}) + k_{out} * (AI2_{in})$
AI-2 inside the cell	$\frac{dAI2_{in}}{dt} = k_{in} * (LsrACDB) * (AI2_{out}) - k_{out} * (AI2_{in}) - k_p * (LsrK) * (AI2_{in})$
ACDB protein synthesis	$\frac{dLsrACDB}{dt} = [K_{nat} + K_I * (IPTG_{ACDB})] * (OD_{600}^{ACDB}) - k_d * (LsrACDB)$
Lsr kinase synthesis	$\frac{dLsrK}{dt} = [K_{nat} + K_I * (IPTG_K)] * (OD_{600}) - k_d * (LsrK)$
Cell density (LsrACDB overexpression)	$\frac{dOD_{600}^{ACDB}}{dt} = \mu_T * (OD_{600}^{ACDB})$
Cell density	$\frac{dOD_{600}}{dt} = \mu * (OD_{600})$

935

936 **Table 3.1: Ordinary differential equations of model.** Uptake of exogenously added AI-2 by each
937 plasmid in the strain LW12

938 Using the described network architecture, our deterministic model yielded simulation

939 results that closely matched the experimental data (**Figure 3.1A**). The simulated values of AI-2

940 uptake for each ‘controller cell’ is illustrated in **Figure 3.1B** and these indicate a broad

941 distribution in the rate of AI-2 uptake through the overexpression of the various uptake

942 mechanisms, and also enrich our understanding of the kinetic balances basis for these

943 phenomena.

944 In all cases, this is a phenomenological “best fit” model that incorporates the molecular

945 features contributing to uptake, and it is a simplification of our previous stochastic model for AI-2

946 uptake [135] and deterministic model for *lsr* gene expression [130]. The AI-2 transport into the

947 cell is described as an interaction of the protein complex LsrACDB with extracellular AI-2, and

948 the phosphorylation of AI-2 to AI-2P (a sequestered form of AI-2 that cannot be secreted back

949 outside the cell) is dependent on the interaction of enzyme LsrK with intracellular AI-2. The

950 induction parameter $IPTG_x$ is used as an input (1 or 0) to specify if a plasmid-encoded protein is

951 overexpressed (e.g. pLsrACDBFG has $IPTG_{ACDB}$ value of 1, and $IPTG_K$ value of 0) in the

952 presence of IPTG (strains without induction showed reduced AI-2 uptake, **Supplementary**

953 **Figure 3.3**). Our prior work on *lsr* gene expression and AI-2 synthesis [130,135] provided an

954 initial range of kinetic parameters; a parameter estimation routine was used to fit the model based

955 on a least squares minimization of the distance between the experimental and modeled data
 956 (Table 3.2). A detailed discussion of rate equations, growth rates, and kinetic parameters can be
 957 found in the **Supplementary material**.

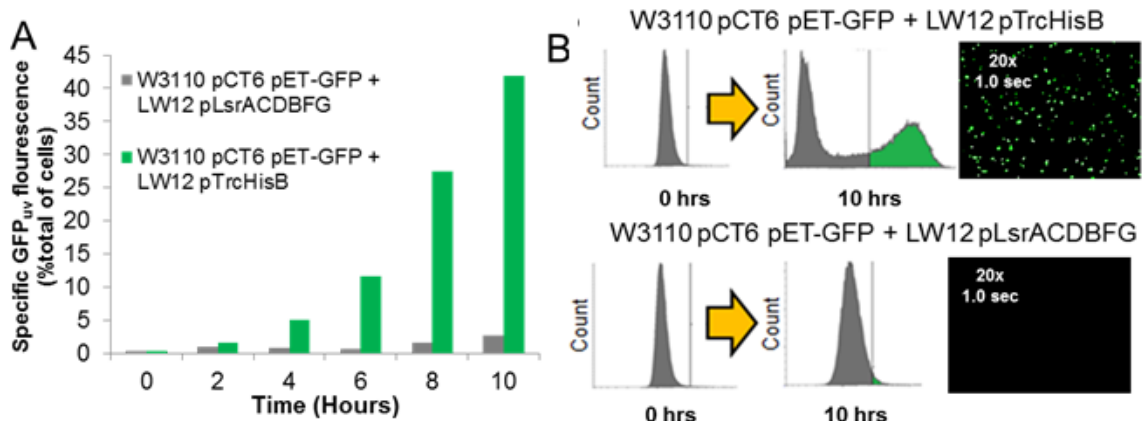
Species	Description	Initial Condition/Range
t	Time	[0, 270] min
$AI2_{out}$	Extracellular AI-2	50 μM
$AI2_{in}$	Intracellular AI-2	0 μM
$IPTG_K$	Plasmid-encoded LsrK	[1,0]
$IPTG_{ACDB}$	Plasmid-encoded LsrACDB	[1,0]
$LsrK$	Kinase	0 μM
$LsrACDB$	ACDB transporter	0 μM
OD_{600}^{ACDB}	Cell density (LsrACDB, LsrACDBFG)	0.4-0.6
OD_{600}	Cell density (LsrK, LsrFG, empty)	0.4-0.6
Parameters	Description	Best fit value
k_{in}	AI-2 import by LsrACDB complex	0.008 $\mu\text{M}^{-1} \text{min}^{-1}$
k_{out}	AI-2 export	0.045 min^{-1}
k_p	AI-2 phosphorylation	0.006 $\mu\text{M}^{-1} \text{min}^{-1}$
K_I	Induced expression	0.9 $\mu\text{M} \text{min}^{-1}$
K_{nat}	Native expression	0.1 $\mu\text{M} \text{min}^{-1}$
k_d	Protein decay	0.02 min^{-1}
μ	Growth rate	0.0056 min^{-1}
μ_T	Growth rate (LsrACDB expression)	0.0044 min^{-1}

958
 959 **Table 3.2: Model species and kinetic rate constants in model of exogenously added AI-2**
 960 **uptake by each plasmid in the strain LW12**

961 3.5.2 Quenching of QS-dependent protein expression

962 We sought to “shut off” W3110 pCT6 pET-GFP_{uv}, a strain that produces and responds to
 963 AI-2 by producing GFP, to provide an independent means to alter heterologous gene expression
 964 [14]. In **Figure 3.2**, we show that a 1:1 mixture of W3110 pCT6 pET-GFP_{uv} with LW12
 965 pLsrACDBFG almost completely suppresses QS-activated gene expression from the WT (AI-2
 966 producing) cells for 10 hours. This is in stark contrast to the empty vector results, which found
 967 that over 50% of the total population was observed to synthesize GFP over the same time period.
 968 Intermediate timepoints show a steady rise in the production of GFP in co-incubations with the
 969 empty vector, while co-incubations with LW12 pLsrACDBFG remained low throughout

970 (Supplementary Figures 3.S4-S5). “Since both the ‘controller cells’ and W3110 pCT6 pET-
 971 EGFP have the same antibiotic resistance, relative population dynamics could not be determined
 972 throughout the incubation. However, since LW12 pTrcHisB has a faster growth rate than LW12
 973 pLsrACDBFG (Table 3.2), purely growth rate dynamics would favor decreased fluorescence in
 974 cultures of LW12 pTrcHisB than LW12 pLsrACDBFG. Because we chose the ‘controller cell’
 975 strain having the greatest uptake rate, LW12 pLsrACDBFG, we would expect that by either using
 976 a lower inoculum fraction or by selecting LW12 pLsrK (the strain that significantly reduced AI-2
 977 levels through overexpression of the kinase) at 50% inoculum we would observe gradations in the
 978 overall fraction of QS positive activity. These results demonstrate “programmed” attenuation of
 979 heterologous protein expression as an indicator of QS phenotype and typically this is an outcome
 980 we seek to maximize. However, such control of the metabolic cue may also have positive
 981 implications for guiding synthetic networks of small populations of cells assembled to coordinate
 982 to produce a desired outcome [13].



983

984 **Figure 3.2 Cell-cell modulation of protein expression.** Panel (A) shows results for two cultures
 985 with an initial state of non-fluorescence. A 1:1 mixture of OD~1 of LW12 pLsrACDBFG or LW12
 986 pTrcHisB is mixed with OD~0.2 of reporter strain W3110 pCT6 pET-GFP. Panel (B) shows FACS
 987 data of the non-fluorescing population of both mixtures and the results 10 hours later.
 988 Microscopic images of the cells at 10 hours are shown, adjusted for clarity.

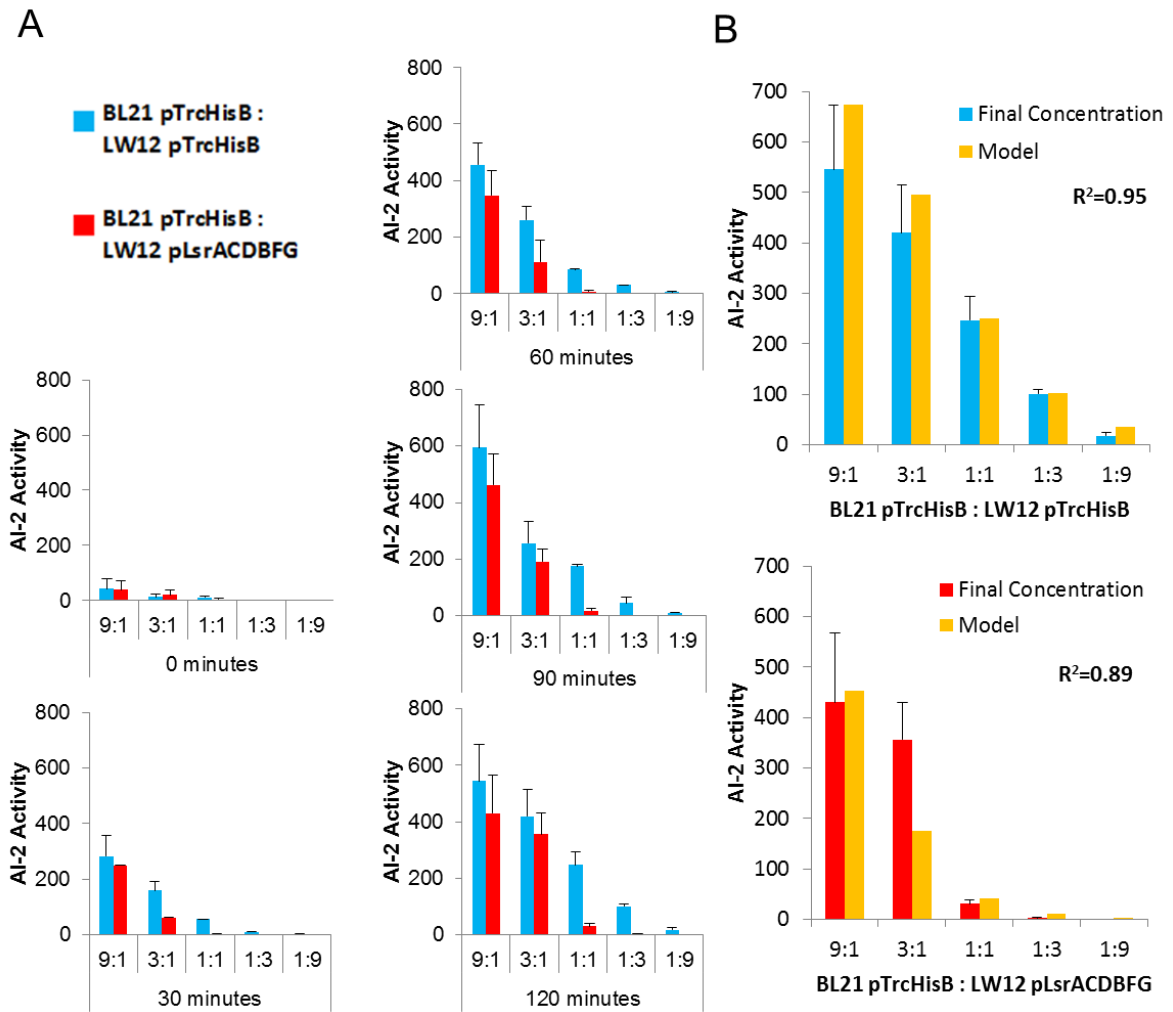
989 **3.5.3 Manipulation of ‘producer cell’ in co-cultures and extension of model**

990 Previously, we illustrated that the *E. coli* strain, BL21 *luxS*⁺, can act as ‘producer cell’ to
991 increase protein expression in QS-dependent systems [14]. To enable the use of these cells to
992 dynamically modulate metabolic cues, we investigated the interaction of the most effective
993 ‘controller cell’, pLsrACDBFG, and the empty vector with strain BL21 *luxS*⁺. We note that BL21
994 does not take up AI-2 from the medium [86], hence the removal of AI-2 here is due solely to the
995 added $\Delta luxS$ ‘controller cells’. In this experiment, BL21 pTrcHisB, LW12 pTrcHisB, and LW12
996 pLsrACDBFG were grown to an OD ~ 0.4 and co-cultures of BL21 pTrcHisB were incubated
997 with either LW12 pTrcHisB or LW12 pLsrACDBFG and aliquoted in culture test tubes at ratios
998 of 9:1, 3:1, 1:1, 1:3, and 1:9. At this point, IPTG (1 mM) was added and samples were harvested
999 every 30 minutes on which AI-2 activity assays were performed and optical density was
1000 measured (**Supplementary Figure 3.2**).

1001 The data in Figure 3.3A depict the AI-2 levels over time for each initial condition (the
1002 initial ratio of BL21 to ‘controller cell’ ranging from 9:1 to 1:9). The initial level of AI-2 is due to
1003 wild-type BL21 in the inoculums (they had secreted AI-2 in precultures). As expected, cultures
1004 with more BL21 initially had higher AI-2 activity levels and remained highest throughout the
1005 incubation. Also, we note that for the control culture, LW12 pTrcHisB (Figure 3.3A blue bars),
1006 there was an appreciable consumption of AI-2 so that we did not find a consistent threefold
1007 decrease in AI-2 as the population shifted in three-fold increments from 9:1 to 1:9. Nonetheless, a
1008 nearly linear decrease was observed with increasing LW12 pTrcHisB cells and this would be
1009 expected. In contrast, the rapid uptake rate of LW12 pLsrACDBFG is perhaps most evident in
1010 cultures where the consumer culture strain was present at an initial ratio of 1:1 or higher. In these
1011 cases, LW12 pLsrACDBFG (Figure 3.3A red bars), prevented significant quantities of AI-2 from
1012 accumulating to even measurable levels in the extracellular environment throughout the time
1013 period, while the empty vector control showed increased accumulation of AI-2 over time at all

1014 ratios. Hence, the co-cultured LW12 pLsrACDBFG cells effectively cleared all QS signaling
1015 among the 'producer' cells at these ratios.

1016



1017

1018 **Figure 3.3 LW12 pLsrACDBFG modulates AI-2 in the microenvironment.** Panel (A) illustrates
 1019 the AI-2 in co-cultures of *E. coli* BL21 (*luxS*⁺) with LW12 pTrcHisB (blue) and LW12 pACDBFG
 1020 (red), respectively, over time in a range of concentration ratios. AI-2 levels were measured with
 1021 AI-2 activity assays every 30 minutes. Each experiment is performed in triplicate with error bars
 1022 indicating standard error. Panel (B) compares the AI-2 activities at 120 minutes with the
 1023 mathematical model generated.

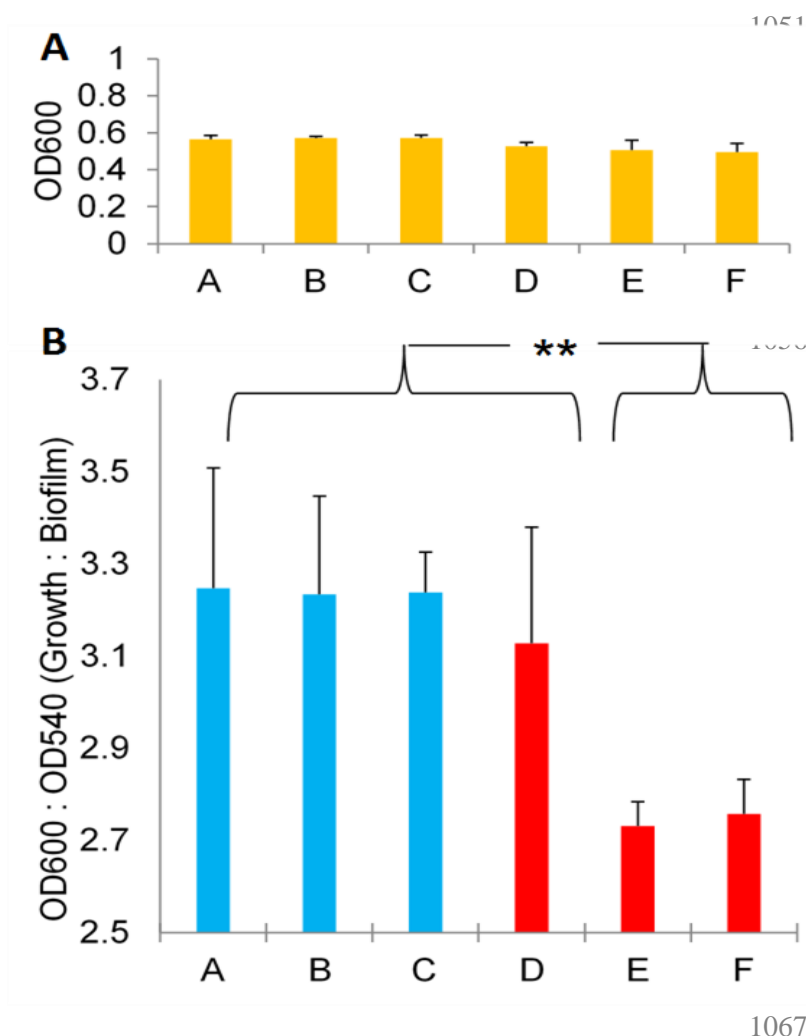
1024 The mathematical model developed in **Table 3.1** was extended to characterize these co-
 1025 cultures (Figure 3.3B), as opposed to the addition of exogenous AI-2 to the earlier simulations
 1026 where AI-2 was exogenously added to ‘controller cell’ cultures (Figure 3.1). We found good
 1027 agreement between the model and the experimental data, and detailed discussion of all rate
 1028 equations, growth rates, and kinetic parameters is provided in the Supplementary material. We

1029 note all rate equations and kinetic parameters used in the uptake profile for exogenously added
1030 AI-2 were unchanged for the co-incubation experiments.

1031 **3.5.4 Chemotaxis and biofilm attenuation**

1032 While this methodology provides a tool to regulate synthetic systems, it may also serve as
1033 a modifier of natural processes such as antibiotic susceptibility, motility, and biofilm formation. It
1034 has been shown that AI-2 has a contributing effect on biofilm formation in the *E. coli* W3110
1035 [136]; therefore, we investigated if LW12 pLsrACDBFG, could interfere with biofilm formation
1036 from this biofilm producer. Co-incubations of W3110 pTrcHisB were reinoculated with either
1037 LW12 pTrcHisB or LW12 pLsrACDBFG and grown in a 96-well plate for 24 hours. In certain
1038 wells, exogenous AI-2 was added to produce greater biofilm formation, and homocysteine, a side-
1039 product of AI-2 synthesis, was added as an additional negative control. Optical density
1040 measurements showed no significant variation in growth (**Figure 3.4A**), thereby suggesting that
1041 this method to obtain biofilm reduction does not exert selective pressure. Biofilm production was
1042 normalized to the final cell density and LW12 pLsrACDBFG showed reduced biofilm formation
1043 by about 20% compared to identical incubations with LW12 pTrcHisB (**Figure 3.4B**). A two-
1044 tailed unpaired Student's t-test was performed between the groupings, and a p-value of 0.0000485
1045 was determined, indicating that the biofilm reduction is significant. Further, the addition of
1046 exogenous AI-2 to the co-incubations (bar 'D') showed a restoration of biofilm formation in co-
1047 culture of LW12 pLsrACDBFG while homocysteine (bar 'E') does not, which further illustrates
1048 that the direct removal of AI-2 by LW12 pLsrACDBFG caused the resultant biofilm reduction.

1049



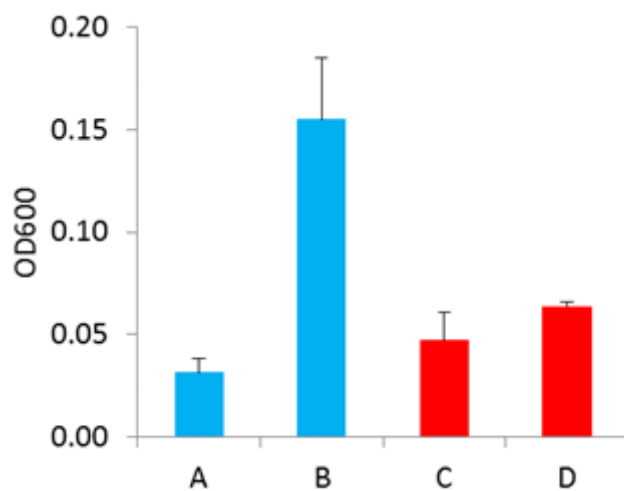
1068 **Figure 3.4: Effects of AI-2 on biofilm production.** Co-incubations of (A) W3110 pTrcHisB : LW12
 1069 pTrcHisB (B) W3110 pTrcHisB : LW12 pTrcHisB + homocysteine (50 μ M) (C) W3110 pTrcHisB :
 1070 LW12 pTrcHisB + AI-2 (50 μ M) (D) W3110 pTrcHisB : LW12 pLsrACDBFG (E) W3110 pTrcHisB :
 1071 LW12 pLsrACDBFG + homocysteine (50 μ M) (F) W3110 pTrcHisB : LW12 pLsrACDBFG + AI-2 (50
 1072 μ M) are mixed at a 1:1 ratio at OD \sim 0.05 and IPTG (1 mM) is added at OD \sim 0.4. Homocysteine
 1073 is added as a negative control to evaluate the effect of exogenous AI-2. Biomass is measured in
 1074 technical triplicate after 24 hours, and each experiment is performed in biological duplicate.
 1075 **Figure 3.4A** illustrates optical density at OD₆₀₀ after 24 hours. **Figure 3.4B** shows the ratio of cell
 1076 density at OD₆₀₀ to biomass measured at OD₅₄₀. A Student's two tailed unpaired t-test was used
 1077 to compare the groupings shown and a significance value of $p = 4.85 \times 10^{-5}$ was determined. All
 1078 error bars indicate one standard deviation.

1079

1080 Similarly, AI-2 acts as a chemoattractant for *E. coli* [137], and we show that LW12

1081 pLsrACDBFG can interfere with chemotaxis through the removal of AI-2. Conditioned media

1082 with exogenously added AI-2 incubated with LW12 pTrcHisB or LW12 pLsrACDBFG was used
1083 in a transwell assay where a culture of “seeker” cells, W3110 $\Delta luxS \Delta lsrFG$, in the bottom
1084 chamber traverse the permeable membrane towards the conditioned media with AI-2 in the top
1085 chamber (see Methods). As shown in **Figure 3.5**, a greater population of “seeker” cells
1086 chemotaxed upwards towards conditioned media from incubations with LW12 and the empty
1087 vector supplemented with AI-2 than LW12 pLsrACDBFG supplemented with AI-2, illustrating
1088 that the clearing of AI-2 by LW12 pLsrACDBFG can block AI-2 mediated chemotaxis.



1089

1090 **Figure 3.5: Effects of AI-2 on chemotaxis.** Migration of CT104 ($\Delta luxS \Delta lsrFG$) in a transwell
1091 incubated for two hours (see Methods) with induced (1 mM IPTG) conditioned media of (A)
1092 LW12 pTrcHisB (B) LW12 pTrcHisB + AI-2 (20 μ M) (C) LW12 pLsrACDBFG and (D) LW12
1093 pLsrACDBFG + AI-2 (20 μ M). Each experiment is performed in biological triplicate. Error bars
1094 indicate one standard deviation.

1095

1096

1097 **3.6 Discussion**

1098 Connecting both natural and synthetic networks, quorum sensing is widely used for a variety
1099 of processes and applications. When we developed the first population based example of a native
1100 regulatory circuit that was rewired to sense and transduce AI-2 to produce proteins, we looked
1101 forward to its potential to be used for “throttled” protein expression[14]. This dynamic control
1102 could help lead to the development of a ‘synthetic switchboard’ to control multiple genes in
1103 industrial bioprocesses [138], and the ‘universal’ signaling molecule AI-2, could be a natural
1104 choice to guide this kind of consortia. Traditional metabolic engineering could also benefit from
1105 microbial consortia, where a division of labor between two communities decreases the net
1106 metabolic load, creates new compounds, and increases productivity [139]. Synthetic
1107 communication systems would provide population-level coordination [140], and by developing
1108 an orthogonal method to control these QS systems, we provide another useful tool to guide
1109 microbial consortia in metabolic engineering applications.

1110 We have previously demonstrated that both native [125] and artificial transcriptional circuits
1111 [14,117] are dependent on the level of signal and that this potentially has widespread application
1112 [27,141,142]. In this work, we developed ‘controller cells, the application of which can actively
1113 modulate extracellular AI-2 concentrations. We show that the most effective ‘controller cell’,
1114 LW12 pLsrACDBFG, can silence heterologous gene expression. Also, this ‘controller cell’ can
1115 independently remove the signal generated from a ‘producer cell’, BL21, revealing the possibility
1116 of dynamic modulation (i.e. up- and down-regulation). We extended the application from
1117 synthetic networks to the naturally occurring processes of biofilm formation and chemotaxis.

1118 Further, the deterministic model developed here helps to delineate the mechanistic
1119 underpinnings that guide QS phenomena. While the increased rate of AI-2 uptake due to
1120 LsrACDB overexpression was expected, increased uptake coincident with LsrK overexpression

1121 was not (**Figure 3.1B**). By examining our model results in the context of the roles of the various
1122 components, we hypothesize that enhanced AI-2 uptake was due to a combination of two related
1123 factors. The first was that phosphorylated AI-2, unlike AI-2, cannot be transported across the
1124 bacterial membrane [32]. Thus, increased LsrK converts more intracellular AI-2 into AI-2P,
1125 increasing net AI-2 influx into the cell. Second, phosphorylated AI-2 acts to derepress LsrR,
1126 consequently resulting in greater expression of the *lsr*-operon from the genome (that is, AI-2P is
1127 assumed to be in rapid equilibrium with LsrR and this level corresponds to the prevailing rate of
1128 LsrK expression). So, faster accumulation of AI-2P should result in faster activation of *lsr* –
1129 mediated components. Of these two factors, we believe that the dominant is that the increased AI-
1130 2P prevents AI-2 from leaking back out of the cell. This was supported by the uptake profile of
1131 cells with pLsrFG, which was not significantly different than the uptake profile of cells with the
1132 empty vector. Theoretically, overexpression of *lsrFG* should result in faster degradation of AI-2P,
1133 which should cause a concomitant decreased expression of the genomic *lsr*-operon and
1134 resultantly, a slower uptake of AI-2. Since the uptake rate was not significantly altered, which
1135 suggests sufficient AI-2P levels in LW12 pLsrFG to maintain transcription of the genomic *lsr*-
1136 operon, then increased levels of AI-2P in LW12 pLsrK from overexpression of LsrK was
1137 correspondingly unlikely to cause much greater activation of the genomic *lsr*-operon.

1138 While we have only simulated conditions that describe the experiments shown, its use as a
1139 predictive tool for further work is envisioned. That is, the intentional modulation of quorum-
1140 sensing molecules by the inclusion of static or growing ‘controller cells’ can provide an
1141 additional level of control for synthetic networks. Further understanding of the kinetic parameters
1142 of the uptake system would guide future manipulation using this control methodology; one might
1143 estimate the quantities of ‘controller cells’ needed to guide protein expression or other processes.
1144 Alternatively, we suggest that similarly engineered commensal *E. coli* may provide a means for
1145 altering behavior in natural ecosystems such as the gut microbiome. Analogously, by extension,

1146 other bacterial species similarly engineered may provide a means to alter the balance of native
1147 niches. To our knowledge these concepts have not been reported. Among the many phenotypes
1148 controlled by AI-2 [8] at least two have been demonstrated in *E. coli* [136,143], and we have
1149 shown here that LW12 pLsrACDBFG can guide these phenotypes (biofilm formation and
1150 chemotaxis). We envision such cells might find utility in minimally disturbing cell-cell processes.
1151 We recognize that the current system uses a “charged” bacterium (induced with IPTG to
1152 overexpress transporter); the advantage being a well-controlled ‘controller cell’. There may be
1153 instances where a completely autonomous system would be more advantageous; it might
1154 interrogate and interact within ecological niches. While challenges clearly remain for tailoring
1155 metabolic cues to spatiotemporally control cell populations, this work provides one additional
1156 potent tool for guiding phenotype among bacterial populations.

1157 **3.7 Supplemental material on mathematical model**

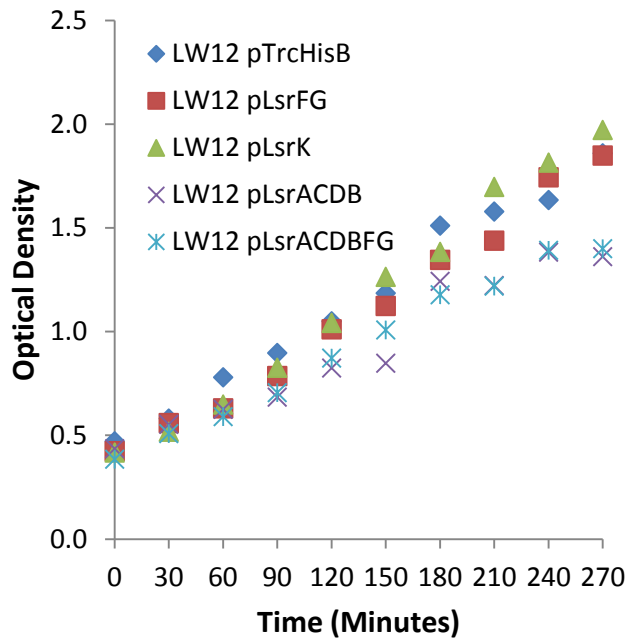
1158 **3.7.1 Mathematical model of ‘controller cells’ with exogenously added AI-2**

1159 The expression of LsrACDB and LsrK are presented as 1st order dependent on cell
1160 density; this presumes that LsrR binding kinetics are rapid relative to the transcription rate and
1161 that LsrR is effectively unbound to the DNA because of the high levels of AI-2P. Since it has
1162 been shown that the alternative transport system is far slower than the *lsr*-mediated system to
1163 uptake AI-2 [130], we have assumed that flux through the alternative pathway is negligible. The
1164 secretion of AI-2 back into the extracellular environment through the transporter TqsA [144] is
1165 assumed to be 1st order. Lastly, the growth rates are fitted to experimental measurements ($R^2 >$
1166 0.90), and it was found that overexpression of the LsrACDB and LsrACDBFG resulted in growth
1167 rates that were slower compared to the other strains (**Supplementary Figure 3.1**).

1168 **3.7.2 Extension of deterministic model to co-incubations with BL21**

1169 The mathematical model developed with exogenous AI-2 is extended to account for co-
1170 incubations with AI-2 producer, BL21 pTrcHisB. All strains were grown to an OD ~ 0.4 and co-
1171 cultures of BL21 pTrcHisB were incubated with either LW12 pTrcHisB or LW12 pLsrACDBFG
1172 and aliquoted in culture test tubes at ratios of 9:1, 3:1, 1:1, 1:3, and 1:9. Rate equations for
1173 incubations of BL21 pTrcHisB with LW12 pTrcHisB or LW12 pLsrACDBFG are listed in **Table**
1174 **S3.3** and **Table S3.4**, respectively. We note that kinetic rate coefficients are unchanged from
1175 incubations with exogenous AI-2 (**Table S3.5**). Further, the production of AI-2 from BL21 is
1176 modeled as a 1st order process, since it has been shown that BL21 accumulates AI-2 in the
1177 extracellular environment with a similar dependence on cell density during exponential growth
1178 [94]. The resuspension of the cultures in various ratios results in various degrees of disturbance,
1179 and a phenomena known as an intermediate lag phase has been found to occur when cells are
1180 disturbed during exponential growth [145-147]. Therefore, a microbial lag phase is included in
1181 the model for strains that were diluted to below a 50% initial co-culture ratio. It is well-known
1182 that the length of the microbial lag phase is dependent on various parameters, including the
1183 deviation from the prior state and the bacterium [145,148]. We used the commonly used growth
1184 model from Baranyi and Roberts (1994) [149], resulting in an adjustment function dependent on
1185 the deviation from the previous state (denoted here as physiological state). The adjustment
1186 function, $\left(\frac{Q_i}{1+Q_i}\right)$, has an initial higher deviance for strains with 10% of the co-culture ratio
1187 compared to strains with 25% of the co-culture ratio. The adjustment function approaches a value
1188 of 1 at a rate dependent on the cell density growth rate. Since LW12 pLsrACDBFG has a slower
1189 growth rate than LW12 pTrcHisB and BL21 pTrcHisB, the adjustment function returns to a value
1190 of 1 slower for LW12 pLsrACDBFG than the other cultures. Lastly, the optical density rates are
1191 fitted from the experimental measurements and show good agreement ($R^2 > 0.87$)
1192 (**Supplementary Figure 3.2**).

1193 **3.8 Supplemental figures**

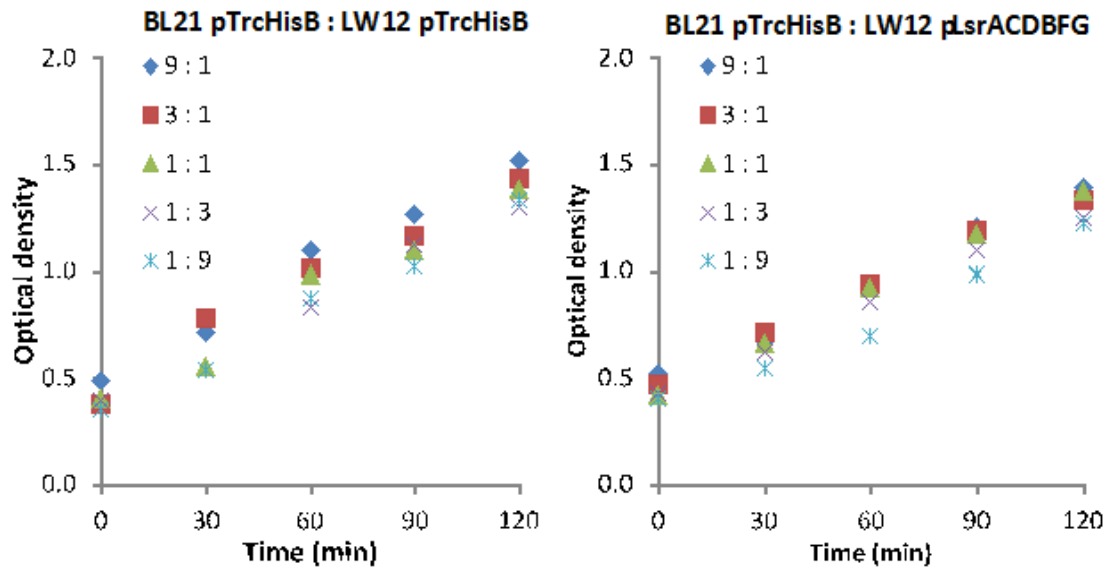


1194
1195

1196 **Figure S3.1: Optical density of individual strains.** OD₆₀₀ of respective strains after reinoculation
1197 and growth to OD ~ 0.4 before the addition of IPTG (1 mM) and AI-2 (50 μM).

1198

1199

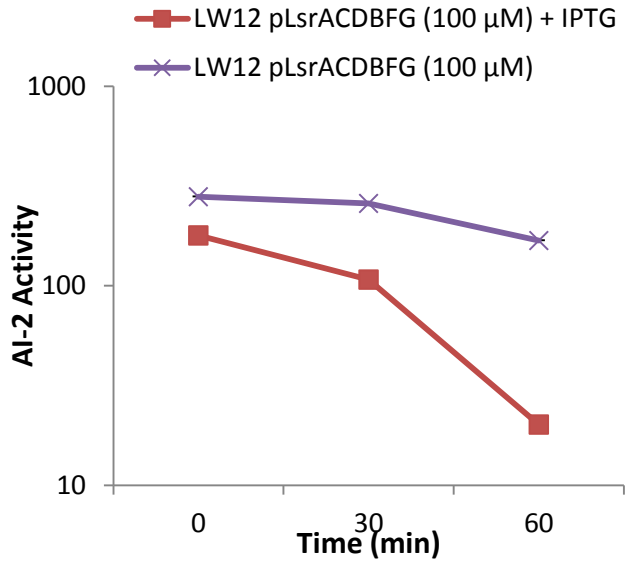


1200

1201 **Figure S3.2: Optical density of co-cultures.** OD₆₀₀ of co-cultures of *E. coli* BL21 with LW12
1202 pTrcHisB or LW12 pLsrACDBFG, respectively, over time at range of concentration ratios

1203

1204



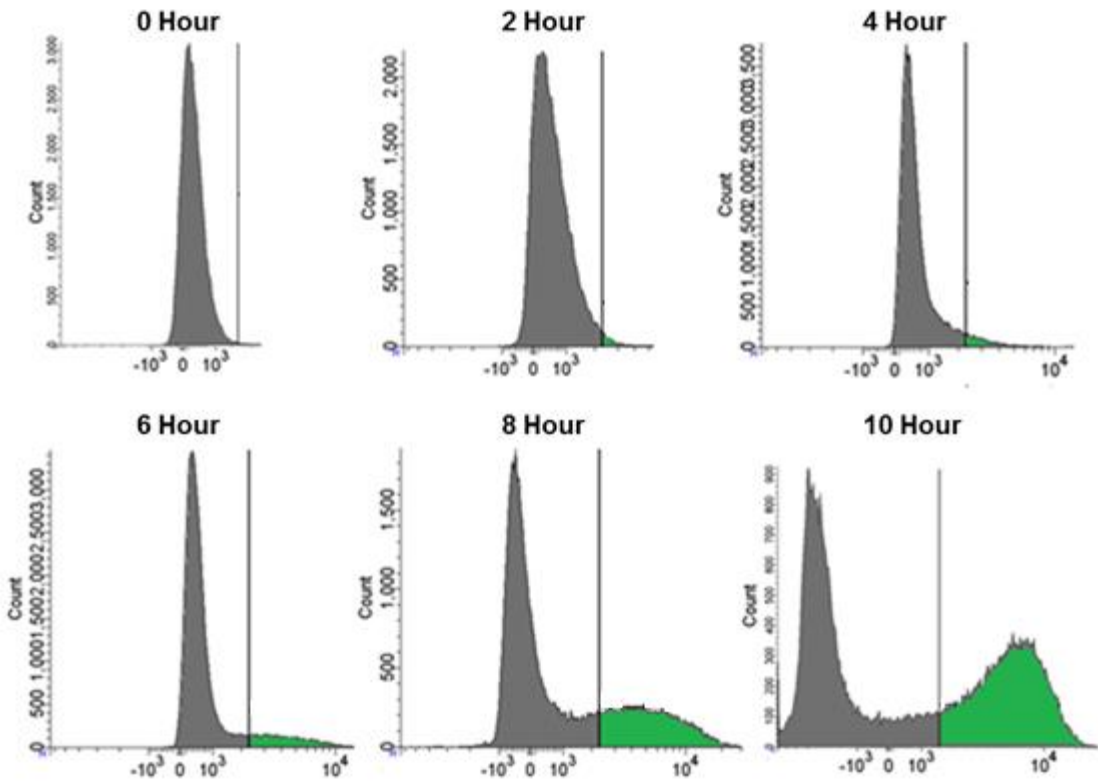
1205

1206 **Figure S3.3: Uninduced uptake rate.** Uptake rate of LW12 pLsrACDBFG with or without the
 1207 presence of IPTG (1 mM)

1208

1209

W3110 pCT6 pET-GFP : LW12 pTrcHisB



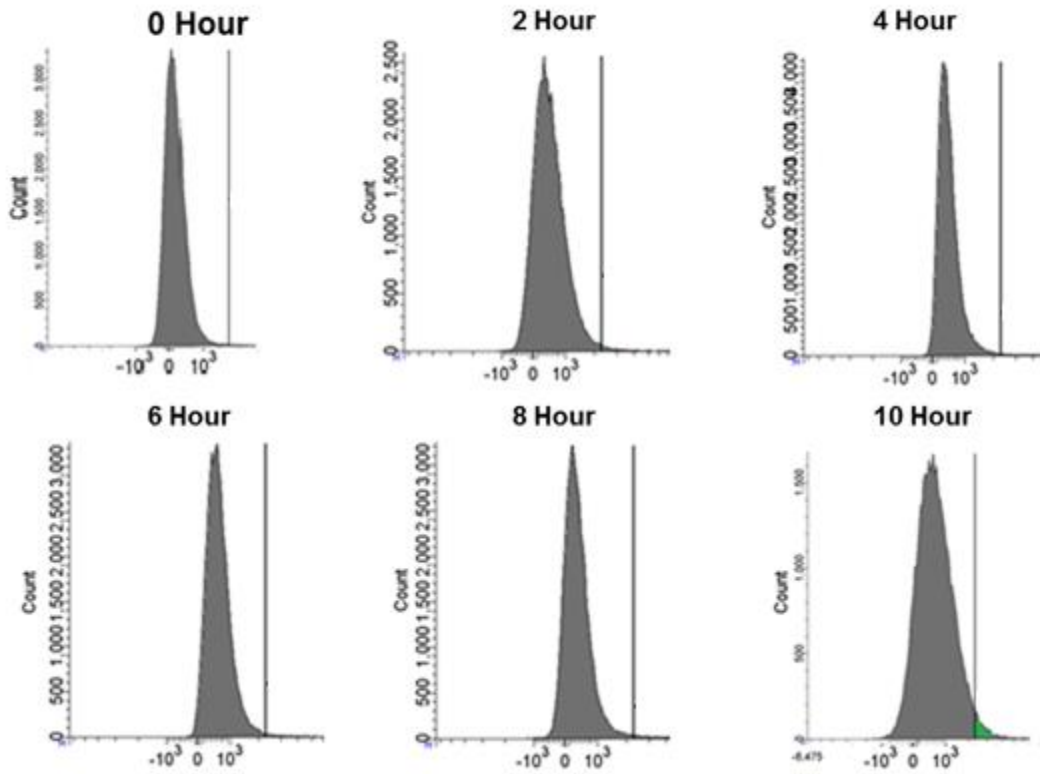
1210

1211 **Figure S3.4: QS reporter with control.** A 1:1 mixture of OD~1 of LW12 pTrcHisB is mixed with
1212 OD~0.2 of reporter strain W3110 pCT6 pET-GFP. Panel shows FACS data of the non-fluorescing
1213 population of both mixtures over time.

1214

1215

W3110 pCT6 pET-GFP : LW12 pLsrACDBFG



1216

1217 **Figure S3.5: QS reporter with controller cell.** A 1:1 mixture of OD~1 of LW12 pLsrACDBFG is
1218 mixed with OD~0.2 of reporter strain W3110 pCT6 pET-GFP. Panel shows FACS data of the non-
1219 fluorescing population of both mixtures over time.

1220

1221

1222

1223

1224 **3.9 Supplemental Tables**

1225

Strains	Description	Source
<i>E. coli</i>		
W3110	K12 strain, wild type, <i>t</i> ⁻ , F ⁻ , IN(<i>rrnD-rrnE</i>)1, <i>rph-1s</i>	Genetic Stock Center Yale University, New Haven, CT
LW12	W3110 Δ <i>luxS</i> ::Kan T	[125]
BL21	B strain, F ⁻ <i>ompT</i> [<i>dcm</i>]/[<i>lon</i>]/ <i>hsdS</i> (_{τ_B} ⁻ M _B ⁻)/ <i>gal</i>	Novagen
<i>V. harveyi</i>		
BB170	BB120 <i>luxN</i> ::Tn5 (sensor 1 ⁻ , sensor 2 ⁺), Km ^r	[69]
Plasmids	Description	Source
pFZY1	<i>galK'-lacZYA</i> transcriptional fusion vector, Ap ^r	[150]
pET200/D-TOPO	Cloning vector, containing T7 promoter, Km ^r	Invitrogen
pTrcHisB	pTrcHis derivative, Ap ^r	Invitrogen
pET200/dsRed	pET200 derivative, containing <i>dsRed</i> , Km ^r	[129]
pCT6	pFZY1 derivative, containing <i>lsrR</i> and <i>lsrR</i> promoter region fused with T7RPol, Ap ^r	[14]
pLsrFG	pTrcHisB derivative, containing <i>lsrFG</i> , Ap ^r	This study
pLsrK	pTrcHisB derivative, containing <i>lsrK</i> , Ap ^r	This study
pLsrACDB	pTrcHisB derivative, containing <i>lsrACDB</i> , Ap ^r	This study
pLsrACDBFG	pTrcHisB derivative, containing <i>lsrACDBFG</i> , Ap ^r	This study

1226 **Table S3.1: All strains and plasmids used in Chapter 3**

1227

1228

1229

1230

Name	Sequence	Relevant Description
pLsrFG Fwd	CGATAAGGATCCGAGCATGGCAGATTTAGACGATATTAAG	Forward primer for cloning <i>lsrFG</i>
pLsrFG Rev	GTACCAGCTGCAGATCTCACGGCATCAAACCATG	Reverse primer for cloning <i>lsrFG</i>
pLsrK Fwd	CGATAAGGATCCGAGCTGAGATGGCTCGACTCTTTACC	Forward primer for cloning <i>lsrK</i>
pLsrK Rev	GTACCAGCTGCAGATCTCGAGCTATAACCCAGGCGCTTTC	Reverse primer for cloning <i>lsrK</i>
pLsrACDB Fwd	CGATAAGGATCCGAGCTCGAGATGCAAACGAGTGATACC	Forward primer for cloning <i>lsrACDB</i>
pLsrACDB Rev	GTACCAGCTGCAGATCTGAGTCAGAAATCGTATTTGCCG	Reverse primer for cloning <i>lsrACDB</i>
pLsrACDBFG Fwd	CGATAAGGATCCGAGCATGCAAACGAGTGATACC	Forward primer for cloning <i>lsrACDBFG</i>
pLsrACDBFG Rev	GTACCAGCTGCAGATCCTCACGGCATCAAACCATG	Reverse primer for cloning <i>lsrACDBFG</i>

1231 **Table S3.2: Oligonucleotide primers used in Chapter 3**

1232

Reaction	Differential Equation
AI-2 outside the cell	$\frac{dAI2_{out}}{dt} = -k_{in} * (LsrACDB) * (AI2_{out}) + k_{out} * (AI2_{in}) + k_{lux} * (OD_{BL21})$
AI-2 inside the cell	$\frac{dAI2_{in}}{dt} = k_{in} * (LsrACDB) * (AI2_{out}) - k_{out} * (AI2_{in}) - k_p * (LsrK) * (AI2_{in})$
ACDB protein synthesis	$\frac{dLsrACDB}{dt} = K_{nat} * (OD_{LW12}^{pTrcHisB}) - k_d * (LsrACDB)$
Lsr kinase synthesis	$\frac{dLsrK}{dt} = K_{nat} * (OD_{LW12}^{pTrcHisB}) - k_d * (LsrK)$
Cell density (BL21)	$if r_b \geq 0.5, \frac{dOD_{BL21}}{dt} = r_b * \mu * (OD_{BL21})$ $else \frac{dOD_{BL21}}{dt} = r_b * \mu * (OD_{BL21}) * \left(\frac{Q_{BL21}}{1 + Q_{BL21}} \right)$
Cell density (LW12 pTrcHisB)	$if r_h \geq 0.5, \frac{dOD_{LW12}^{pTrcHisB}}{dt} = r_h * \mu * (OD_{LW12}^{pTrcHisB})$ $else \frac{dOD_{LW12}^{pTrcHisB}}{dt} = r_h * \mu * (OD_{LW12}^{pTrcHisB}) * \left(\frac{Q_{LW12}^{pTrcHisB}}{1 + Q_{LW12}^{pTrcHisB}} \right)$
Physiological state (BL21)	$\frac{dQ_{BL21}}{dt} = \mu * (Q_{BL21})$
Physiological state (LW12 pTrcHisB)	$\frac{dQ_{LW12}^{pTrcHisB}}{dt} = \mu * (Q_{LW12}^{pTrcHisB})$

1233

1234

1235

Table S3.3: Rate equations used in co-incubations of BL21 pTrcHisB with LW12 pTrcHisB

Reaction	Differential Equation
AI-2 outside the cell	$\frac{dAI2_{out}}{dt} = -k_{in} * (LsrACDB) * (AI2_{out}) + k_{out} * (AI2_{in}) + k_{lux} * (OD_{BL21})$
AI-2 inside the cell	$\frac{dAI2_{in}}{dt} = k_{in} * (LsrACDB) * (AI2_{out}) - k_{out} * (AI2_{in}) - k_p * (LsrK) * (AI2_{in})$
ACDB protein synthesis	$\frac{dLsrACDB}{dt} = K_I * (OD_{LW12}^{pLsrACDBFG}) + K_{nat} * (OD_{LW12}^{pLsrACDBFG}) - k_d * (LsrACDB)$
Lsr kinase synthesis	$\frac{dLsrK}{dt} = K_{nat} * (OD_{LW12}^{pLsrACDBFG}) - k_d * (LsrK)$
Cell density (BL21)	$\text{if } r_b \geq 0.5, \frac{dOD_{BL21}}{dt} = r_b * \mu * (OD_{BL21})$ $\text{else } \frac{dOD_{BL21}}{dt} = r_b * \mu * (OD_{BL21}) * \left(\frac{Q_{BL21}}{1 + Q_{BL21}} \right)$
Cell density (LW12 pTrcHisB)	$\text{if } r_v \geq 0.5, \frac{dOD_{LW12}^{pLsrACDBFG}}{dt} = r_v * \mu_v * (OD_{LW12}^{pLsrACDBFG})$ $\text{else } \frac{dOD_{LW12}^{pLsrACDBFG}}{dt} = r_v * \mu_v * (OD_{LW12}^{pLsrACDBFG}) * \left(\frac{Q_{LW12}^{pLsrACDBFG}}{1 + Q_{LW12}^{pLsrACDBFG}} \right)$
Physiological state (BL21)	$\frac{dQ_{BL21}}{dt} = \mu * (Q_{BL21})$
Physiological state (LW12 pTrcHisB)	$\frac{dQ_{LW12}^{pLsrACDBFG}}{dt} = \mu_v * (Q_{LW12}^{pLsrACDBFG})$

1236

1237

1238

Table S3.4: Rate equations used in co-incubations of BL21 pTrcHisB and LW12 pLsrACDBFG

Species	Description	Initial Condition/Range
t	Time	[0, 120] min
$AI2_{out}$	Extracellular AI-2	[0, 4] μM
$AI2_{in}$	'Controller' intracellular AI-2	0 μM
$IPTG_K$	Overexpression of LsrK	[1,0]
$IPTG_{ACDB}$	Overexpression of LsrACDB	[1,0]
$LsrK$	Kinase	0 μM
$LsrACDB$	ACDB transporter	0 μM
$OD_{LW12}^{pTrcHisB}$	Cell density (LW12 pTrcHisB)	0.04-0.54
$OD_{LW12}^{pLsrACDBFG}$	Cell density (LW12 LsrACDBFG)	0.04-0.54
OD_{BL21}	Cell density (BL21 pTrcHisB)	0.04-0.54
r_b	Ratio of BL21 pTrcHisB	[.90, .75, .50, .25, .10]
r_h	Ratio of LW12 pTrcHisB	[.10, .25, .50, .75, .90]
r_v	Ratio of LW12 pLsrACDBFG	[.10, .25, .50, .75, .90]
Q_{BL21}	Physiological state BL21 pTrcHisB	[0, 0, 0, 1.5, 1]
$Q_{LW12}^{pTrcHisB}$	Physiological state LW12 pTrcHisB	[1, 1.5, 0, 0, 0]
$Q_{LW12}^{pLsrACDBFG}$	Physiological state LW12 pLsrACDBFG	[1, 1.5, 0, 0, 0]
Parameters	Description	Best fit value
k_{in}	AI-2 import by LsrACDB complex	$0.008 \mu\text{M}^{-1} \text{min}^{-1}$
k_{out}	AI-2 export	0.045min^{-1}
k_p	AI-2 phosphorylation	$0.006 \mu\text{M}^{-1} \text{min}^{-1}$
K_I	Induced expression	$0.9 \mu\text{M} \text{min}^{-1}$
K_{nat}	Native expression	$0.1 \mu\text{M} \text{min}^{-1}$
k_{lux}	AI-2 production	$0.45 \mu\text{M} \text{min}^{-1}$
k_d	Protein decay	0.02min^{-1}
μ	Growth rate (BL21 / LW12, pTrcHisB)	0.010min^{-1}
μ_v	Growth rate (LW12 pLsrACDBFG)	0.007min^{-1}

1239

1240

1241

1242

Table S3.5: Kinetic rate constants and parameters used in co-cultures

1243 **3.10 Supplemental Material on Mathematical Model**

1244 **Mathematical model of ‘controller cells’ with exogenously added AI-2**

1245 The expression of LsrACDB and LsrK are presented as 1st order dependent on
1246 cell density; this presumes that LsrR binding kinetics are rapid relative to the
1247 transcription rate and that LsrR is effectively unbound to the DNA because of the high
1248 levels of AI-2P. Since it has been shown that the alternative transport system is far slower
1249 than the *lsr*-mediated system to uptake AI-2 [130], we have assumed that flux through the
1250 alternative pathway is negligible. The secretion of AI-2 back into the extracellular
1251 environment through the transporter TqsA [144] is assumed to be 1st order. Lastly, the
1252 growth rates are fitted to experimental measurements ($R^2 > 0.90$), and it was found that
1253 overexpression of the LsrACDB and LsrACDBFG resulted in growth rates that were
1254 slower compared to the other strains (**Supplementary Figure 3.1**).

1255 **Extension of deterministic model to co-incubations with BL21**

1256 The mathematical model developed with exogenous AI-2 is extended to account
1257 for co-incubations with AI-2 producer, BL21 pTrcHisB. All strains were grown to an OD
1258 ~ 0.4 and co-cultures of BL21 pTrcHisB were incubated with either LW12 pTrcHisB or
1259 LW12 pLsrACDBFG and aliquoted in culture test tubes at ratios of 9:1, 3:1, 1:1, 1:3, and
1260 1:9. Rate equations for incubations of BL21 pTrcHisB with LW12 pTrcHisB or LW12
1261 pLsrACDBFG are listed in **Table S3.3** and **Table S3.4**, respectively. We note that kinetic
1262 rate coefficients are unchanged from incubations with exogenous AI-2 (**Table S3.5**).
1263 Further, the production of AI-2 from BL21 is modeled as a 1st order process, since it has
1264 been shown that BL21 accumulates AI-2 in the extracellular environment with a similar
1265 dependence on cell density during exponential growth [94]. The resuspension of the

1266 cultures in various ratios results in various degrees of disturbance, and a phenomena
1267 known as an intermediate lag phase has been found to occur when cells are disturbed
1268 during exponential growth [145-147]. Therefore, a microbial lag phase is included in the
1269 model for strains that were diluted to below a 50% initial co-culture ratio. It is well-
1270 known that the length of the microbial lag phase is dependent on various parameters,
1271 including the deviation from the prior state and the bacterium [145,148]. We used the
1272 commonly used growth model from Baranyi and Roberts (1994) [149], resulting in an
1273 adjustment function dependent on the deviation from the previous state (denoted here as
1274 physiological state). The adjustment function, $\left(\frac{q_i}{1+q_i}\right)$, has an initial higher deviance for
1275 strains with 10% of the co-culture ratio compared to strains with 25% of the co-culture
1276 ratio. The adjustment function approaches a value of 1 at a rate dependent on the cell
1277 density growth rate. Since LW12 pLsrACDBFG has a slower growth rate than LW12
1278 pTrcHisB and BL21 pTrcHisB, the adjustment function returns to a value of 1 slower for
1279 LW12 pLsrACDBFG than the other cultures. Lastly, the optical density rates are fitted
1280 from the experimental measurements and show good agreement ($R^2 > 0.87$)
1281 **(Supplementary Figure 3.2).**

1282 **Chapter 4: Generation of ‘quantized quorums’ through dose-dependent**
1283 **encapsulated bacteria**

1284 The following work is prepared to be submitted into *ACS Synthetic Biology*.

1285 **4.1 Abstract**

1286 Bacteria secrete and recognize communication molecules to coordinate action in a
1287 process known as quorum sensing (QS), which plays a role in natural processes such as biofilm
1288 formation, antibiotic susceptibility, and motility. QS is used to connect synthetic networks with
1289 QS molecules such as acyl homoserine lactones, autoinducer-2 and oligopeptides. Previously, we
1290 engineered a suite of ‘controller cells’ that elucidated the dynamics of the uptake mechanisms and
1291 were used to quench QS and modulate QS dependent phenotypes such as biofilm formation.
1292 However, these ‘controller cells’ required an equivalent ratio of induced controller cell population
1293 to target QS cell population, an undesirable scenario in many microbiological applications. In this
1294 work, we rationally design a high-efficiency (HE) ‘controller cell’ that provides the most rapid
1295 uptake of the quorum sensing molecule autoinducer-2 (AI-2), without the addition of an
1296 exogenous inducing agent, to guide QS populations in a sequestered, encapsulated environment.
1297 This is done through the expression of every element of the *lsr*-system, with the exception of the
1298 *lsr* repressor, on a two-promoter constitutive plasmid. In addition to greatly increased uptake rate,
1299 this HE ‘controller cell’ is unaffected by the presence of glucose, thereby providing the
1300 possibility to affect cell processes in diverse, polymicrobial environments as well as glucose
1301 feedstock bioreactors. We show that these HE cells can silence quorum sensing at much lower
1302 cell populations than previous ‘controller cells’, and then show that through HE encapsulation
1303 inside the well-studied alginate-chitosan capsule motif, we can quench quorum sensing in target
1304 QS populations from a sequestered environment. Lastly, we sought to enable quantized
1305 subpopulation of QS-activated cells and in a dose-dependent fashion, tune QS-mediated gene
1306 expression. We have previously described the generation of ‘quantized quorums’ through

1307 differences in AI-2 sensitivity[151], and here, we build on this by producing these quorums in a
1308 user-mediated fashion. These encapsulated bacteria provide orthogonal control to drive protein
1309 expression while maintaining minimal interaction and interference with the system, with
1310 applications in metabolic engineering and human disease.

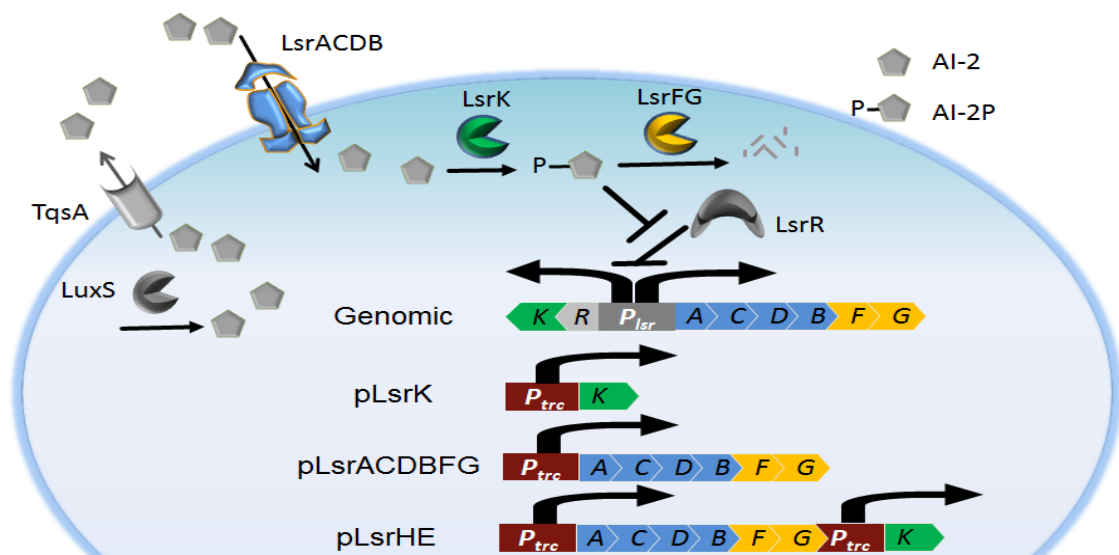
1311 **4.2 Introduction**

1312 Quorum sensing (QS) is a process used by many microorganisms to coordinate action in
1313 a cell-density dependent manner through small signaling molecules. Microorganisms survey their
1314 local environment through the production and transduction of QS molecules. This coordination is
1315 necessary in natural bacterial networks such as biofilm formation, virulence factor secretion, and
1316 antibiotic production which can be critical to survival, but are fruitless if only enacted by a single
1317 member of the community. When the critical threshold for QS molecules is reached, indicating a
1318 sufficient cell population, a ‘quorum’ is obtained and bacteria can initiate gene expression as a
1319 community to coordinate behavior of a population on a larger scale[152]. Extending beyond
1320 natural processes, synthetic biologists have incorporated these QS components into synthetic
1321 circuits to generate sophisticated systems such as bistable networks, pulse generators, spatio-
1322 temporal activation of gene expression, and predator-prey ecosystems [106].

1323 Recently, we developed “controller cells” to quench QS-dependent protein expression
1324 and phenotypic outcomes such as biofilm formation and chemotaxis (in review). These cells
1325 provided an orthogonal means of manipulation of natural and synthetic gene networks and
1326 phenotypes. However, these controller cells needed large amounts of bacteria directly interacting
1327 with the system to block communication, required the addition of an exogenous inducing agent,
1328 functioned only in the absence of glucose—a common nutrient in a variety of environments. The
1329 requirement of an induced, direct interaction of a large controller cell population to actuate
1330 quorum sensing suppression may not be suitable for many applications. Ideally, we could not

1331 only quench, but tune QS-dependent response in a target population through a sequestered,
 1332 separated controller cell population.

1333 In this work, we sought to extend our prior work to encapsulate a controller cell inside a
 1334 multifunctional polysaccharide capsule to tune protein expression of QS-dependent protein
 1335 expression systems, without direct interaction with the QS culture, the need for an inducing agent,
 1336 or the exclusion of glucose. We rationally designed a high-efficiency (HE) ‘controller cell’ that
 1337 would provide rapid uptake of AI-2 without the need for an inducing agent, such as IPTG. In this
 1338 design, we build off of our prior work where we separately overexpressed the three main
 1339 components responsible for the uptake and degradation of AI-2 from the environment (**Scheme**
 1340 **1**): AI-2 transport into the cell through the protein complex LsrACDB, phosphorylation of AI-2 to
 1341 AI-2P, a form of AI-2 that cannot cross the cell membrane, by the kinase LsrK, and degradation
 1342 of AI-2P by the isomerase LsrG and cleavage by LsrF.



1343
 1344 **Scheme 4: Schematic of the *lsr*-system in *E. coli* and engineered plasmids.** LuxS generates AI-2,
 1345 which is exported out of the cell by TqsA. The ABC-transporter complex, LsrACDB, brings AI-2
 1346 into the cell where it is subsequently phosphorylated by LsrK into AI-2P. AI-2P derepresses LsrR,
 1347 the global regulator of the *lsr* operon, from the genome allowing transcription of the *lsr*-genes.
 1348 AI-2P is degraded through a two-step process by enzymes LsrG and LsrF. The engineered
 1349 plasmids pLsrK, pLsrACDBFG, and pLsrHE are illustrated with constitutive transcription through
 1350 the leakiness of the P_{trc} promoter.

1351 Our previous work revealed that the separate overexpression of LsrK and LsrACDB both
1352 resulted in increased uptake, and we hypothesized that the overexpression of both mechanisms
1353 would result in greater uptake than overexpression of each separately. Therefore, a two promoter
1354 system on a single plasmid was designed to overexpress all aspects of the *lsr*-system, save the *lsr*
1355 repressor, and we rely on ‘leaky’ transcription from the *trc* promoter (i.e. IPTG is not added). As
1356 a host strain, we previously used a $\Delta luxS$ synthase knockout to enable investigation of the kinetics
1357 involved in AI-2 uptake. In this study, to fully enable AI-2 uptake, we used the strain SH1c, a
1358 $\Delta luxS \Delta lsrR$ double knockout that does not require a quorum of phosphorylated AI-2 to activate
1359 the *lsr* system. Further, since the metabolic pathway that is responsible for AI-2 uptake and
1360 phosphorylation is greatly impaired when glucose is present due to the reduction of transcription
1361 factor cAMP-CRP [125], our previously engineered ‘controller cells’ could not be applied in
1362 glucose-rich environments. The HE ‘controller cell’ constitutively expresses the *lsr*-system using
1363 the *trc* promoter, independently of genomic transcription of the *lsr* system through the *lsr*
1364 promoter, which removes the need for the cAMP-CRP transcription factor.

1365 We show that the HE ‘controller cell’ provides the most rapid uptake of AI-2 compared
1366 to all previously engineered cells, and that it is the only one to effectively remove all AI-2 from
1367 the extracellular environment in the presence of glucose. Further, the HE cells can silence QS-
1368 dependent protein expression communication not only at very low cell quantities, but also when
1369 encapsulated inside a biocompatible capsule. We sought to encapsulate these cells to maintain
1370 population separation while being able to effectively remove AI-2 and interfere with quorum
1371 sensing. Recent work has shown that ‘engineered’ population control through killer proteins can
1372 achieve adjustable steady state populations [16,153,154], and we aim to engineer quantized active
1373 subpopulations with minimal interaction. To achieve this, the ‘controller cells’ were encapsulated
1374 in a porous chitosan-alginate capsule. The improved HE controller cell is needed to overcome the
1375 diffusion limits of small molecules into capsules and the comparatively small bacterial

1376 populations encapsulated to effectively uptake AI-2, as empty vector controls show no significant
1377 reduction in AI-2 levels.

1378 We show that higher dosages of these encapsulated HE controller cells can quench QS
1379 signaling, which can be envisioned to be used as a quorum quenching [35,155] treatment to
1380 reduce the expression of harmful phenotypes while maintaining separation from the encapsulated
1381 bacteria. Our overarching goal was to not only quench protein expression, but to guide a QS-
1382 dependent system that would minimally interact with the controller cell populations. Tunable
1383 protein expression is a highly desired property and has been pursued through methods such as
1384 proteases [156,157], riboregulators[158], and RNAi[159]. We show here that we can tune protein
1385 expression by adjusting the quorum activated population through capsule dosage. We also
1386 envision that by enabling controlled manipulation of quorums, this tool could be used to assay
1387 threshold responses[159], manipulate complex genetic circuits [138], and develop and interrogate
1388 spatially-patterned cell populations[160,161].

1389 **4.3 Materials and Methods**

1390 **4.3.1 Plasmid construction**

1391 Plasmids were constructed according to standard procedures[123]. Briefly, plasmid
1392 pLsrACDBFG (Invitrogen) was used as the backbone to construct plasmids pLsrHE. The plasmid
1393 plsrK was used as template to PCR the promoter to the termination region, inclusive of the lsrK
1394 gene using Q5 polymerase (New England Biolabs). This PCR insert was ligated into XhoI-
1395 digested pLsrACDBFG using Gibson assembly[124] and then transformed into SH1c (W3110
1396 $\Delta luxS \Delta lsrR$) (Cite). Oligonucleotide primers were obtained from Integrated DNA Technologies
1397 (Coralville, IA) and are listed in **Table S1** (Supplementary Information).

1398 **4.3.2 AI-2 Assay**

1399 Cultured media was tested for AI-2 activity through the assay using *Vibrio harveyi*
1400 reporter strain BB170 [69]. In short, BB170, supplemented with kanamycin (50 ug/mL), was
1401 grown for 16 hours with shaking at 30°C in AB media. These cultures were diluted 1:5,000 in
1402 fresh AB media, and aliquoted into 12 x 75-mm tubes (Fisher Scientific). Cultured media samples
1403 were added to these BB170 cultures to obtain a final concentration of 10% (vol/vol). The
1404 resulting bioluminescence was measured by quantifying light production with a lumenometer
1405 (Glomax Multi- Jr) and assays points were selected so that values were in the linear range. Data
1406 are presented as “fold change” compared to the negative control, and all conditions were tested in
1407 triplicate. In experiments with supplemented chemically-synthesized AI-2, we report AI-2
1408 activity normalized to the initial concentration, and subsequent points are correlated to AI-2
1409 concentration using a prepared standard curve, as performed in prior studies (CITE mBIO).

1410 **4.3.3 Synthetic AI-2 uptake profiles**

1411 Chemically synthesized AI-2 [127] was generously provided by the Sintim research
1412 group. Each strain was reinoculated by diluting an overnight culture to 3% volume in 10 mL of
1413 LB and 10 mL of LB supplemented with 1% glucose, respectively. These cells were grown in a
1414 50 mL culture flask to an optical density (OD) ~ 0.4 at 30°C with 250 RPM shaking. AI-2 was
1415 then added to obtain a final concentration of 100µM. Optical density was measured and samples
1416 were harvested every half hour for AI-2 activity assays. The average bioluminescence for samples
1417 at t = 0 were denoted as 100 µM, and subsequent AI-2 activity values were normalized to the
1418 standard curve generated.

1419 **4.3.4 Modulation of autoinduced protein expression**

1420 SH1c pTrcHisB, and SH1c pLsrSV were reinoculated at 3% of overnight culture in 4 mL
1421 of LB in 15 mL culture tubes and grown to an OD ~ 0.4-0.6 at 37°C with ampicillin. W3110

1422 pCT6 pET_EGFP [14], a strain of *E.coli* that responds to the level of the AI-2 concentration by
1423 expressing GFP, was grown to an OD ~ 0.1, was reinoculated at 3% overnight culture in 10 mL
1424 of LB in 50 mL culture flasks and grown to OD ~ 0.2. Co-cultures of W3110 pCT6 pET-EGFP
1425 incubated with either LW12 pTrcHisB or LW12 pLsrACDBFG were aliquoted in culture test
1426 tubes at ratios of 1:1, 2:1, 3:1, 6:1 and 8:1. Fluorescence was measured with a **plate reader**.

1427 **4.3.5 Capsule preparation**

1428 SH1c pTrcHisB and SH1c pLsrSV were reinoculated at 3% overnight culture in and
1429 grown to an OD~0.4-0.6 in 4 mL of LB supplemented with ampicillin (50 µg/mL) and 4 mL LB
1430 supplemented with 1% glucose and ampicillin (50 µg/mL), respectively. Cells were concentrated
1431 (5x) in their respective medias before being mixed with a 1:1 mixture of 2% alginate. A 1:1
1432 mixture of 2% alginate with bacteria in LB is added dropwise with a 22 gauge needle into a
1433 stirring mixture of 4 mL of 1.5% chitosan and 2 ml of 0.25 M CaCl₂ in 10 mL beaker. Each
1434 capsule is then washed 3 times with 200 uL of DPBS supplemented with 0.1 M CaCl₂.

1435 **4.3.6 AI-2 uptake profile in capsules**

1436 Capsules were placed in 12 well plates (**Corning**) with 2 mL of LB supplemented with
1437 20 µM AI-2, 50 µM Amp and 0.1 M CaCl₂ and 2 mL of LB supplemented with 20 µM AI-2, 1%
1438 glucose, 50 µM Amp and 0.1 M CaCl₂. A 150 µL sample is harvested every 30 minutes for for
1439 AI-2 activity assays.

1440 **4.3.7 Modulation of protein expression through encapsulated bacteria**

1441 W3110 pCT6 pET-EGFP was grown to OD ~ 0.2 and then resuspended in an equivalent volume
1442 of LB supplemented with ampicillin (50µg/mL). Capsules were added in each well of a 48 well
1443 plate (Corning) that contained 0.25 mL the W3110 pCT pET-EGFP culture. Flow cytometric

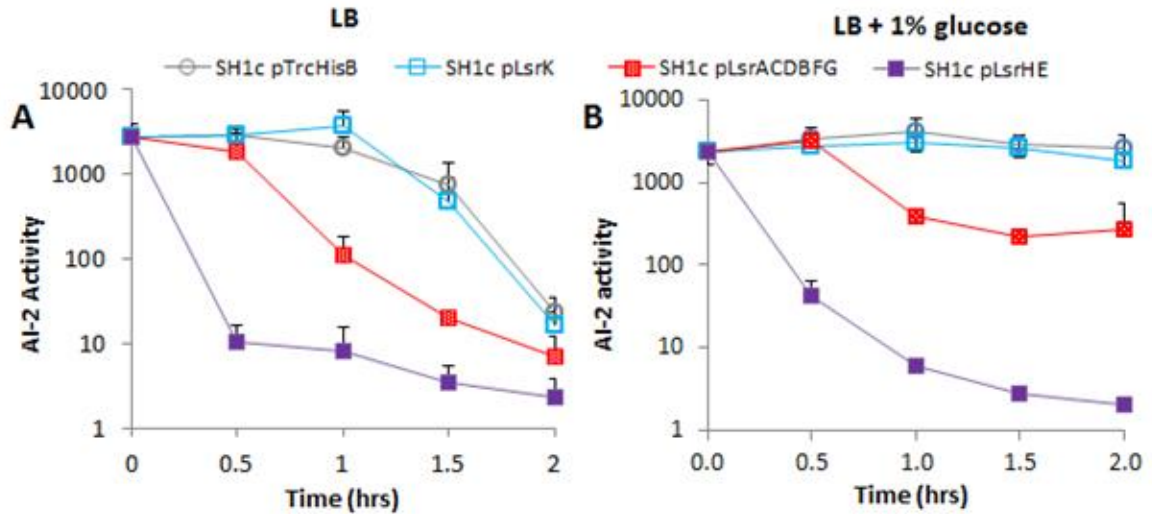
1444 analysis was performed using a FACSCanto II™ Flow Cytometer (Becton Dickinson) and all raw
1445 data were analyzed with BD FACSDiva™ 6.0 software (Becton Dickinson).

1446 **4.4 Results and Discussion**

1447 **4.4.1 AI-2 uptake profiles of controller cells with and without glucose**

1448 We characterized the uptake rates of our ‘controller cells’ by adding a fixed amount of
1449 exogenous AI-2 and monitoring AI-2 activity levels over time (**Figure 4/1A**). To determine this,
1450 we grew each culture in LB or LB supplemented with 1% glucose to an OD~0.4 and then added
1451 100 μM of AI-2. While all controller cells displayed uptake of AI-2 in the presence of LB (left
1452 panel), the SH1c pLsrHE was clearly the fastest, with a rapid quenching by the first 30 minute
1453 timepoint. The uptake rate of SH1c pLsrACDBFG, which showed the most rapid uptake in our
1454 prior work, illustrated faster uptake dynamics than the empty vector, but clearly slower than SH1c
1455 pLsrHE. The controller cell SH1c pLsrK showed no significant uptake differences than the empty
1456 vector. Our prior work had shown that overexpression of LsrK provides a significant increase in
1457 uptake rate in the $\Delta luxS$ knockout strain LW12, but we find here that in the $\Delta luxS \Delta lsrR$ double
1458 knockout strain, that plasmid expression of LsrK does not alter the uptake rates. This suggests by
1459 deleting *lsrR*, the gene responsible for the repression of the *lsr*-operon, the constant genomic
1460 transcription of *lsrK* already rapidly reduces intracellular AI-2 levels, so that additional
1461 overexpression of the kinase through pLsrK has negligible effects.

1462



1463

1464 **Figure 4.1: AI-2 uptake profiles.** Each plasmid was transformed into SH1c (W3110 $\Delta lsrR \Delta luxS$)
 1465 and grown to $OD \sim 0.4$ in either LB (Panel A) or LB supplemented with 1% glucose (Panel B)
 1466 before the addition of $100 \mu M$ of AI-2. AI-2 activity assays (see Methods) were used to measure
 1467 AI-2 levels. Experiment performed in biological triplicate.

1468 While all controller cells removed AI2 from the environment in LB, we expected the
 1469 addition of 1% glucose (**Figure 4.1B**) to interfere greatly with uptake in strains relying on
 1470 genomic transcription of at least one component of the *lsr*-system (i.e. SH1c with all plasmids
 1471 except pLsrHE). This effect on genomic transcription of the *lsr*-operon is attributed to the export
 1472 of cAMP out of the cell and down-regulation of catabolite repressor protein (CRP), which are
 1473 transcription factors for *lsr* gene transcription[125]. As expected, in the empty vector, the
 1474 extracellular AI-2 levels were not significantly reduced. Likewise, SH1c pLsrK showed no
 1475 significant drop in AI-2 levels, as the downregulation of the ABC-transporter did not allow
 1476 significant uptake of AI-2 for subsequent intracellular phosphorylation. While AI-2 can also enter
 1477 through the slower intracellular transport of the alternative system [130], these dynamics were
 1478 likely too slow to overcome the downregulation of genomic *lsrACDB*. Surprisingly, despite the
 1479 downregulation of genomic *lsrK*, SH1c pLsrACDBFG did reduce AI-2 from the extracellular
 1480 environment, albeit at a much slower rate compared to incubations with LB alone. Prior studies
 1481 have shown that *lsrK* knockouts do not reduce extracellular AI-2 concentrations, as the
 1482 phosphorylation of AI-2 by LsrK is needed to prevent secretion of AI-2 back into to the

1483 extracellular environment [32]. Therefore, we expected that SH1c pLsrACDBFG would exhibit a
1484 similar uptake profile as the empty vector in glucose due to the down-regulation of *lsrACDB*.
1485 This surprising reduction by SH1c pLsrACDBFG may be due to the second independent
1486 promoter of LsrK [125], and suggests that this promoter may not be directly influenced by CRP-
1487 cAMP. As expected, SH1c pLsrHE exhibited only a small reduction in uptake rate since the
1488 downregulation of genomic transcription of *lsr*-components was supplemented with the
1489 unaffected transcription from the two-promoter plasmids.

1490 **4.4.2 Quenching of protein expression**

1491 To demonstrate that the HE ‘controller cell’ can interfere with QS-dependent actions, we
1492 sought to interfere with W3110 pCT6 pET-EGFP, a reporter strain that generates and transduces
1493 the AI-2 signal to produce GFP. Previously, we have shown that we can quench protein
1494 expression in this reporter system, by inducing the controller cell culture for 3 hours and
1495 resuspending in a 1:1 mixture with the reporter system (in review). In **Figure 4.2**, we grew
1496 W3110 pCT6 pET-EGFP, SH1c pTrcHisB, and SH1c pLsrHE to OD~0.4, and co-cultured
1497 W3110 pCT6 pET-EGFP with SH1c pTrcHisB and SH1c pLsrHE for 6 hours at a range of
1498 mixture ratios. The empty vector could quench AI-2 at ratios of 1:1 compared to the reporter
1499 strain, but in proportions with higher amounts of the reporter strain, the amount of protein
1500 expression shifts higher. In contrast, co-cultures with our improved ‘controller cell’ SH1c pLsrHE
1501 quenched protein expression even at proportions as high as 8:1.

1502

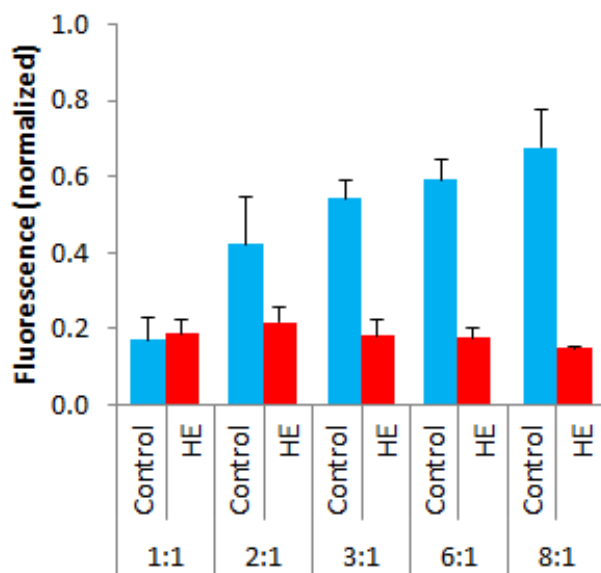


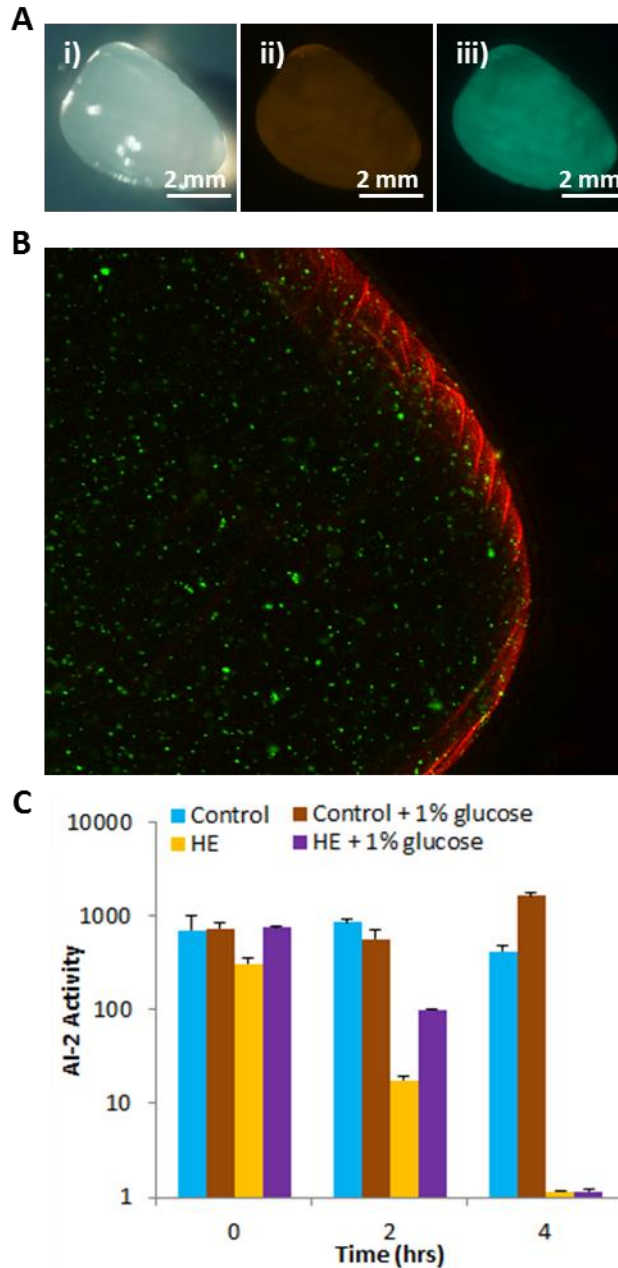
Figure 4.2. Modulation of protein expression. A range of concentration ratios of W3110 pCT6 pET-EGFP and SH1c pTrcHisB or SH1c pLsrHE are incubated for six hours before fluorescence intensity is measured on a plate reader and normalized to pure cultures of W3110 pCT6 pET-EGFP (positive control) and SH1c pTrcHisB (negative control). Experiment performed in biological duplicate.

1516

1517 4.4.3 Encapsulated bacteria remove extracellular AI-2

1518 We have previously shown the ability to encapsulate fusion proteins that could produce
 1519 AI-2 from the precursor, SAH, that would secrete from the capsule and signal QS-sensitive cells
 1520 [162]. Here, we sought to encapsulate controller cells to modulate QS expression through the
 1521 removal of AI-2 from the QS-dependent protein expression system. With an estimated pore size
 1522 of less than 17nm [163], bacteria are easily retained inside the alginate matrix [164,165], and we
 1523 used the well-studied alginate chitosan capsule method made through the extrusion technique
 1524 [166]. Alginate entraps the bacteria and is surrounded by a hard chitosan shell. The pores in the
 1525 alginate-chitosan allow small molecules such as AI-2 to pass, but contains larger items such as
 1526 enzymes and bacteria within. Briefly, bacteria were grown to an OD ~ 0.4-0.6, concentrated 5X,
 1527 and then mixed with a 2% alginate solution. The resulting mixture was added dropwise to a
 1528 stirring chitosan/CaCl₂ solution (see Methods). To confirm that the bacteria are contained within
 1529 the alginate matrix, we stained the bacterial membranes with calcein and used rhodamine dyed
 1530 chitosan to visualize the orientation of the capsule. As **Figure 4.3A** and **4.3B** illustrate, these

1531 chitosan forms a thin layer at the edge to provide support, and the bacteria are within the alginate
1532 inner core [162].
1533



1534

1535 **Figure 4.3: Encapsulated bacteria uptake profiles.** Bacteria are mixed with 2% alginate in a 1:1
 1536 ratio before being dropped into a chitosan-CaCl₂ mixture. Panel (A) shows a stereomicroscopic
 1537 (i) bright field image of the capsule (ii) RFP-filtered image of the rhodamine-labeled chitosan,
 1538 and (iii) GFP-filtered image of Syto9 labeled bacteria. Panel (B) is a confocal image of the
 1539 capsule with Syto9 labeled bacteria (green) and rhodamine labeled chitosan (red). Panel (C)
 1540 shows the AI-2 uptake profile of encapsulated bacteria. Concentrated (5X) SH1c pTrcHisB and
 1541 SH1c pLsrHE cultures in LB and LB supplemented with 1% glucose are mixed at a 1:1 ratio with
 1542 2% alginate before being dropped into a mixture of chitosan and CaCl₂ to encapsulate bacteria.
 1543 Four capsules are then placed in 2 mL of LB supplemented with 20 μM of AI-2, and samples are
 1544 harvested every 2 hours to measure AI-2 activity with AI-2 assays. Experiment performed in
 1545 biological triplicate and a representative sample is illustrated.

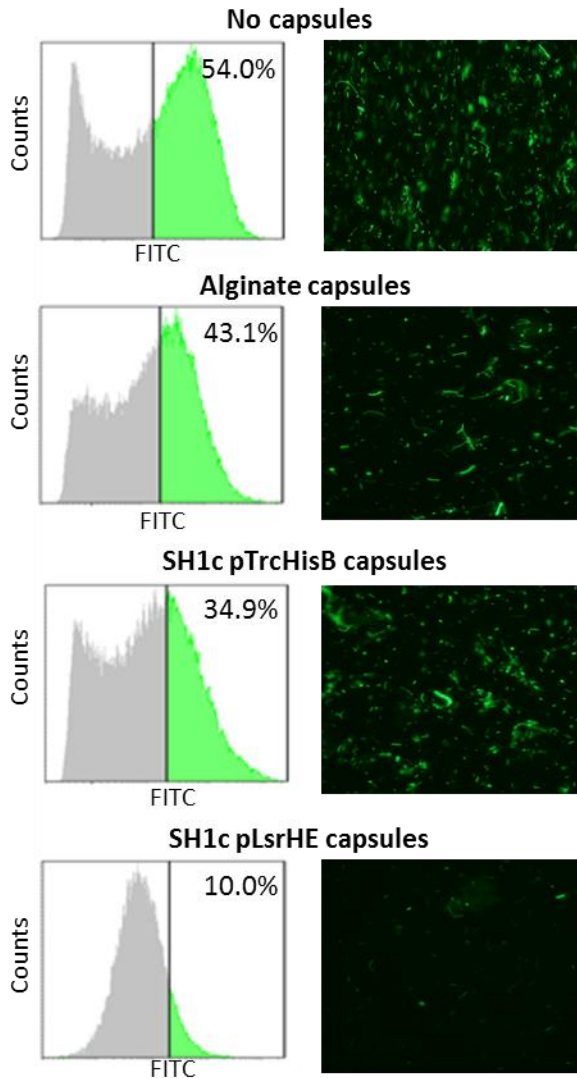
1546 Based on our prior work where entrapped enzymes inside the alginate-chitosan capsule
1547 could synthesize AI-2 that diffused out of the capsule [162], we encapsulated bacteria and tested
1548 the AI-2 uptake rate. Four capsules of SH1c pTrcHisB and SH1c pLsrHE were mixed with 20
1549 μM of exogenous AI-2, and AI-2 levels were monitored over time. As **Figure 4.3C** illustrates,
1550 encapsulated HE ‘controller cells’ remove exogenous AI-2 from the environment, either with or
1551 without glucose, while the empty vector did not show any detectable reduction in the AI-2
1552 environment. As in **Figure 4.1**, glucose only causes a small reduction in AI-2 uptake rate in SH1c
1553 pLsrHE. Bacterial load in each capsule was determined by dissolving each capsule in sodium
1554 citrate before and after incubation and streaking diluted portions on antibiotic selective plates.
1555 Colony-forming units (CFU) count showed an initial cell load of $\sim 1.1 \times 10^7$ cells that grew to a
1556 final count of $\sim 1.4 \times 10^8$ cells (data not shown).

1557 **4.4.4 Encapsulated HE ‘controller cell’ can quench and tune quorum sensing**

1558 We have shown that SH1c pLsrHE can quench protein expression of a QS-dependent
1559 system with a comparatively small amount of bacteria (**Figure 4.2**) and that encapsulated SH1c
1560 pLsrHE can remove exogenous AI-2 despite a limited bacterial load (**Figure 4.4**). We applied the
1561 encapsulated bacteria to growing cultures of W3110 pCT6 pET-EGFP to silence QS dependent
1562 communication (see Methods). As **Figure 4.5** shows, no capsules, alginate capsules and SH1c
1563 pTrcHisB encapsulated capsules all resulted in bimodal cell populations. Each of these cultures
1564 displayed a bimodal population, and microscopic images show a bright, fluorescent population. In
1565 incubations with SH1c pLsrSV, however, a unimodal population was observed and microscopic
1566 images display a much smaller and dimmer fluorescent population.

1567

1568

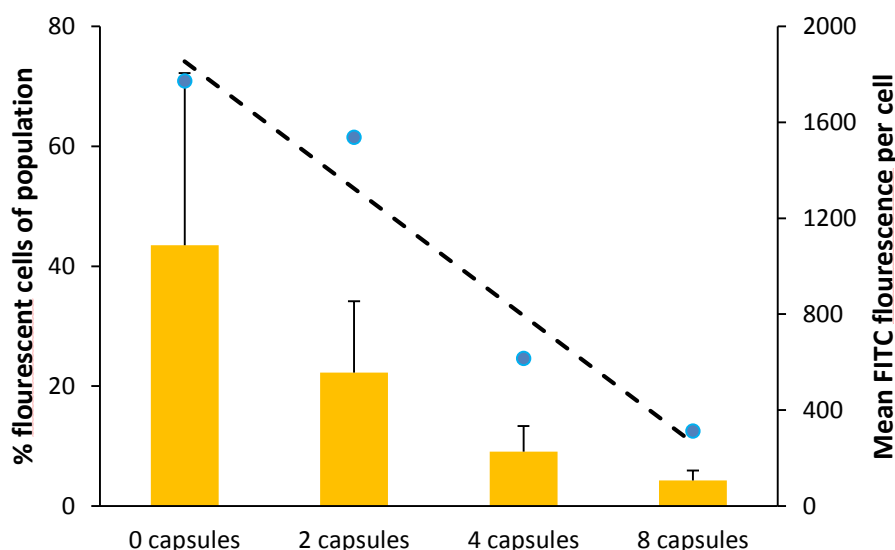


1569

1570 **Figure 4.4: Encapsulated bacteria silence cell-cell communication.** Cultures of W3110 pCT6 pET-
 1571 EGFP were grown to an $OD \sim 0.1$, and then incubated for 10 hours alone or with 8 capsules of
 1572 alginate, SH1c pTrcHisB, and SH1c pLsrS.V. Cultures were then evaluated using flow cytometry
 1573 (left panels) and microscopic images (right panels).

1574 Finally, we sought to externally “tune” autonomous protein expression through
 1575 encapsulated controller cells to obtain graduations of QS active subpopulations. Growing cultures
 1576 of W3110 pCT6 pET-EGFP were grown in the presence of 8, 4, and 2 capsules of HE ‘controller
 1577 cells’, as well as a culture without capsules. Capsules loaded with the HE ‘controller cell’ showed
 1578 a dose-dependent guiding of protein expression with the doubling of capsule dose from 2 to 4 to 8
 1579 causing a concomitant reduction in brightness and fluorescent cell population (**Figure 4.6**). A

1580 linear reduction in fluorescent population was observed ($R^2 = 0.94$), and a linear fit found a 22%
 1581 reduction in population with the doubling of capsule dosage. **Supplementary Figure 4.1** shows
 1582 the graduated reductions from a bimodal system (0 capsules) to a unimodal system (8 capsules).
 1583 **Supplementary Figure 4.2** displays the same information graphed on forward and side scatter.
 1584 Through the further development of mathematical models, we can envision the *a priori*
 1585 determination of QS-active subpopulations. While there has been promising work to develop
 1586 adjustable threshold switches through direct mediation of transcription or translation, this work
 1587 shows the first tunable protein expression system through the use of biocompatible capsules that
 1588 provide minimal interaction to the system.



1589

1590 **Figure 4.5: Tuning protein expression with varying doses of encapsulated bacteria.** Cultures of
 1591 W3110 pCT6 pET-EGFP were grown to an $OD \sim 0.1$, and then incubated for 10 hours alone or with
 1592 8, 4 and 2 capsules of SH1c pLsrHE. Cultures were then evaluated using flow cytometry with
 1593 data points (blue) representing the fluorescent population and bar graphs (yellow) representing
 1594 the mean fluorescence. A linear trendline is fitted to the fluorescent population and an R^2 value
 1595 is provided.

1596

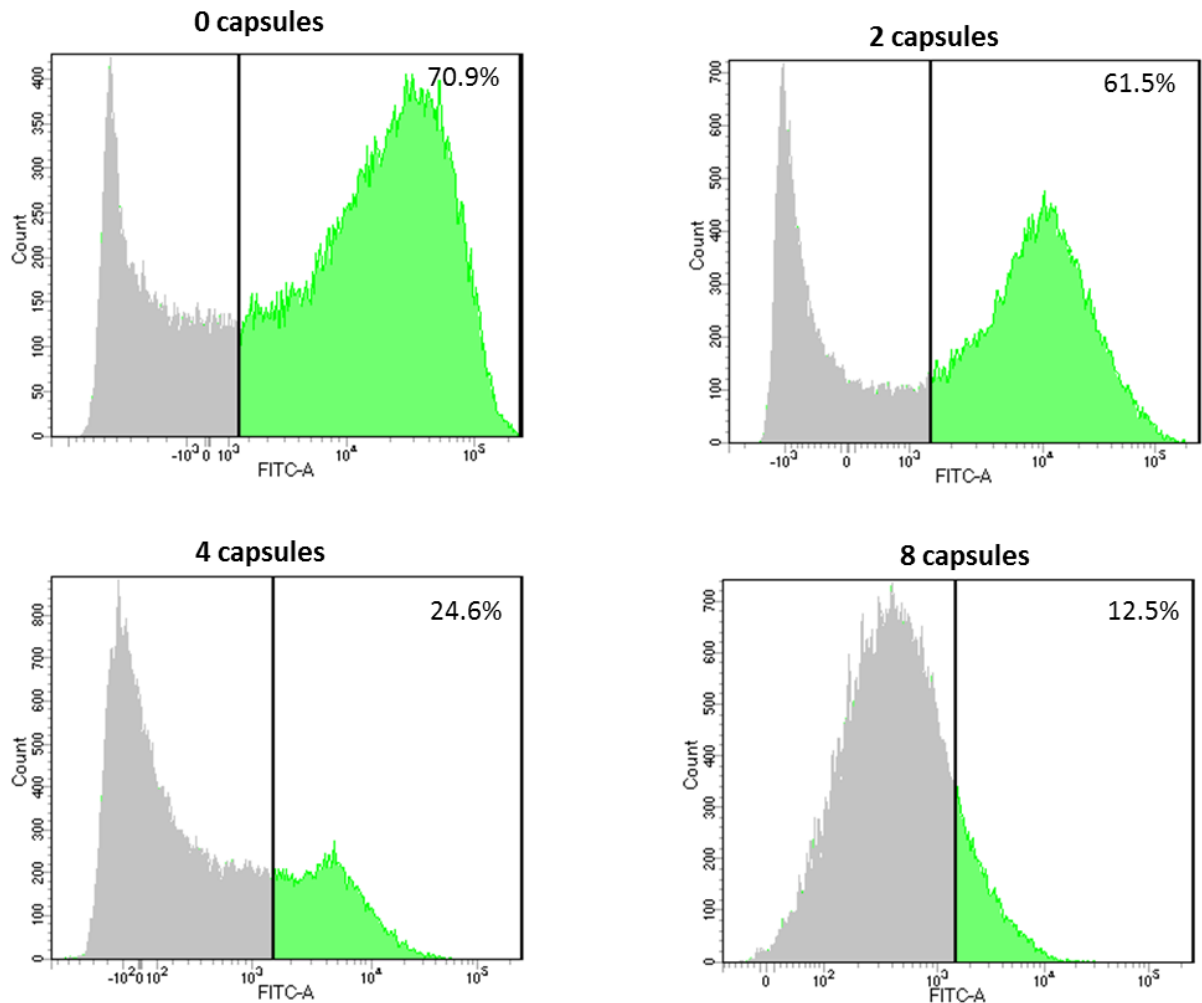
1597

1598

1599

1601

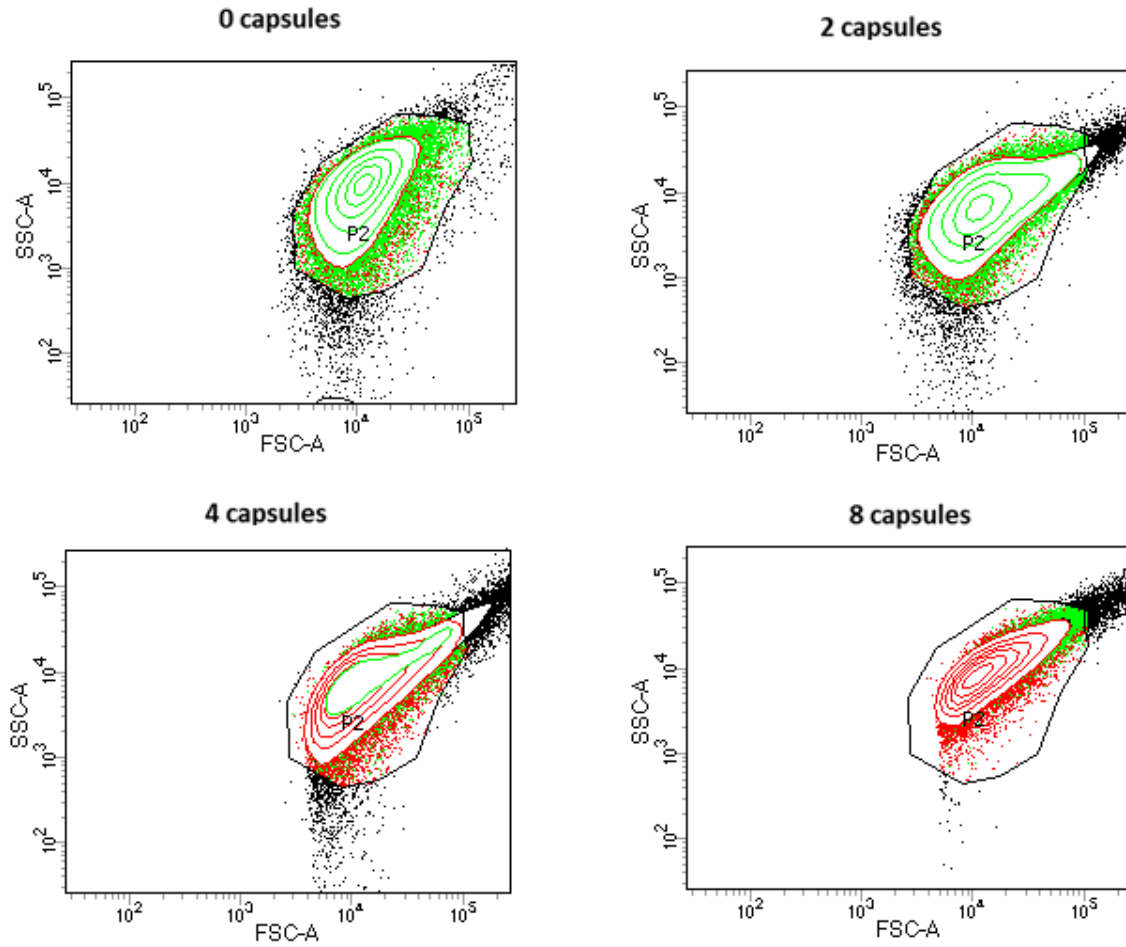
4.5 Supplemental Figures



1602

1603 **Figure S1: FACS histogram of EGFP expression with doses of encapsulated bacteria.** Cultures of
1604 W3110 pCT6 pET-EGFP were grown to an OD~0.1, and then incubated for 10 hours alone or with
1605 8, 4 and 2 capsules of SH1c pLsrHE. Cultures were then evaluated using flow cytometry.
1606 Percentages of fluorescent populations through gating is noted in the top right hand corner of
1607 each panel.

1608



1609

1610 **Figure S2: FACS histogram of EGFP expression with gating on side and forward scatter**
 1611 **illustrated.** Illustrated is Figure S1 graphed on gating for side and forward scatter. Black dots
 1612 indicate all events, red dots indicate a non-fluorescent event, and green dots indicate a
 1613 fluorescent event.

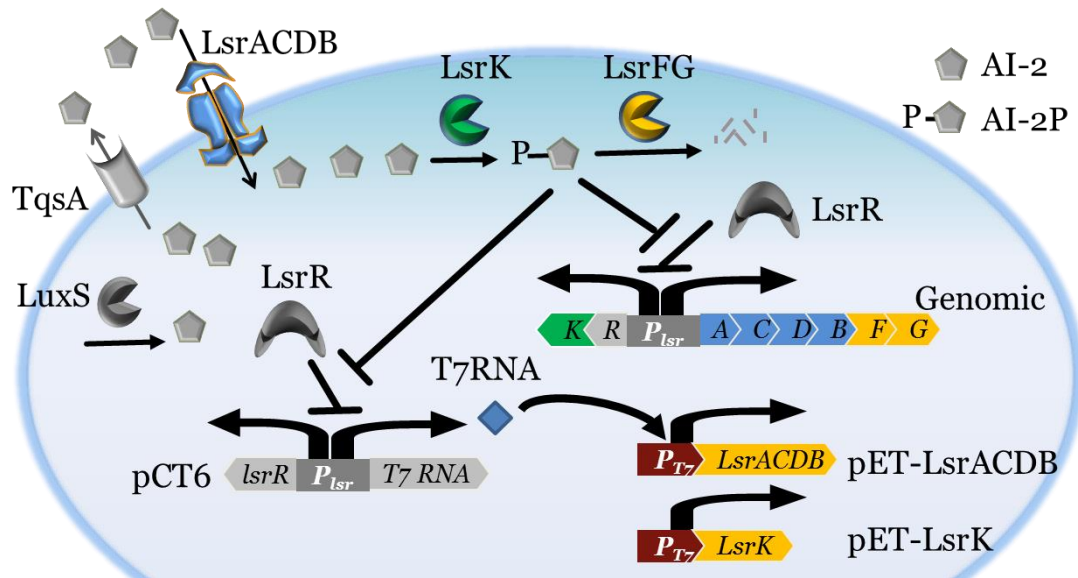
1614

1615 **Chapter 5: Autonomous cell-guided quorum quenching**

1616 In our group, we have leveraged QS systems to engineer protein expression systems that
1617 are driven by QS signaling molecules [14]. A central challenge in metabolic engineering is
1618 balancing the distribution of microbial resources to maximize overexpression pathways come at
1619 the expense of endogenous pathways, which has been described as a ‘zero-sum game’[109]. *E.*
1620 *coli*, the bacterium of choice for recombinant protein production, conveys the stress of
1621 overexpressing heterologous genes through AI-2 [116]. A creative approach to leveraging this
1622 behavior for protein production is to use QS to autonomously produce recombinant proteins,
1623 which we have done using *E. coli* and its ‘universal’ QS molecule, autoinducer-2 [167]. We wish
1624 to use this same approach to develop an autonomous ‘controller cell’. This is a direction that will
1625 provide a useful tool in situations where the use of autonomous “cell-mediated” cells is more
1626 preferable to the “user-mediated” approach as outlined in this work (Chapters 3 and 4), such as the
1627 use of “surveillance bacteria” in GI tracts.

1628 **5.2.1 Autonomous controller cell generates positive feedback loop**

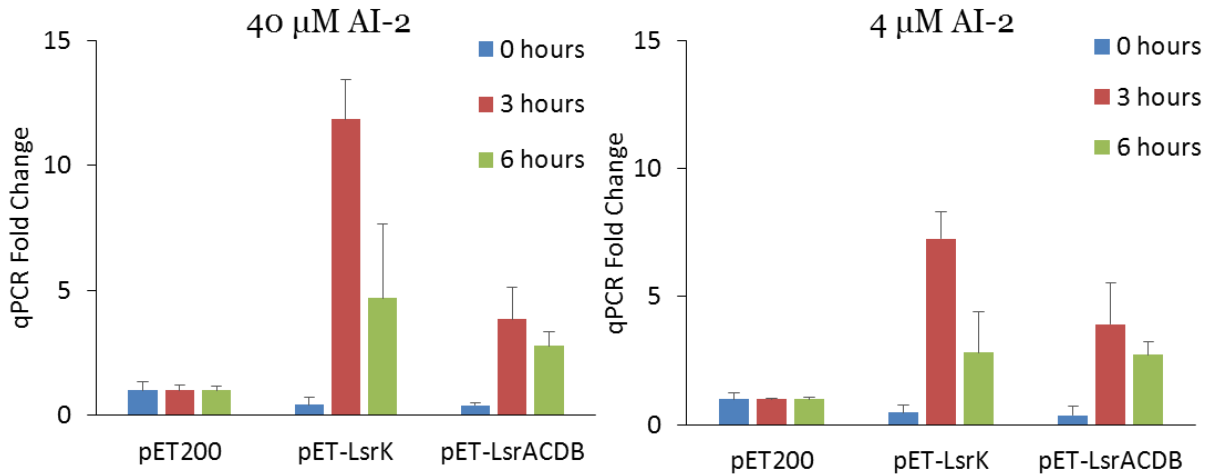
1629 In Chapters 3 and 4, we developed controller cells that were characterized with inducible
1630 or constitutive expression. While we believe these ‘user-mediated’ controller cells are useful in a
1631 variety of applications, one could envision autonomous ‘cell-mediated’ controller cells that are
1632 only active in the presence of the QS molecule AI-2. Used to interrogate and alter their
1633 environments, these autonomous controller cells would ideally be activated and sensitive to the
1634 the presence of AI-2, report a signal indicating the presence of the QS molecule, and actuate a
1635 response by uptaking AI-2 and processing the signal. We sought to enable this through the pCT6
1636 system. **Figure 5.1** shows the schematic, where phosphorylated AI-2 derepresses the pCT6
1637 plasmid causing the transcription of the pET plasmid. The pET plasmid, in this case makes LsrK
1638 or LsrACDB, instead of GFP. Phosphorylated AI-2 would cause the upregulation of the
1639 components responsible for the generation of phosphorylated AI-2.



1640

1641 **Figure 5.1: Schematic of 'autonomous controller cell'.** Phosphorylated AI-2 causes the
 1642 expression of T7RNA polymerase that transcribes LsrACDB and LsrK.
 1643

1644 We first show that this positive feedback loop indeed cause greater activation of the pET
 1645 plasmid, through qPCR, as seen in **Figure 5.2**. Strains were grown to an OD~0.4 and exogenous
 1646 AI-2 at 40 and 4 μM were added. qPCR results show greater expression of the pET transgene in
 1647 the pET-LsrK and pET-LsrACDB plasmids, than the empty vector pET200 control at both
 1648 concentrations. As expected, the extent of upregulation in the autonomous controller cells is
 1649 higher at 40 μM than 4 μM.

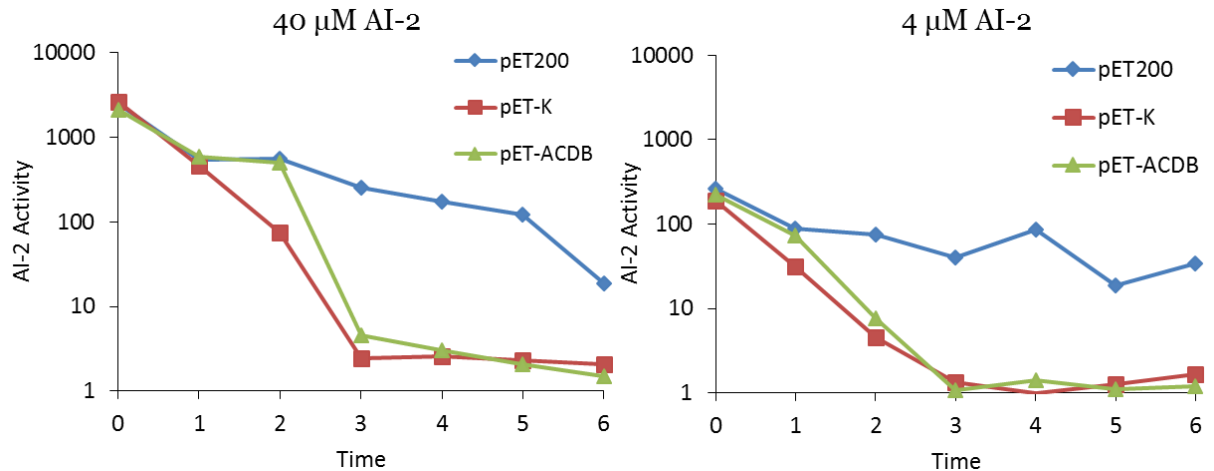


1650

1651 **Figure 5.2: qPCR of autonomous controller cells.** MDAI2 pCT6 with plasmids pET200, pET-LsrK
 1652 and pET-LsrACDB are grown to OD~0.4. Left panel shows qPCR results of pET transgene when 40
 1653 μM of AI-2 is added. Right panel shows qPCR results pET transgene when 4 μM of AI-2 is added.

1654 **5.2.2 Autonomous controller uptake AI-2 in accelerated fashion and increases sensitivity**

1655 We measured actuation by also monitoring the AI-2 levels in the experiment above (OD~
 1656 0.4 with the addition of exogenous AI-2). As **Figure 5.3** illustrates, when 40 μM of AI-2 is
 1657 added, the empty vector pET200 control shows a slow removal of AI-2 over the course of 6
 1658 hours. The autonomous controller cells, both rapidly clear AI-2 within 3 hours. When 4 μM of
 1659 AI-2 is added, the pET200 control is virtually unresponsive to the level AI-2, while the
 1660 autonomous cells once again remove AI-2 within 3 hours, illustrating the increased sensitivity of
 1661 these cells.



1662

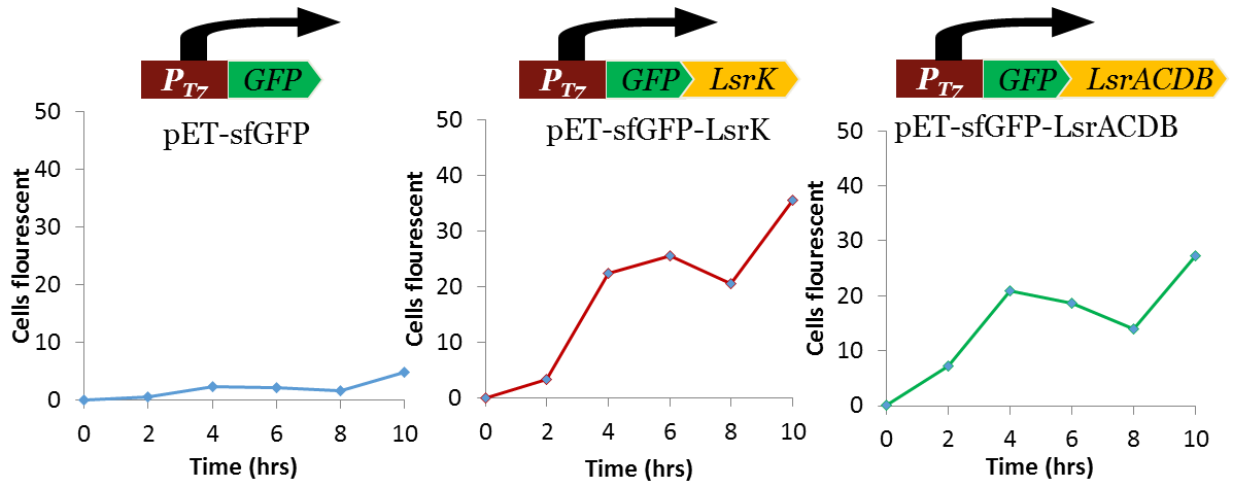
1663 **Figure 5.3: AI-2 uptake of autonomous controller cells.** MDAI2 pCT6 with plasmids pET200, pET-
 1664 LsrK and pET-LsrACDB are grown to OD~0.4. Left panel shows AI-2 levels when 40 μM of AI-2 is
 1665 added. Right panel shows AI-2 levels when 4 μM of AI-2 is added.

1666 5.2.3 Autonomous controller uptake provides signal of AI-2 uptake

1667 Lastly, we would like these autonomous cells to secrete a signal when they uptake AI-2.

1668 To enable this, we cloned a GFP reporter gene upstream of the *lsrACDB* and *lsrK* genes. We
 1669 grew the strains to OD~0.4 and added 40 μM of exogenous AI-2. Fluorescence was measured
 1670 with flow cytometry every 2 hours and the results are shown in **Figure 5.4**. By creating this
 1671 positive feedback loop that increases transcription of the pET transgene, the reporter gene is
 1672 expressed at much higher levels in the autonomous controller cells than in the empty vector
 1673 control.

1674



1675

1676 **Figure 5.4: AI-2 uptake of autonomous controller cells.** MDA12 pCT6 with plasmids pET-sfGFP,
 1677 pET-sfGFP-LsrK and pET-sfGFP-LsrACDB are grown to OD~0.4. Exogenous AI-2 (40 μ M) is added
 1678 and fluorescence is measured every 2 hours with flow cytometry.

1679 **5.3 Applications of autonomous controller cell**

1680 We believe the autonomous controller cells would be useful as a tool in both synthetic
 1681 and natural networks. We hope to input these bacteria inside an animal model and show that these
 1682 cells can interfere with QS-dependent phenotypes such as bioluminescence inside a living system.

1683

1684

1685 **Chapter 6: Conclusions, contributions and future directions**

1686

1687 **6.1 Summary**

1688 This dissertation details our work to investigate the interkingdom effects of the
1689 nonpathogenic *E. coli* secretome, including AI-2, on colonic epithelial cells, and the development
1690 of controller cells to guide intrakingdom phenotypes. This work has currently generated two
1691 published papers in mBio and Metabolic Engineering, an additional paper in preparation, and 5
1692 international conferences.

1693 We have shown here for the first time the global transcriptomic effects of the *E. coli*
1694 secretome on human epithelial cells. The secretome was shown to have an inflammatory
1695 response, with the upregulation of many genes in the cytokine-cytokine receptor pathway, the
1696 chemokine signaling pathway, and others, while also upregulating negative feedback regulators
1697 of the NOD-like signaling pathway and the NFkB pathway. We further show that AI-2 may also
1698 have a transcriptional inflammatory response that is initially upregulated at 6 hours before being
1699 downregulated at 24 hours. We hypothesize that this pattern fits the motif of a tight interplay
1700 between the host and microbiota, where metabolites can cause perturbations in the host cell which
1701 are restored through negative feedback elements[68].

1702 After determining the AI-2 may contribute an initial inflammatory response to IECs, we
1703 progressed to the second aim of our work, to develop ‘controller cells’ that could rapidly remove
1704 AI-2 and affect QS-dependent phenotypes. We selected a *luxS* null mutant that could not generate
1705 AI-2 as a host strain, and transformed inducible plasmids that overexpressed each aspect of the
1706 AI-2 uptake mechanism. We found two ‘knobs’ for AI-2 uptake: phosphorylation of AI-2 by
1707 LsrK and transport into the cell by LsrACDB. Our mathematical model closely recapitulated the
1708 experimental results, and our work provides a clearer elucidation of the dynamics involved in the
1709 *lsr*-system. We provide phenotypic applications such as chemotaxis and biofilm formation.

1710 Our overall goal was to develop controller cells that could modulate the target QS
1711 population while being sequestered in a separate environment. To do this, we extended the work
1712 by creating a HE controller cell that overexpresses every component of the *lsr*-system, save the
1713 repressor. We transform this inside a *luxS lsrR* double knockout mutant strain, a strain shown by
1714 Xavier et al, to provide more rapid uptake of AI-2 than a *luxS* null mutant alone [35]. We chose a
1715 single *luxS* mutant in the previous work to more clearly investigate the *lsr* dynamics, but in this
1716 work, to fully enable AI-2 uptake, we chose the double knockout strain. This HE controller cell
1717 provides the most rapid uptake of AI-2, without the addition of an inducing agent or the absence
1718 of glucose. This HE controller cell provides the needed rapid uptake to not only quench, but tune
1719 QS response while sequestered inside an alginate-chitosan capsule. This capsule provides a proof-
1720 of-concept to deliver encapsulated bacteria to modulate QS.

1721 Lastly, we developed an autonomous quorum quenching system that rapidly removes AI-
1722 2 without a stimulus. We have characterized the system with AI-2 kinetic rates, transcriptional
1723 profiles and protein expression. We plan to further characterize the system with a detailed
1724 mathematical model, and apply the system to *in vivo* murine models.

1725 **6.2 Contributions to Science**

1726 We provide the first global transcriptomic analysis of nonpathogenic *E. coli* secretome on
1727 epithelial cells, and reveal that IECs respond to secretomes by activating defense-related
1728 pathways. We found that IECs “listen in” on QS molecule AI-2, but modulate response at later
1729 times.

1730 We developed induced ‘controller cells’ that quench synthetic QS networks and applied these
1731 induced ‘controller cells’ to modulate QS-dependent phenotypes, including biofilm formation and
1732 chemotaxis. Through a mathematical model of our “controller cells”, we elucidated the
1733 mechanisms of AI-2 processing in the *lsr* system.

1734 Using the mathematical model we generated in our induced controller cells, we set about
1735 developing high-efficiency controller cells that uptake AI-2 at a fastest rate, without an inducing
1736 agent. In this application, we encapsulated HE cells inside biocompatible capsules and illustrated
1737 that it can quench and guide QS networks in discrete ‘quantized quorums’. Not only can this
1738 method be used to quench QS and study QS dependent phenotypes such as antibiotic resistance,
1739 but as the capsules hold in bacteria and most proteins, the effects of secretome on IECs may be
1740 minimized in *in vivo* applications.

1741 Lastly, we provide a quorum quenching platform that is self-directed. This provides the first
1742 quorum quenching application that is autonomous, and by rewiring the system, improve protein
1743 production yield. This system may be used in W3110 cells to improve the autonomous protein
1744 production system previously developed by our laboratory.

1745 **6.3 Future directions**

1746 We feel there are many exciting new directions and applications from this work. One
1747 application already mentioned is that the directed quantized quorums can be used to study
1748 quorum sensing dependent phenotypes. Previously, we have shown that by adding discrete
1749 quantities of AI-2, we can develop ‘self-assembled’ quorums using *luxS* knockout *E. coli* [151].
1750 However, this system requires knocking out the gene *luxS*, a vital gene in *E. coli* metabolism.
1751 Studying QS by removing *luxS* confounds the conclusions that can be drawn [168]. The HE-
1752 capsules allow a general platform to manipulate any *lsr*-autoinduction system, as well as possibly
1753 any AI-2 producing bacterial species, which numbers over 80 different species. By allowing the
1754 gradual reduction in QS population, we can determine answer QS questions, such as, “How many
1755 QS cells are needed to defend the population against an antibiotic?”

1756 While we have already mentioned using the autoinduced quorum quenching cells for an
1757 *in vivo* application, we could also use them as a rapid dynamic gene expression system. These
1758 systems have been hypothesized for use in microfluidic chips, where they are combined in a plug

1759 and play application [161]. Further, these cells could be used in a breadboard like production
1760 switchboard, where cells are localized [169] and respond rapidly to different intensities of the
1761 ‘universal’ AI-2 signal.

1762

1763

1764 **References**

1765

- 1766 1. Ng WL, Bassler BL (2009) Bacterial quorum-sensing network architectures. Annual review of
1767 genetics 43: 197-222.
- 1768 2. Jayaraman A, Wood TK (2008) Bacterial quorum sensing: signals, circuits, and implications for
1769 biofilms and disease. Annu Rev Biomed Eng 10: 145-167.
- 1770 3. Ahmer BMM (2004) Cell-to-cell signalling in Escherichia coli and Salmonella enterica.
1771 Molecular Microbiology 52: 933-945.
- 1772 4. Walters M, Sperandio V (2006) Quorum sensing in Escherichia coli and Salmonella.
1773 International Journal of Medical Microbiology 296: 125-131.
- 1774 5. Nealson K, Hastings JW (1979) Bacterial bioluminescence: its control and ecological
1775 significance. Microbiological reviews 43: 496.
- 1776 6. Nasser W, Reverchon S (2007) New insights into the regulatory mechanisms of the LuxR
1777 family of quorum sensing regulators. Analytical and bioanalytical chemistry 387: 381-
1778 390.
- 1779 7. Fuqua C, Greenberg EP (2002) Listening in on bacteria: acyl-homoserine lactone signalling.
1780 Nature Reviews Molecular Cell Biology 3: 685-695.
- 1781 8. Pereira CS, Thompson JA, Xavier KB (2013) AI-2-mediated signalling in bacteria. FEMS
1782 microbiology reviews 37: 156-181.
- 1783 9. Quan DN, Bentley WE (2012) Gene network homology in prokaryotes using a similarity search
1784 approach: Queries of quorum sensing signal transduction. PLoS computational biology 8:
1785 e1002637.
- 1786 10. Monod J, Jacob F. General conclusions: teleonomic mechanisms in cellular metabolism,
1787 growth, and differentiation; 1961. Cold Spring Harbor Laboratory Press. pp. 389-401.
- 1788 11. Gardner TS, Cantor CR, Collins JJ (2000) Construction of a genetic toggle switch in Escherichia
1789 coli. Nature 403: 339-342.
- 1790 12. Khalil AS, Collins JJ (2010) Synthetic biology: applications come of age. Nature Reviews
1791 Genetics 11: 367-379.
- 1792 13. Cameron DE, Bashor CJ, Collins JJ (2014) A brief history of synthetic biology. Nature Reviews
1793 Microbiology 12: 381-390.
- 1794 14. Tsao C-Y, Hooshangi S, Wu H-C, Valdes JJ, Bentley WE (2010) Autonomous induction of
1795 recombinant proteins by minimally rewiring native quorum sensing regulon of E. coli.
1796 Metabolic engineering 12: 291-297.
- 1797 15. Prindle A, Samayoa P, Razinkov I, Danino T, Tsimring LS, et al. (2012) A sensing array of
1798 radically coupled genetic 'biopixels'. Nature 481: 39-44.
- 1799 16. Balagaddé FK, Song H, Ozaki J, Collins CH, Barnet M, et al. (2008) A synthetic Escherichia coli
1800 predator-prey ecosystem. Molecular systems biology 4.
- 1801 17. Swofford CA, Van Dessel N, Forbes NS (2015) Quorum-sensing Salmonella selectively trigger
1802 protein expression within tumors. Proceedings of the National Academy of Sciences 112:
1803 3457-3462.
- 1804 18. Duan F, March JC (2010) Engineered bacterial communication prevents Vibrio cholerae
1805 virulence in an infant mouse model. Proceedings of the National Academy of Sciences
1806 107: 11260-11264.
- 1807 19. Silver PA, Way JC, Arnold FH, Meyerowitz JT (2014) Synthetic biology: Engineering explored.
1808 Nature 509: 166-167.

- 1809 20. Telford G, Wheeler D, Williams P, Tomkins P, Appleby P, et al. (1998) The *Pseudomonas*
1810 *aeruginosa* Quorum-Sensing Signal Molecule N-(3-Oxododecanoyl)-L-Homoserine Lactone
1811 Has Immunomodulatory Activity. *Infection and Immunity* 66: 36-42.
- 1812 21. Williams SC, Patterson EK, Carty NL, Griswold JA, Hamood AN, et al. (2004) *Pseudomonas*
1813 *aeruginosa* autoinducer enters and functions in mammalian cells. *Journal of*
1814 *bacteriology* 186: 2281-2287.
- 1815 22. Bryan A, Watters C, Koenig L, Youn E, Olmos A, et al. (2010) Human transcriptome analysis
1816 reveals a potential role for active transport in the metabolism of *Pseudomonas*
1817 *aeruginosa* autoinducers. *Microbes and Infection* 12: 1042-1050.
- 1818 23. Kendall MM, Sperandio V (2007) Quorum sensing by enteric pathogens. *Current opinion in*
1819 *gastroenterology* 23: 10-15.
- 1820 24. Sperandio V, Torres AG, Jarvis B, Nataro JP, Kaper JB (2003) Bacteria–host communication:
1821 the language of hormones. *Proceedings of the National Academy of Sciences* 100: 8951-
1822 8956.
- 1823 25. Shiner EK, Rumbaugh KP, Williams SC (2005) Interkingdom signaling: Deciphering the
1824 language of acyl homoserine lactones. *FEMS Microbiology Reviews* 29: 935-947.
- 1825 26. Arias CA, Murray BE (2009) Antibiotic-resistant bugs in the 21st century—a clinical super-
1826 challenge. *New England Journal of Medicine* 360: 439-443.
- 1827 27. Roy V, Adams BL, Bentley WE (2011) Developing next generation antimicrobials by
1828 intercepting AI-2 mediated quorum sensing. *Enzyme and Microbial Technology* 49: 113-
1829 123.
- 1830 28. García-Contreras R, Maeda T, Wood TK (2013) Resistance to quorum-quenching compounds.
1831 *Applied and environmental microbiology* 79: 6840-6846.
- 1832 29. Duan F, March JC (2008) Interrupting *Vibrio cholerae* infection of human epithelial cells with
1833 engineered commensal bacterial signaling. *Biotechnology and bioengineering* 101: 128-
1834 134.
- 1835 30. Wright JS, Jin R, Novick RP (2005) Transient interference with staphylococcal quorum sensing
1836 blocks abscess formation. *Proceedings of the National Academy of Sciences of the*
1837 *United States of America* 102: 1691-1696.
- 1838 31. LaSarre B, Federle MJ (2013) Exploiting Quorum Sensing To Confuse Bacterial Pathogens.
1839 *Microbiology and Molecular Biology Reviews* 77: 73-111.
- 1840 32. Roy V, Fernandes R, Tsao C-Y, Bentley WE (2010) Cross species quorum quenching using a
1841 native AI-2 processing enzyme. *ACS chemical biology* 5: 223-232.
- 1842 33. Roy V, Smith JA, Wang J, Stewart JE, Bentley WE, et al. (2010) Synthetic analogs tailor native
1843 AI-2 signaling across bacterial species. *Journal of the American Chemical Society* 132:
1844 11141-11150.
- 1845 34. Thompson JA, Oliveira RA, Djukovic A, Ubeda C, Xavier KB (2015) Manipulation of the
1846 Quorum Sensing Signal AI-2 Affects the Antibiotic-Treated Gut Microbiota. *Cell Reports*.
- 1847 35. Xavier KB, Bassler BL (2005) Interference with AI-2-mediated bacterial cell–cell
1848 communication. *Nature* 437: 750-753.
- 1849 36. Wang Z, Gerstein M, Snyder M (2009) RNA-Seq: a revolutionary tool for transcriptomics.
1850 *Nature Reviews Genetics* 10: 57-63.
- 1851 37. Ewing B, Hillier LD, Wendl MC, Green P (1998) Base-calling of automated sequencer traces
1852 using Phred. I. Accuracy assessment. *Genome research* 8: 175-185.
- 1853 38. Volkman SK, Sabeti PC, DeCaprio D, Neafsey DE, Schaffner SF, et al. (2006) A genome-wide
1854 map of diversity in *Plasmodium falciparum*. *Nature genetics* 39: 113-119.
- 1855 39. Trapnell C, Pachter L, Salzberg SL (2009) TopHat: discovering splice junctions with RNA-Seq.
1856 *Bioinformatics* 25: 1105-1111.

- 1857 40. Langmead B, Trapnell C, Pop M, Salzberg SL (2009) Ultrafast and memory-efficient alignment
1858 of short DNA sequences to the human genome. *Genome Biol* 10: R25.
- 1859 41. Thorvaldsdóttir H, Robinson JT, Mesirov JP (2012) Integrative Genomics Viewer (IGV): high-
1860 performance genomics data visualization and exploration. *Briefings in bioinformatics*.
- 1861 42. Anders S, Huber W (2010) Differential expression analysis for sequence count data. *Genome*
1862 *Biol* 11: R106.
- 1863 43. Tarca AL, Draghici S, Khatri P, Hassan SS, Mittal P, et al. (2009) A novel signaling pathway
1864 impact analysis. *Bioinformatics* 25: 75-82.
- 1865 44. Dwyer DJ, Kohanski MA, Collins JJ (2009) Role of reactive oxygen species in antibiotic action
1866 and resistance. *Current opinion in microbiology* 12: 482-489.
- 1867 45. Zargar A, Quan DN, Carter KK, Guo M, Sintim HO, et al. (2015) Bacterial Secretions of
1868 Nonpathogenic *Escherichia coli* Elicit Inflammatory Pathways: a Closer Investigation of
1869 Interkingdom Signaling. *mBio* 6: e00025-00015.
- 1870 46. Sekirov I, Russell SL, Antunes LCM, Finlay BB (2010) Gut microbiota in health and disease.
1871 *Physiological reviews* 90: 859-904.
- 1872 47. Peterson LW, Artis D (2014) Intestinal epithelial cells: regulators of barrier function and
1873 immune homeostasis. *Nature Reviews Immunology* 14: 141-153.
- 1874 48. Rakoff-Nahoum S, Paglino J, Eslami-Varzaneh F, Edberg S, Medzhitov R (2004) Recognition of
1875 Commensal Microflora by Toll-Like Receptors Is Required for Intestinal Homeostasis.
1876 *Cell* 118: 229-241.
- 1877 49. Bansal T, Alaniz RC, Wood TK, Jayaraman A (2010) The bacterial signal indole increases
1878 epithelial-cell tight-junction resistance and attenuates indicators of inflammation.
1879 *Proceedings of the National Academy of Sciences* 107: 228-233.
- 1880 50. Medzhitov R (2001) Toll-like receptors and innate immunity. *Nature Reviews Immunology* 1:
1881 135-145.
- 1882 51. Inohara N, Nunez G (2003) NODs: intracellular proteins involved in inflammation and
1883 apoptosis. *Nature Reviews Immunology* 3: 371-382.
- 1884 52. Creagh EM, O'Neill LA (2006) TLRs, NLRs and RLRs: a trinity of pathogen sensors that co-
1885 operate in innate immunity. *Trends in immunology* 27: 352-357.
- 1886 53. Nord CE, Kager L, Heimdahl A (1984) Impact of antimicrobial agents on the gastrointestinal
1887 microflora and the risk of infections. *The American journal of medicine* 76: 99-106.
- 1888 54. Lyte M (2013) Microbial Endocrinology in the Microbiome-Gut-Brain Axis: How Bacterial
1889 Production and Utilization of Neurochemicals Influence Behavior. *PLoS pathogens* 9:
1890 e1003726.
- 1891 55. Curtis MM, Sperandio V (2011) A complex relationship: the interaction among symbiotic
1892 microbes, invading pathogens, and their mammalian host. *Mucosal immunology* 4: 133-
1893 138.
- 1894 56. Hughes DT, Sperandio V (2008) Inter-kingdom signalling: communication between bacteria
1895 and their hosts. *Nature Reviews Microbiology* 6: 111-120.
- 1896 57. Iyer LM, Aravind L, Coon SL, Klein DC, Koonin EV (2004) Evolution of cell-cell signaling in
1897 animals: did late horizontal gene transfer from bacteria have a role? *TRENDS in Genetics*
1898 20: 292-299.
- 1899 58. Rutherford ST, Bassler BL (2012) Bacterial quorum sensing: its role in virulence and
1900 possibilities for its control. *Cold Spring Harbor perspectives in medicine* 2: a012427.
- 1901 59. Rasko DA, Sperandio V (2010) Anti-virulence strategies to combat bacteria-mediated
1902 disease. *Nature Reviews Drug Discovery* 9: 117-128.

- 1903 60. Borruel N, Casellas F, Antolín M, Llopis M, Carol M, et al. (2003) Effects of nonpathogenic
 1904 bacteria on cytokine secretion by human intestinal mucosa. *The American journal of*
 1905 *gastroenterology* 98: 865-870.
- 1906 61. Kelly D, Campbell JI, King TP, Grant G, Jansson EA, et al. (2004) Commensal anaerobic gut
 1907 bacteria attenuate inflammation by regulating nuclear-cytoplasmic shuttling of PPAR- γ
 1908 and RelA. *Nature immunology* 5: 104-112.
- 1909 62. Haller D, Bode C, Hammes WP, Pfeifer AMA, Schiffrin EJ, et al. (2000) Non-pathogenic
 1910 bacteria elicit a differential cytokine response by intestinal epithelial cell/leucocyte co-
 1911 cultures. *Gut* 47: 79-87.
- 1912 63. Kamada N, Maeda K, Inoue N, Hisamatsu T, Okamoto S, et al. (2008) Nonpathogenic
 1913 *Escherichia coli* Strain Nissle 1917 Inhibits Signal Transduction in Intestinal Epithelial
 1914 Cells. *Infection and Immunity* 76: 214-220.
- 1915 64. Lammers K, Helwig U, Swennen E, Rizzello F, Venturi A, et al. (2002) Effect of probiotic
 1916 strains on interleukin 8 production by HT29/19A cells. *The American journal of*
 1917 *gastroenterology* 97: 1182-1186.
- 1918 65. Martinez-Medina M, Aldeguer X, Lopez-Siles M, González-Huix F, López-Oliu C, et al. (2009)
 1919 Molecular diversity of *Escherichia coli* in the human gut: New ecological evidence
 1920 supporting the role of adherent-invasive *E. coli* (AIEC) in Crohn's disease. *Inflammatory*
 1921 *Bowel Diseases* 15: 872-882.
- 1922 66. Yoon SH, Han M-J, Jeong H, Lee CH, Xia X-X, et al. (2012) Comparative multi-omics systems
 1923 analysis of *Escherichia coli* strains B and K-12. *Genome Biol* 13: R37.
- 1924 67. Yoon S, Jeong H, Kwon S-K, Kim J (2009) Genomics, Biological Features, and Biotechnological
 1925 Applications of *Escherichia coli* B: "Is B for better?!". In: Lee S, editor. *Systems Biology*
 1926 *and Biotechnology of Escherichia coli*: Springer Netherlands. pp. 1-17.
- 1927 68. Lozupone CA, Stombaugh JI, Gordon JI, Jansson JK, Knight R (2012) Diversity, stability and
 1928 resilience of the human gut microbiota. *Nature* 489: 220-230.
- 1929 69. Bassler BL, Greenberg EP, Stevens AM (1997) Cross-species induction of luminescence in the
 1930 quorum-sensing bacterium *Vibrio harveyi*. *Journal of bacteriology* 179: 4043-4045.
- 1931 70. Baruch M, Belotserkovsky I, Hertzog BB, Ravins M, Dov E, et al. (2014) An Extracellular
 1932 Bacterial Pathogen Modulates Host Metabolism to Regulate Its Own Sensing and
 1933 Proliferation. *Cell* 156: 97-108.
- 1934 71. Kendall MM, Gruber CC, Parker CT, Sperandio V (2012) Ethanolamine controls expression of
 1935 genes encoding components involved in interkingdom signaling and virulence in
 1936 enterohemorrhagic *Escherichia coli* O157: H7. *MBio* 3: e00050-00012.
- 1937 72. Swamy M, Jamora C, Havran W, Hayday A (2010) Epithelial decision makers: in search of
 1938 the 'epimune'. *Nature immunology* 11: 656-665.
- 1939 73. Abreu MT, Vora P, Faure E, Thomas LS, Arnold ET, et al. (2001) Decreased expression of Toll-
 1940 like receptor-4 and MD-2 correlates with intestinal epithelial cell protection against
 1941 dysregulated proinflammatory gene expression in response to bacterial
 1942 lipopolysaccharide. *The Journal of Immunology* 167: 1609-1616.
- 1943 74. Naik S, Kelly EJ, Meijer L, Pettersson S, Sanderson IR (2001) Absence of Toll-like receptor 4
 1944 explains endotoxin hyporesponsiveness in human intestinal epithelium. *Journal of*
 1945 *pediatric gastroenterology and nutrition* 32: 449-453.
- 1946 75. Suzuki M, Hisamatsu T, Podolsky DK (2003) Gamma Interferon Augments the Intracellular
 1947 Pathway for Lipopolysaccharide (LPS) Recognition in Human Intestinal Epithelial Cells
 1948 through Coordinated Up-Regulation of LPS Uptake and Expression of the Intracellular
 1949 Toll-Like Receptor 4-MD-2 Complex. *Infection and Immunity* 71: 3503-3511.

- 1950 76. Jeon HJ, Choi J-H, Jung I-H, Park J-G, Lee M-R, et al. (2010) CD137 (4–1BB) deficiency reduces
1951 atherosclerosis in hyperlipidemic mice. *Circulation* 121: 1124-1133.
- 1952 77. Liew FY, Xu D, Brint EK, O'Neill LA (2005) Negative regulation of toll-like receptor-mediated
1953 immune responses. *Nature Reviews Immunology* 5: 446-458.
- 1954 78. Perkins ND (2007) Integrating cell-signalling pathways with NF-[kappa]B and IKK function.
1955 *Nat Rev Mol Cell Biol* 8: 49-62.
- 1956 79. Ma A, Malynn BA (2012) A20: linking a complex regulator of ubiquitylation to immunity and
1957 human disease. *Nature Reviews Immunology* 12: 774-785.
- 1958 80. Vereecke L, Beyaert R, van Loo G (2009) The ubiquitin-editing enzyme A20 (TNFAIP3) is a
1959 central regulator of immunopathology. *Trends in immunology* 30: 383-391.
- 1960 81. Hausmann E, Raisz L, Miller W (1970) Endotoxin: stimulation of bone resorption in tissue
1961 culture. *Science* 168: 862-864.
- 1962 82. Ishihara Y, Nishihara T, Maki E, Noguchi T, Koga T (1991) Role of interleukin-1 and
1963 prostaglandin in in vitro bone resorption induced by *Actinobacillus*
1964 *actinomycetemcomitans* lipopolysaccharide. *Journal of periodontal research* 26: 155-
1965 160.
- 1966 83. Angrisano T, Pero R, Peluso S, Keller S, Sacchetti S, et al. (2010) LPS-induced IL-8 activation in
1967 human intestinal epithelial cells is accompanied by specific histone H3 acetylation and
1968 methylation changes. *BMC microbiology* 10: 172.
- 1969 84. Pugin JM, Schürer-Maly C, Leturcq D, Moriarty A, Ulevitch RJ, et al. (1993)
1970 Lipopolysaccharide activation of human endothelial and epithelial cells is mediated by
1971 lipopolysaccharide-binding protein and soluble CD14. *Proceedings of the National*
1972 *Academy of Sciences* 90: 2744-2748.
- 1973 85. Cario E, Rosenberg IM, Brandwein SL, Beck PL, Reinecker H-C, et al. (2000)
1974 Lipopolysaccharide activates distinct signaling pathways in intestinal epithelial cell lines
1975 expressing Toll-like receptors. *The Journal of Immunology* 164: 966-972.
- 1976 86. Studier FW, Daegelen P, Lenski RE, Maslov S, Kim JF (2009) Understanding the Differences
1977 between Genome Sequences of *Escherichia coli* B Strains REL606 and BL21(DE3) and
1978 Comparison of the *E. coli* B and K-12 Genomes. *Journal of Molecular Biology* 394: 653-
1979 680.
- 1980 87. Pereira CS, de Regt AK, Brito PH, Miller ST, Xavier KB (2009) Identification of functional LsrB-
1981 like autoinducer-2 receptors. *Journal of bacteriology* 191: 6975-6987.
- 1982 88. Li J, Wang L, Hashimoto Y, Tsao CY, Wood TK, et al. (2006) A stochastic model of *Escherichia*
1983 *coli* AI-2 quorum signal circuit reveals alternative synthesis pathways. *Molecular systems*
1984 *biology* 2.
- 1985 89. Mota LJ, Cornelis GR (2005) The bacterial injection kit: type III secretion systems. *Annals of*
1986 *medicine* 37: 234-249.
- 1987 90. Tateda K, Ishii Y, Horikawa M, Matsumoto T, Miyairi S, et al. (2003) The *Pseudomonas*
1988 *aeruginosa* autoinducer N-3-oxododecanoyl homoserine lactone accelerates apoptosis
1989 in macrophages and neutrophils. *Infection and Immunity* 71: 5785-5793.
- 1990 91. Shiner E, Terentyev D, Bryan A, Sennoune S, Martinez-Zaguilan R, et al. (2006) *Pseudomonas*
1991 *aeruginosa* autoinducer modulates host cell responses through calcium signalling.
1992 *Cellular microbiology* 8: 1601-1610.
- 1993 92. Karlin D, Mastromarino A, Jones R, Stroehlein J, Lorentz O (1985) Fecal skatole and indole
1994 and breath methane and hydrogen in patients with large bowel polyps or cancer.
1995 *Journal of cancer research and clinical oncology* 109: 135-141.

- 1996 93. Zuccato E, Venturi M, Di Leo G, Colombo L, Bertolo C, et al. (1993) Role of bile acids and
1997 metabolic activity of colonic bacteria in increased risk of colon cancer after
1998 cholecystectomy. *Digestive diseases and sciences* 38: 514-519.
- 1999 94. Zhu J, Pei D (2008) A LuxP-Based Fluorescent Sensor for Bacterial Autoinducer II. *ACS*
2000 *Chemical Biology* 3: 110-119.
- 2001 95. Charlton TS, De Nys R, Netting A, Kumar N, Hentzer M, et al. (2000) A novel and sensitive
2002 method for the quantification of N-3-oxoacyl homoserine lactones using gas
2003 chromatography–mass spectrometry: application to a model bacterial biofilm.
2004 *Environmental Microbiology* 2: 530-541.
- 2005 96. Zargar A, Quan DN, Emamian M, Tsao CY, Wu H-C, et al. (2015) Rational design of ‘controller
2006 cells’ to manipulate protein and phenotype expression. *Metabolic engineering* 30: 61-
2007 68.
- 2008 97. Bailey JE (1991) Toward a science of metabolic engineering. *Science* 252: 1668-1675.
- 2009 98. Stephanopoulos G, Vallino JJ (1991) Network rigidity and metabolic engineering in
2010 metabolite overproduction. *Science(Washington)* 252: 1675-1681.
- 2011 99. Jarboe LR, Zhang X, Wang X, Moore JC, Shanmugam K, et al. (2010) Metabolic engineering
2012 for production of biorenewable fuels and chemicals: contributions of synthetic biology.
2013 *BioMed Research International* 2010.
- 2014 100. Stephanopoulos G, Kelleher J (2001) How to make a superior cell. *Science* 292: 2024-2025.
- 2015 101. Kramer BP, Fischer M, Fussenegger M (2005) Semi-synthetic mammalian gene regulatory
2016 networks. *Metabolic engineering* 7: 241-250.
- 2017 102. Malphettes L, Fussenegger M (2006) Impact of RNA interference on gene networks.
2018 *Metabolic engineering* 8: 672-683.
- 2019 103. Boyle PM, Silver PA (2012) Parts plus pipes: synthetic biology approaches to metabolic
2020 engineering. *Metabolic engineering* 14: 223-232.
- 2021 104. Keasling JD (2012) Synthetic biology and the development of tools for metabolic
2022 engineering. *Metabolic engineering* 14: 189-195.
- 2023 105. Weber W, Fussenegger M (2011) Molecular diversity—the toolbox for synthetic gene
2024 switches and networks. *Current opinion in chemical biology* 15: 414-420.
- 2025 106. Purnick PE, Weiss R (2009) The second wave of synthetic biology: from modules to systems.
2026 *Nature reviews Molecular cell biology* 10: 410-422.
- 2027 107. Nielsen J, Fussenegger M, Keasling J, Lee SY, Liao JC, et al. (2014) Engineering synergy in
2028 biotechnology. *Nature chemical biology* 10: 319-322.
- 2029 108. Way JC, Collins JJ, Keasling JD, Silver PA (2014) Integrating Biological Redesign: Where
2030 Synthetic Biology Came From and Where It Needs to Go. *Cell* 157: 151-161.
- 2031 109. Solomon KV, Prather KL (2011) The zero-sum game of pathway optimization: Emerging
2032 paradigms for tuning gene expression. *Biotechnology journal* 6: 1064-1070.
- 2033 110. Farmer WR, Liao JC (2000) Improving lycopene production in *Escherichia coli* by
2034 engineering metabolic control. *Nature biotechnology* 18: 533-537.
- 2035 111. Kobayashi H, Kærn M, Araki M, Chung K, Gardner TS, et al. (2004) Programmable cells:
2036 interfacing natural and engineered gene networks. *Proceedings of the National*
2037 *Academy of Sciences of the United States of America* 101: 8414-8419.
- 2038 112. Tsao C-Y, Quan DN, Bentley WE (2012) Development of the quorum sensing
2039 biotechnological toolbox. *Current Opinion in Chemical Engineering* 1: 396-402.
- 2040 113. Fuqua WC, Winans SC, Greenberg EP (1994) Quorum sensing in bacteria: the LuxR-LuxI
2041 family of cell density-responsive transcriptional regulators. *Journal of bacteriology* 176:
2042 269.

- 2043 114. Surette MG, Bassler BL (1998) Quorum sensing in *Escherichia coli* and *Salmonella*
 2044 typhimurium. *Proceedings of the National Academy of Sciences* 95: 7046-7050.
- 2045 115. Bentley WE, Mirjalili N, Andersen DC, Davis RH, Kompala DS (1990) Plasmid-encoded
 2046 protein: the principal factor in the "metabolic burden" associated with recombinant
 2047 bacteria. *Biotechnology and bioengineering* 35: 668-681.
- 2048 116. DeLisa MP, Valdes JJ, Bentley WE (2001) Quorum signaling via AI-2 communicates the
 2049 "Metabolic Burden" associated with heterologous protein production in *Escherichia coli*.
 2050 *Biotechnology and bioengineering* 75: 439-450.
- 2051 117. Tsao C-Y, Wang L, Hashimoto Y, Yi H, March JC, et al. (2011) LuxS Coexpression Enhances
 2052 Yields of Recombinant Proteins in *Escherichia coli* in Part through Posttranscriptional
 2053 Control of GroEL. *Applied and Environmental Microbiology* 77: 2141-2152.
- 2054 118. Kuipers OP, de Ruyter PG, Kleerebezem M, de Vos WM (1998) Quorum sensing-controlled
 2055 gene expression in lactic acid bacteria. *Journal of Biotechnology* 64: 15-21.
- 2056 119. Tamsir A, Tabor JJ, Voigt CA (2011) Robust multicellular computing using genetically
 2057 encoded NOR gates and chemical 'wires'. *Nature* 469: 212-215.
- 2058 120. Wood TK, Hong SH, Ma Q (2011) Engineering biofilm formation and dispersal. *Trends in*
 2059 *Biotechnology* 29: 87-94.
- 2060 121. Basu S, Mehreja R, Thiberge S, Chen M-T, Weiss R (2004) Spatiotemporal control of gene
 2061 expression with pulse-generating networks. *Proceedings of the National Academy of*
 2062 *Sciences of the United States of America* 101: 6355-6360.
- 2063 122. Carter KK, Valdes JJ, Bentley WE (2012) Pathway engineering via quorum sensing and sRNA
 2064 riboregulators—interconnected networks and controllers. *Metabolic engineering* 14:
 2065 281-288.
- 2066 123. Sambrook J, Fritsch EF, Maniatis T (1989) *Molecular cloning: Cold spring harbor laboratory*
 2067 *press New York*.
- 2068 124. Gibson DG, Young L, Chuang R-Y, Venter JC, Hutchison CA, et al. (2009) Enzymatic assembly
 2069 of DNA molecules up to several hundred kilobases. *Nat Meth* 6: 343-345.
- 2070 125. Wang L, Hashimoto Y, Tsao C-Y, Valdes JJ, Bentley WE (2005) Cyclic AMP (cAMP) and cAMP
 2071 receptor protein influence both synthesis and uptake of extracellular autoinducer 2 in
 2072 *Escherichia coli*. *Journal of bacteriology* 187: 2066-2076.
- 2073 126. Zargar A, Quan DN, Carter KK, Guo M, Sintim HO, et al. (2015) Bacterial Secretions of
 2074 Nonpathogenic *Escherichia coli* Elicit Inflammatory Pathways: a Closer Investigation of
 2075 Interkingdom Signaling. *mBio* 6.
- 2076 127. Smith JAI, Wang J, Nguyen-Mau S-M, Lee V, Sintim HO (2009) Biological screening of a
 2077 diverse set of AI-2 analogues in *Vibrio harveyi* suggests that receptors which are
 2078 involved in synergistic agonism of AI-2 and analogues are promiscuous. *Chemical*
 2079 *Communications*: 7033-7035.
- 2080 128. Liu Y, Terrell JL, Tsao CY, Wu HC, Javvaji V, et al. (2012) Biofabricating Multifunctional Soft
 2081 Matter with Enzymes and Stimuli-Responsive Materials. *Advanced Functional Materials*
 2082 22: 3004-3012.
- 2083 129. Wu HC, Tsao CY, Quan DN, Cheng Y, Servinsky MD, et al. (2013) Autonomous bacterial
 2084 localization and gene expression based on nearby cell receptor density. *Molecular*
 2085 *systems biology* 9.
- 2086 130. Hooshangi S, Bentley WE (2011) LsrR quorum sensing "switch" is revealed by a bottom-up
 2087 approach. *PLoS computational biology* 7: e1002172.
- 2088 131. Taga ME, Miller ST, Bassler BL (2003) Lsr-mediated transport and processing of AI-2 in
 2089 *Salmonella typhimurium*. *Molecular Microbiology* 50: 1411-1427.

- 2090 132. Xue T, Zhao L, Sun H, Zhou X, Sun B (2009) LsrR-binding site recognition and regulatory
2091 characteristics in Escherichia coli AI-2 quorum sensing. *Cell Res* 19: 1258-1268.
- 2092 133. Xavier KB, Miller ST, Lu W, Kim JH, Rabinowitz J, et al. (2007) Phosphorylation and
2093 Processing of the Quorum-Sensing Molecule Autoinducer-2 in Enteric Bacteria. *ACS*
2094 *Chemical Biology* 2: 128-136.
- 2095 134. Marques JC, Lamosa P, Russell C, Ventura R, Maycock C, et al. (2011) Processing the
2096 Interspecies Quorum-sensing Signal Autoinducer-2 (AI-2): Characterization of phospho-
2097 (S)-4,5-dihydroxy-2,3-pentanedione isomerization by LsrG Protein *Journal of Biological*
2098 *Chemistry* 286: 18331-18343.
- 2099 135. Li J, Wang L, Hashimoto Y, Tsao CY, Wood TK, et al. (2006) A stochastic model of Escherichia
2100 coli AI-2 quorum signal circuit reveals alternative synthesis pathways. *Molecular systems*
2101 *biology* 2.
- 2102 136. Barrios AFG, Zuo R, Hashimoto Y, Yang L, Bentley WE, et al. (2006) Autoinducer 2 controls
2103 biofilm formation in Escherichia coli through a novel motility quorum-sensing regulator
2104 (MqsR, B3022). *Journal of bacteriology* 188: 305-316.
- 2105 137. Hegde M, Englert DL, Schrock S, Cohn WB, Vogt C, et al. (2011) Chemotaxis to the quorum-
2106 sensing signal AI-2 requires the Tsr chemoreceptor and the periplasmic LsrB AI-2-binding
2107 protein. *Journal of bacteriology* 193: 768-773.
- 2108 138. Lu TK, Khalil AS, Collins JJ (2009) Next-generation synthetic gene networks. *Nat Biotech* 27:
2109 1139-1150.
- 2110 139. Shong J, Jimenez Diaz MR, Collins CH (2012) Towards synthetic microbial consortia for
2111 bioprocessing. *Current Opinion in Biotechnology* 23: 798-802.
- 2112 140. Marchand N, Collins CH (2013) Peptide-based communication system enables Escherichia
2113 coli to Bacillus megaterium interspecies signaling. *Biotechnology and bioengineering*
2114 110: 3003-3012.
- 2115 141. Hooshangi S, Bentley WE (2008) From unicellular properties to multicellular behavior:
2116 bacteria quorum sensing circuitry and applications. *Current Opinion in Biotechnology*
2117 19: 550-555.
- 2118 142. Aurand TC, Russell MS, March JC (2012) Synthetic signaling networks for therapeutic
2119 applications. *Current Opinion in Biotechnology* 23: 773-779.
- 2120 143. Xavier KB, Bassler BL (2005) Regulation of Uptake and Processing of the Quorum-Sensing
2121 Autoinducer AI-2 in Escherichia coli. *Journal of bacteriology* 187: 238-248.
- 2122 144. Herzberg M, Kaye IK, Peti W, Wood TK (2006) YdgG (TqsA) Controls Biofilm Formation in
2123 Escherichia coli K-12 through Autoinducer 2 Transport. *Journal of bacteriology* 188: 587-
2124 598.
- 2125 145. Swinnen IAM, Bernaerts K, Dens EJJ, Geeraerd AH, Van Impe JF (2004) Predictive modelling
2126 of the microbial lag phase: a review. *International Journal of Food Microbiology* 94: 137-
2127 159.
- 2128 146. Koseki S, Nonaka J (2012) Alternative approach to modeling bacterial lag time, using logistic
2129 regression as a function of time, temperature, pH, and sodium chloride concentration.
2130 *Applied and Environmental Microbiology* 78: 6103-6112.
- 2131 147. Mertens L, Van Derlinden E, Van Impe JF (2012) Comparing experimental design schemes in
2132 predictive food microbiology: optimal parameter estimation of secondary models.
2133 *Journal of Food Engineering* 112: 119-133.
- 2134 148. Cuny C, Lesbats M, Dukan S (2007) Induction of a Global Stress Response during the First
2135 Step of Escherichia coli Plate Growth. *Applied and Environmental Microbiology* 73: 885-
2136 889.

- 2137 149. Baranyi J, Roberts TA (1994) A dynamic approach to predicting bacterial growth in food.
2138 International Journal of Food Microbiology 23: 277-294.
- 2139 150. Koop AH, Hartley ME, Bourgeois S (1987) A low-copy-number vector utilizing β -
2140 galactosidase for the analysis of gene control elements. Gene 52: 245-256.
- 2141 151. Servinsky MD, Terrell JL, Tsao C-Y, Wu H-C, Quan DN, et al. (2015) Directed assembly of a
2142 bacterial quorum. The ISME journal.
- 2143 152. Choudhary S, Schmidt-Dannert C (2010) Applications of quorum sensing in biotechnology.
2144 Applied microbiology and biotechnology 86: 1267-1279.
- 2145 153. You L, Cox RS, Weiss R, Arnold FH (2004) Programmed population control by cell-cell
2146 communication and regulated killing. Nature 428: 868-871.
- 2147 154. Weber W, Daoud-El Baba M, Fussenegger M (2007) Synthetic ecosystems based on
2148 airborne inter- and intrakingdom communication. Proceedings of the National Academy
2149 of Sciences 104: 10435-10440.
- 2150 155. Dong Y-H, Zhang L-H (2005) Quorum sensing and quorum-quenching enzymes. J Microbiol
2151 43: 101-109.
- 2152 156. Prindle A, Selimkhanov J, Li H, Razinkov I, Tsimring LS, et al. (2014) Rapid and tunable post-
2153 translational coupling of genetic circuits. Nature 508: 387-391.
- 2154 157. Cameron DE, Collins JJ (2014) Tunable protein degradation in bacteria. Nat Biotech 32:
2155 1276-1281.
- 2156 158. Callura JM, Dwyer DJ, Isaacs FJ, Cantor CR, Collins JJ (2010) Tracking, tuning, and
2157 terminating microbial physiology using synthetic riboregulators. Proceedings of the
2158 National Academy of Sciences 107: 15898-15903.
- 2159 159. Deans TL, Cantor CR, Collins JJ (2007) A tunable genetic switch based on RNAi and repressor
2160 proteins for regulating gene expression in mammalian cells. Cell 130: 363-372.
- 2161 160. Basu S, Gerchman Y, Collins CH, Arnold FH, Weiss R (2005) A synthetic multicellular system
2162 for programmed pattern formation. Nature 434: 1130-1134.
- 2163 161. Bentley WE, Zargar A, Payne GF (2013) Plug and Play? Interconnected multifunctional chips
2164 for enhancing efficiency of biopharmaceutical R&D. Pharmaceutical Bioprocessing 1:
2165 225-228.
- 2166 162. Gupta A, Terrell JL, Fernandes R, Dowling MB, Payne GF, et al. (2013) Encapsulated fusion
2167 protein confers "sense and respond" activity to chitosan-alginate capsules to
2168 manipulate bacterial quorum sensing. Biotechnology and bioengineering 110: 552-562.
- 2169 163. Klein J, Stock J, Vorlop KD (1983) Pore size and properties of spherical Ca-alginate
2170 biocatalysts. European journal of applied microbiology and biotechnology 18: 86-91.
- 2171 164. Lin J, Yu W, Liu X, Xie H, Wang W, et al. (2008) In Vitro and in Vivo characterization of
2172 alginate-chitosan-alginate artificial microcapsules for therapeutic oral delivery of live
2173 bacterial cells. Journal of Bioscience and Bioengineering 105: 660-665.
- 2174 165. Park SJ, Lee YK, Cho S, Uthaman S, Park IK, et al. (2014) Effect of chitosan coating on a
2175 bacteria-based alginate microrobot. Biotechnology and bioengineering.
- 2176 166. Krasaekoopt W, Bhandari B, Deeth H (2003) Evaluation of encapsulation techniques of
2177 probiotics for yoghurt. International Dairy Journal 13: 3-13.
- 2178 167. Tsao C-Y, Hooshangi S, Wu H-C, Valdes JJ, Bentley WE (2010) Autonomous induction of
2179 recombinant proteins by minimally rewiring native quorum sensing regulon of *E. coli*.
2180 Metabolic engineering 12: 291-297.
- 2181 168. Vendeville A, Winzer K, Heurlier K, Tang CM, Hardie KR (2005) Making 'sense' of metabolism:
2182 autoinducer-2, LuxS and pathogenic bacteria. Nature Reviews Microbiology 3: 383-396.

2183 169. Betz JF, Cheng Y, Tsao C-Y, Zargar A, Wu H-C, et al. (2013) Optically clear alginate hydrogels
2184 for spatially controlled cell entrapment and culture at microfluidic electrode surfaces.
2185 Lab on a Chip 13: 1854-1858.
2186
2187